HEAVY METAL INTERACTIONS WITH NUCLEIC ACID DERIVATIVES: A NUCLEAR MAGNETIC RESONANCE STUDY

A thesis submitted to
THE UNIVERSITY OF CAPE TOWN
in fulfilment of the requirements
for the degree of
DOCTOR OF PHILOSOPHY

by

KLAUS R KOCH

Department of Inorganic Chemistry,
University of Cape Town,
Rondebosch,
Cape Town,
South Africa.

August 1979

ACKNOWLEDGEMENTS

My sincere thanks to my supervisor Professor G.V. Fazakerley, whose patient guidance and friendship has contributed immeasurably to the successful completion of this work. To Professor P.W. Linder and Professor L.R. Nassimbeni, my gratitude for their encouragement and many valuable comments during the course of this work.

A special thank you to Professor H.M.N.H. Irving who has guided and assisted me in so many ways.

To my colleagues, David Reid, Marco Celotti, Alan Hutton and Bob Wright and the many others who contributed in making my stay at U.C.T. so enjoyable, a sincere thank you.

Finally, but not least, I wish to express my sincere gratitude to Mr Ivor Finter for his excellent maintenance of the most critical factor in this work, the N.M.R. spectrometers. To all those who contributed in some small way I am deeply indebted.

I wish to acknowledge with thanks financial assistance from the Council for Scientific and Industrial Research and the University of Cape Town.

ABSTRACT

PART I

The aqueous solution conformation of SAH and SAM has been investigated using lanthanide probes. SAH at pH 7.0 interacts normally with lanthanide aquo ions and lanthanide-EDTA complexes via coordination at the carboxyl group. The conformation of the homocysteine fragment is found to be extended but bent back towards the adenine base. SAM does not interact with lanthanide aquo ions in the pH region 2-7. It does form complexes with lanthanide-EDTA species via an ion-pairing mechanism rather than direct coordination. In addition to lanthanide probes, 250 M Hz ^{1}H n.m.r. spectra yielded vicinal J_{HH} coupling constants from which the ribose conformation in both SAM and SAH could be more accurately determined.

The conformation of SAH can best be described as 75% *anti*/^{3}E with an extended homocysteine moiety. The $^{3}E \rightleftharpoons {}^{2}E$ ratio is found to be approximately 1:1 in both SAH and SAM. In contrast SAM is found to show a pseudo-cyclic conformation of the methionine group in which the carboxyl group lies near to the sulphonium centre held presumably by ion-pairing. SAM is found to favour 60% *anti*/^{3}E.

PART II

A ^{1}H and ^{13}C n.m.r. study of some *cis*-$[Pt(NH_3)X_2]Y_2$ type complexes of imidazoles, pyrimidines, 3-substituted pyridines and selected nucleosides has been undertaken. In general ^{2}J, ^{3}J and ^{4}J ^{195}Pt - ^{13}C coupling constants are observed for most species studied. The shift and coupling constant trends are compared and discussed in terms of the present state of theoretical knowledge governing these parameters.

Both water and DMSO were used as solvent, but in the latter extensive solvolysis occured and is consequently not recommended for studies of this type.

GLOSSARY OF SYMBOLS

$A/\hbar$	hyperfine coupling constant
B_1	power of observing r.f. field
f	ratio of nuclei in bound and unbound state
g	nuclear g factor
I	nuclear spin quantum number
k	Boltzmann's constant
Mo	equilibrium magnetisation
r	metal-proton internuclear distance
S	total electron spin
T	absolute temperature
T_1	longitudinal relaxation time
T_2	transverse relaxation time
T_{iM}	i = 1,2 relaxation rate of bound site
T_{ip}	i = 1,2 paramagnetic contribution to the relaxation rate
τ_c	dipolar correlation time
τ_e	scalar correlation time
τ_M	lifetime of bound state
τ_r	rotational correlation time
τ_s	electron spin relaxation time
μ	ionic strength
μ	nuclear magnetic moment
$\Delta\nu$	line width (in Hz) at half height
ω_I	nuclear Lamor frequency
ω_s	electron Lamor frequency
$\Delta\omega_M$	chemical shift of nucleus in bound state

CONTENTS

PART I

CHAPTER I : INTRODUCTION

INTRODUCTION

The conformation of molecules in solution has become of considerable interest to both chemists and biochemists in recent years. The importance of determining the conformation of small biologically significant molecules becomes clear when details of enzyme catalysis are considered.

In this study, we have undertaken to discover the conformations of S-adenosyl-L-methionine (SAM) and S-adenosyl-L-homocysteine (SAH) in dilute aqueous solution. For this purpose lanthanide shift and relaxation probes were selected to perturb the ^{1}H n.m.r. spectra of the above compounds. It may be useful to give a brief description of some aspects of methyl group biosynthesis since both SAM and SAH are intimately involved in biological transmethylation reactions.

1.1 Methyl Group Metabolism

Methyl groups are ubiquitously distributed in nature and their metabolism is of vital importance to the understanding of a great many biochemical reaction pathways. Following the experimental confirmation of the concept of methyl-group transfer to carbon, nitrogen, oxygen and sulphur atoms by Du Vigneaud [1], there has been active interest in methyl group metabolism. A very significant fact about biological transmethylation reactions is that the vast majority involve the methionine moiety, although not usually in its simplest form [2]. It has been found that methionine becomes 'active' in the form of S-adenosyl-L-methionine. The structural formulae of SAM and its principal metabolite, SAH is shown in Fig 1.1.

For the biosynthesis of methionine the absolute requirements are: homocysteine, serine, tetrahydrofolic acid (FH_4), adenosinetriphosphate (ATP), nicotinamide-adenine dinucleotide (reduced NADH), pyridoxal-

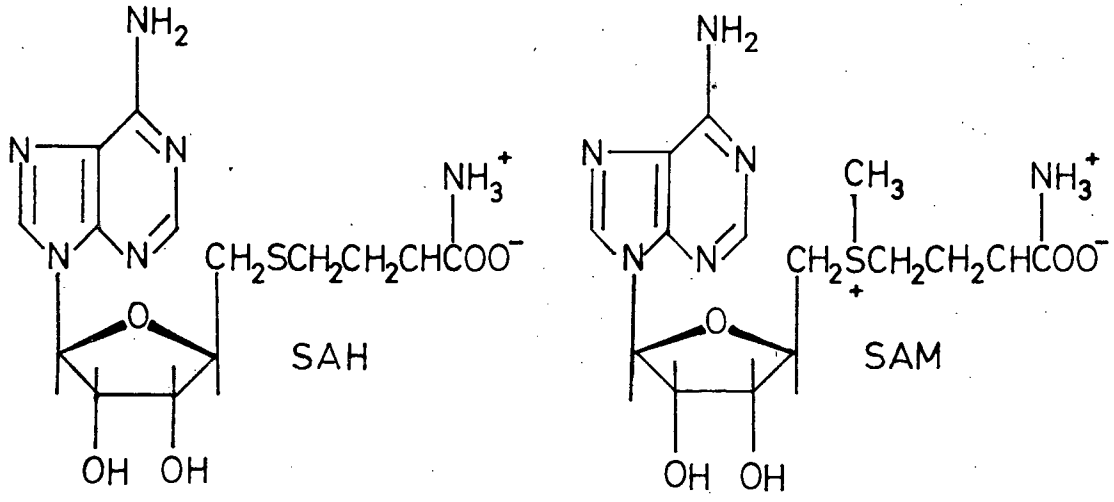

Figure 1.1: The structural formulae of SAM and SAH

phosphate and a flavine-adenine mono or dinucleotide (FAD or FMN). In addition a coenzyme, deoxyadenosylcobalamin, containing vitamin B_{12} is required. Broadly speaking the formation of methionine involves three stages *viz.*,

(i) the β-carbon of serine is transferred to tetrahydrofolic acid FH_4 to form N^5,N^{10}-methenyltetrahydrofolic acid ($h^{5\text{-}10}FH_4$).

(ii) $h^{5\text{-}10}FH_4$ is next reduced to a methylated folic acid derivative at nitrogen-5 *i.e.* m^5FH_4. Reduction presumably takes place *via* a reduced FAD pathway.

(iii) finally, homocysteine is methylated by m^5FH_4 in the presence of ATP, Mg^{2+}, NADH, FAD and an enzyme incorporating vitamin B_{12}.

These processes are shown schematically in Fig 1.2.

The fact that so many requirements for the synthesis of methionine exist underlines the complexity of the reaction pathways, all of which are catalysed by one or another enzyme.

The picture has been made more complicated by the discovery of Cantoni *et al.* [3] that the actual methyl-donor is S-adenosylmethionine (SAM). SAM

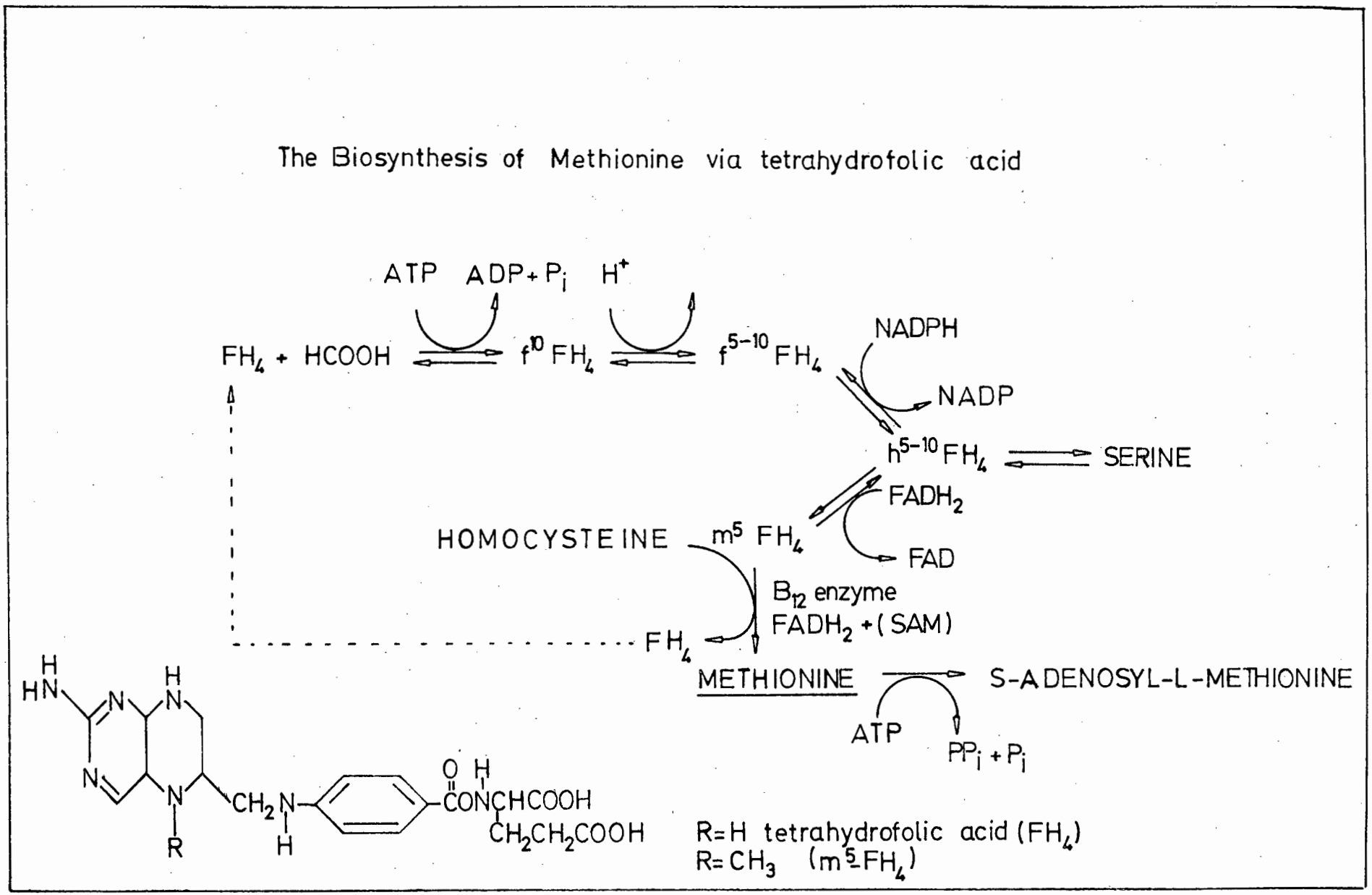

Figure 1.2: Biosynthesis of methionine and SAM.

is apparently formed from methionine and ATP in what is seen as an unprecedented biological reaction. The adenosyl moiety is condensed with methionine, while the terminal γ-phosphate and a pyrophosphate group is liberated. There is evidence that highly purified preparations of the enzyme involved in SAM synthesis also hydrolyse the initially formed triphosphate (PPP_i) group. This group remains almost totally bound to the enzyme until hydrolysis occurs. What is important is that only SAM markedly increases the rate of hydrolysis of PPP_i, suggesting an enzyme site which 'recognises' SAM unambiguously. The overall reaction may then be described by the following scheme.

$$Me + E + ATP \longrightarrow Me\cdots E\cdots ATP$$

$$Me\cdots E\cdots ATP \longrightarrow SAM\cdots E\cdots PPP_i$$

$$SAM\cdots E\cdots PPP_i \longrightarrow SAM + E + PP + P_i$$

$$Me + ATP \longrightarrow SAM + PP + P_i$$

Where Me : Methionine

E : the enzyme involved

P_i, PP, PPP_i the mono, di and triphosphate.

Mudd [4] has estimated free energy contributions for the various reactions above and shown that ΔG is very favourable to the forward reaction,

$$Me\cdots E\cdots ATP \longrightarrow SAM\cdots E\cdots PPP_i \qquad \Delta G = -8.5 \text{ Kcal/mole}$$

with major contributions from the binding energies of SAM and PPP_i to the enzyme. These findings have been supported by kinetic data which show that the overall backward reaction rate is *ca* 5×10^{-6} of the forward rate.

1.2 Biological Methyl-transfer Reactions

By far the majority of all transmethylation reactions that occur in nature involve SAM [2,5]. These reactions proceed *via* the onium pole, in which the methyl group attached to the charged sulphonium centre is transferred to the acceptor site. The methyl-transfer reaction is exergonic while a methylpherase enzyme is always involved.

Durell has estimated free energies associated with a number of simple methyl-transfer reactions [6]. If a proton is released during the course of such reactions the physiological pH makes a major contribution to the overall free energies involved. However an interesting result was presented for the following reaction:

$$(CH_3)_2S^+CH_2COO^- \quad (A) \quad + \quad CH_3SCH_2CH_2CH(NH_3^+)COO^- \longrightarrow CH_3SCH_2COO^- + (CH_3)_2S^+CH_2CH_2CH(NH_3^+)COO^- \quad (B)$$

At both pH = 0 and pH = 7, ΔG has been estimated to be -15.06 kJ $mole^{-1}$.

The notable difference in stability between the two dimethylsulphonium compounds A and B was not explained. It may be seen that B is S-methyl-L-methionine, the methyl analogue of SAM.

1.3 Survey of Previous Work

Despite many biochemical studies of transmethylation reactions as outlined in section 1.1, there have been few detailed investigations of the properties of the co-enzyme SAM and the compound, SAH, resulting from its de-methylation.

Mudd *et al.* investigated a number of sulphonium compounds including SAH and SAM calorimetrically [7]. It was found that an unusually high enthalpy change accompanies transmethylation reactions involving SAM, the basis of which was not clear. Related observations had been made previously by Durell [6]. In a subsequent investigation Mudd *et al.* measured the pK_a values for SAH and SAM, as well as recording their optical rotatory dispersion, infrared and ultraviolet spectra with a view to obtaining their conformation in solution [8]. It was argued that SAM assumed a "reasonably but not completely extended conformation", the molecule apparently being highly hydrated. The adenine ring was suggested to be predominantly *anti* in both SAH and SAM, but to a lesser extent in the latter case. The *syn* and *anti* adenine ring conformations in terms of rotation about the N(9)-C(1') glycosidic bond [9] is given in Fig 1.3.

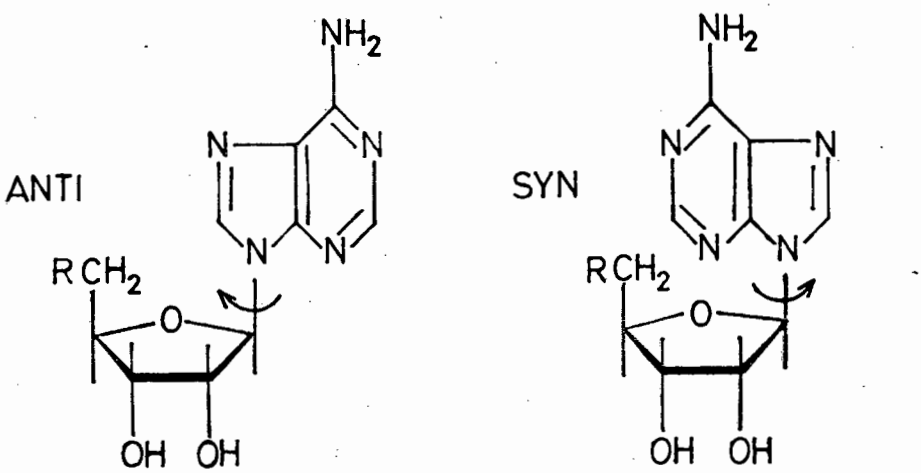

Figure 1.3: The *syn* and *anti* adenine conformations about the glycosidic N(9)-C(1') bond.

Mudd *et al.* concluded that strong coulombic interactions were unlikely because of the relatively 'normal' pK_a values that were obtained.

More recently, a ^1H n.m.r. study of a large variety of adenine nucleosides [11], suggested a strong preference of most of the derivatives for the *anti* conformation of the adenine ring, with a parallel *gauche, gauche*

C-5' substituent conformation [10]. SAH and SAM were found to conform to the generalisation postulated. This study was followed by a circular dichroism study of a similar range of compounds [12], the pertinent conclusion being that compounds such as SAM and SAH assume an average conformation of a *gauche,gauche/anti* type. The torsion angle, ϕ_{CN}, was thought to lie closer to 0°, substantially different from the value ϕ_{CN} = -40°, which is typical for solid monoclinic AMP and ATP [13,14].

An interesting study of the *in vitro* decomposition of S-methylmethionine-sulphonium (SMM) salts in aqueous solution revealed the decomposition products to be dimethyl sulphide and the homoserine lactone [15]. Evidence suggested that the carboxylate moiety partakes in the lactone formation (and demethylation of the sulphonium centre) by an intramolecular neighbouring-group participation mechanism [16], this being particularly evident in mildly acidic to neutral solutions. This mechanism requires that the deprotonated carboxylate moiety interacts electrostatically with the positively charged sulphonium pole of methylmethionine. Fig 1.4 shows such a neighbouring-group participation mechanism.

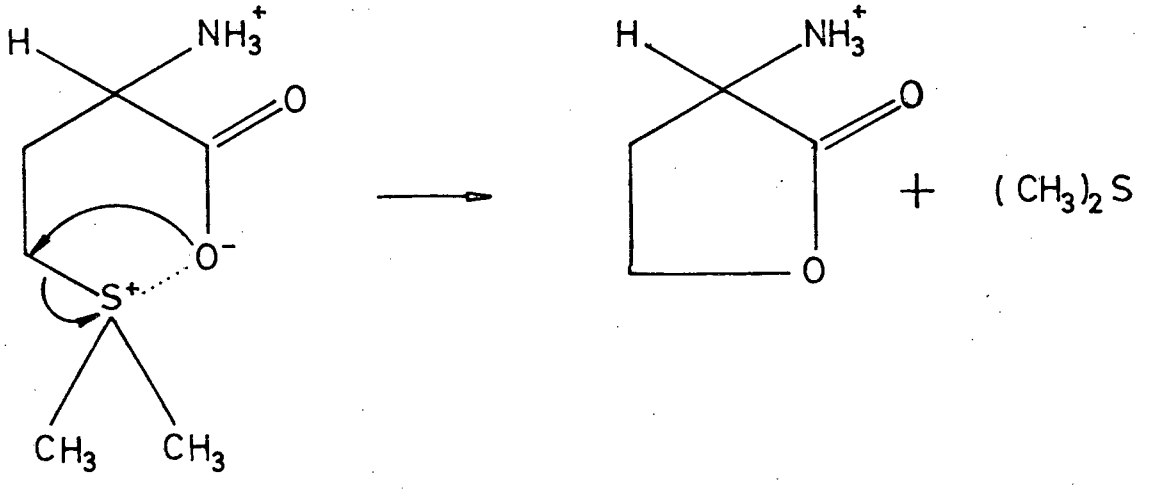

Figure 1.4: The proposed neighbouring-group participation mechanism (after Ramirez [13]).

A crystal structure of S-methyl-L-methionine hydrochloride shows the molecule to be extended, linked to its neighbours by extensive hydrogen bonding and coulombic interactions [17]. Intramolecular van der Waal's potential-energy calculations reveal that especially for the zwitterionic and anionic forms of SMM, a cyclic conformation in which the deprotonated carboxylate moiety lies close to the positive sulphonium centre is strongly favoured. This model was qualitatively supported by a ^{1}H n.m.r. study.

The absolute configuration (in terms of the Cahn, Ingold and Prelog convention) at the sulphonium center of SAM was recently deduced from the crystal structure of (R)-[((S)-3-amino-3-carboxypropyl)(carboxymethyl-methylsuphonium]2,4,6-trinitrobenzenesulphonate, which is the diastereomer of the degradation product of naturally occurring SAM [18]. Since SAM gives rise to the (S)-sulphonium diastereomer, it follows that SAM is thus correctly formulated as 5'-[((3S)-3-amino-3-carboxypropyl)methyl-(S)-sulphino]-5'-deoxyadenosine.

1.4 Objectives of Research

It is evident from previous studies that considerable debate about the conformation of molecules such as SAM and SAH exists. The conflicting picture that emerges from various studies outlined underlines the need for a more direct investigation of conformation.

Two questions need to be answered *viz.*,

(i) are the conformations of SAM and SAH similar or very different?

(ii) is it possible to determine the conformation of SAM and SAH in dilute aqueous solution by means of lanthanide shift and relaxation probes?

In view of what is known about the solution conformation of SAM and SAH. it is tempting to postulate that the methionine moiety in SAM adopts a six-membered cyclic conformation, in which the carboxyl group interacts coulombically with the positive sulphonium centre. There appears to be no reason to expect a similar intra-molecular interaction in the case of SAH.

The objective of this study is to discover the conformation of SAH and SAM in dilute aqueous solution, by means of lanthanide shift and relaxation probes. Additionally the vicinal and geminal coupling constants measured at 250 M Hz are expected to yield quantitative information about the ribose conformation.

PART I

CHAPTER II : THEORY AND METHODS

THEORY

The basic theory of the nuclear magnetic resonance experiment will be assumed since this is well understood and given in many standard texts [19-24]. What will be dealt with here are only those aspects of direct relevance to this work.

2.1 Definition of Nuclear Relaxation Times

The small excess of nuclear magnetic moments in the lower energy level over those in the higher level in the presence of an external magnetic field $\overline{B}_o$, makes it possible to obtain a resonance absorption. Such an absorption of energy would induce transitions between the Zeemann energy levels resulting in an equilisation of the population of ground and excited states, thus saturation would occur. In order to obtain a continuous absorption of energy there must exist a mechanism by which the system of magnetic moments returns to its equilibrium Botzmann distribution. This is achieved by a first-order rate process characterized by a *spin-lattice relaxation time*, T_1. This spin-lattice relaxation time represents the time taken for the nuclei to reach the equilibrium distribution by interactions with the lattice or molecular framework.

In addition to interactions with the lattice, nuclei interact amongst themselves. Each nuclear spin-dipole generates its own local magnetic field, $\overline{B}_{loc}$, which from classical eletromagnetic theory can be given as

$$\overline{B}_{loc} = \pm \frac{\mu(3\cos^2\theta - 1)}{r^3} \qquad (2.1)$$

Here, θ is the angle between $\overline{B}_o$ and vector, $\overline{r}$, joining the spin-dipole to some point under consideration. The dependence of $\overline{B}_{loc}$ on r^{-3} shows that such dipole-dipole interactions only operate over small absolute distances.

Brownian motion in liquids causes rapid tumbling of the nuclear dipoles, thus the vector sum of the local magnetic fields averages to zero (since $\cos^2\theta$ tends to 1/3). Nevertheless, two like nuclei in close contact may experience a spread in their Larmor precession frequency given by

$$\Delta\nu = \frac{2\pi\,\mu\,\bar{B}_{loc}}{Ih} \qquad (2.2)$$

This spread in precession frequency gives rise to many resonance conditions close in frequency and thus results in a broadened spectral line. The line is broader than anticipated on the basis of the uncertainty principle taking account only of spin-lattice (T_1) relaxation processes. The time constant for two like nuclei precessing in phase at a particular instant, to precess out of phase (due to $\bar{B}_{loc}$ fluctuations) is termed the *spin-spin relaxation time*, T_2.

There is another important mechanism contributing to T_2 relaxation, the so called "flip-flop energy enchange". Consider two like nuclei (i.e. same γ_I), one of which undergoes a transition from one spin state to another. This transition results in a change in $\bar{B}_{loc}$ at the precession frequency, which induces a transition in the second nucleus. By such a mechanism, the two nuclei may exchange energy adiabatically, reducing the life-time of a particular excited state without an overall energy change of the system. By the uncertainty principle, the resonance line-width is thus broadened and the spin-spin relaxation time may be approximately defined as the life time of the excited state. T_2 is related to the n.m.r. line width by

$$\nu_{\frac{1}{2}} = \frac{1}{\pi T_2} \qquad (2.3)$$

Where $\nu_{\frac{1}{2}}$ is the half height width of a Lorentzian resonance line.

Perhaps one of the most convenient ways of visualizing the above mentioned relaxation times lies in the concept of the rotating reference frame. Since one is never concerned with a single nuclear moment, it is more convenient to consider the macroscopic resultant magnetization vector, $\overline{M}$, representing the z-component of an ensemble of identical magnetic moments precessing about $\overline{B}_o$. At the thermal equilibrium $\overline{M}$ will point in the direction of $\overline{B}_o$ appearing stationary to the rotating observer. Fig.2.1 shows this idea graphically.

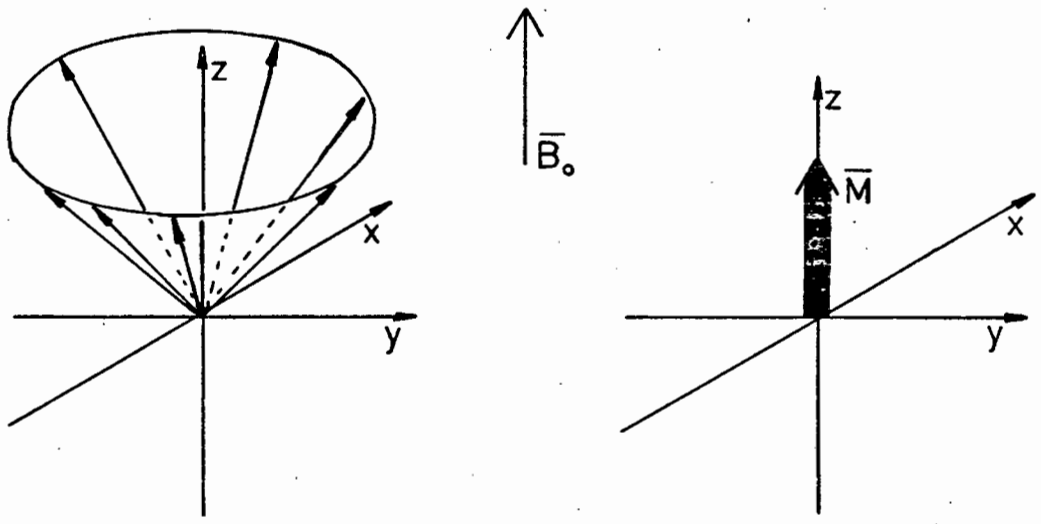

Figure 2.1: The resultant magnetization vector $\overline{M}$.

To perform a resonance experiment one must apply a small magnetic field $\overline{B}_1$ at right angles to $\overline{B}_o$, say along the x-axis, precessing at the Larmor frequencies of the nuclei. To the rotating observer, $\overline{B}_1$ appears as a stationary field vector along the x-axis. The effect of $\overline{B}_1$ is to tilt $\overline{M}$ in the z-y plane, the components M_x and M_y become finite with a concomittant decrease in the magnitude of M_z. The physical situation corresponds to a "phasing" of the precessing nuclei which, at thermal equilibrium, precess about z with a random distribution of phases (the result of a non-uniform $\overline{B}_o$ within the sample).

The extent to which $\overline{M}$ is tilted in the z-y plane depends on the magnitude of both $\overline{B}_1$ and t_p, the time during which $\overline{B}_1$ is applied. It may be shown that the angle, θ, through which $\overline{M}$ is tilted is given by

$$\theta = \gamma/\overline{B}_1/t_p \quad \text{(radians)} \tag{2.4}$$

If at constant $\overline{B}_1$, t_p is such that $\theta = \pi$, $\overline{M}$ is totally inverted, as shown in Fig 2.2

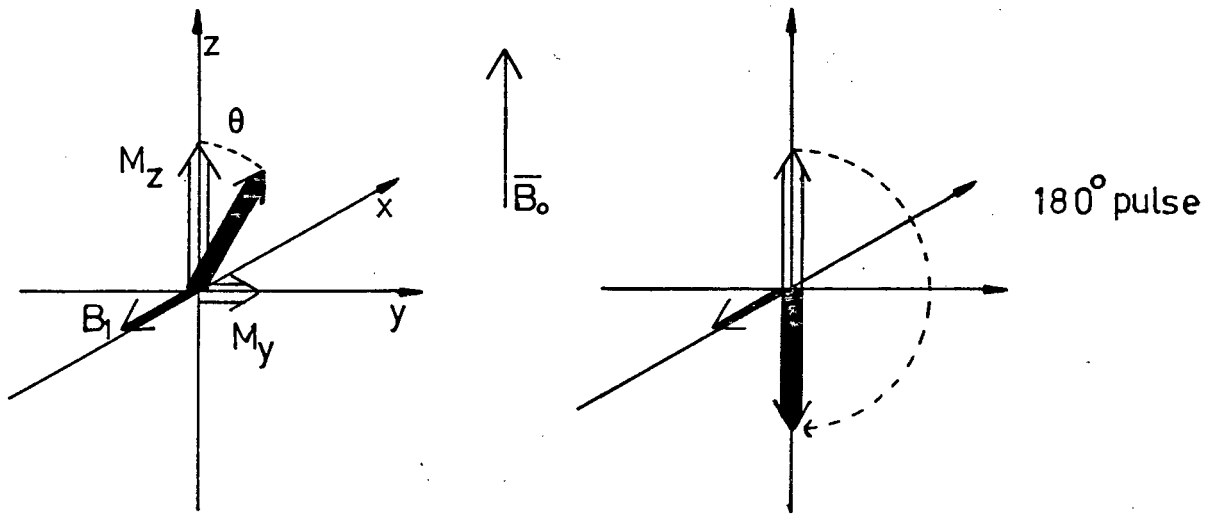

Figure 2.2: Application of an excitation pulse which rotates the magnetization $\overline{M}$ in the z-y plane, through angle θ.

M decays back to its equilibrium orientation with time constant T_1, the spin-lattice, or alternatively the longitudinal, relaxation time. Because of natural processes that cause nuclei to exchange energy with each other e.g. by the flip-flap mechanism referred to above, the M_x and M_y components also relax by the progressive loss of phase coherence between the magnetic moment vectors. The adiabatic dephasing of M_x and M_y is characterized by the spin-spin relacation time also known as the transverse relaxation time. These ideas may be elegantly described by the Bloch differential equations [25,26] (refer to Fig 2.2).

$$\frac{dM_x}{dt} = (M_y B_z - M_z B_1 \sin 2\pi rt) - \frac{M_x}{T_2} \qquad (2,5a)$$

$$\frac{dM_y}{dt} = -(M_x B_z - M_z B_1 \cos 2\pi rt) - \frac{M_y}{T_2} \qquad (2.5b)$$

$$\frac{dM_z}{dt} = -(M_x B_1 \sin 2\pi rt + M_y B_1 \cos 2\pi rt) - \frac{M_z - M_o}{T_1} \qquad (2.5c)$$

Inspection of equations (2.5) gives the following important generalizations about the nature of T_1 and T_2 relaxation processes:-

(i) Both T_1 and T_2 relaxation is induced by fluctuating local magnetic fields.

(ii) T_1 processes arise from magnetic fields that have only x and y components.

(iii) By contrast, T_2 relaxation is induced by fluctuating magnetic fields that have components in the x, y and z directions.

(iv) In general it may be shown that $T_2^* < T_2 < T_1$, where T_2^* includes a contribution from the external magnetic field inhomogeneity such that $1/T_2^* = 1/T_2 + \gamma(\Delta B_o)/2$. where ΔB_o represents the static magnetic field inhomogeneity.

To summarise it may be appropriate to list some of the various types of relaxation mechanisms that have been studied in much detail. In principle any mechanism which gives rise to fluctuating magnetic fields, can induce nuclear magnetic relazation. The following processes are considered to be the most important contributors to T_1 spin-lattice interactions (some, of course, also effect T_2 processes):-

(i) Magnetic dipole-dipole interaction.

(ii) Electric quadrupolar interaction.

(iii) Spin-rotation interaction.

(iv) Scalar-coupling relaxation.

(v) Chemical shift anisotropy interaction.

2.2. *Paramagnetic Relaxation*

An unpaired electron generates a local magnetic field. Due to rapid random molecular motion, the resultant fluctuating magnetic field provides a relaxation mechanism. Since the electron's magnetic field moment is about a thousand times greater than that of a proton, paramagnetic species are expected to be very efficient relaxation agents. This is indeed observed as exemplified by a reduction of the relaxation rate for the protons in benzene by a factor of 5 when dissolved oxygen is removed.

The paramagnetic relaxation is mostly coupled to the nuclei by a dipole-dipole mechanism, although sometimes also by a scalar interaction transmitted through a chemical bond. In general one may write for any fluctuating magnetic field mechanism contributing to relaxation rates,

$$T^{-1} = E^2 f(\tau_c) \qquad (2.6)$$

where E represents the magnitude of the particular interaction and τ_c is the molecular correlation time. The quantity τ_c can be thought of as the average time between molecular collisions which gives a measure of the frequency of variation of the magnetic interactions between nuclei. If τ_c is short, then nuclei quickly lose 'memory' of such magnetic interactions, since for rapid molecular tumbling local magnetic fields fluctuate rapidly.

The relaxation times, T_1 and T_2, for nuclei bound near to a paramagnetic species have been given explicitly by Solomon and Bloembergen [42,45]. The relaxation rates $(T_{1M})^{-1}$ and $(T_{2M})^{-1}$ refer to the condition in which the metal is bound to ligand. In particular $(T_{1M})^{-1}$ and $(T_{2M})^{-1}$ may be given as:-

$$(T_{1M})^{-1} = \frac{2\gamma_I^2 g^2 S(S+1)\beta^2}{15\, r^6}\left[\frac{3\tau_c}{1+\omega_I^2\tau_c^2} + \frac{7\tau_c}{1+\omega_S^2\tau_c^2}\right] + \frac{2}{3}S(S+1)\left[\frac{A}{\hbar}\right]^2\cdot\left[\frac{\tau_e}{1+\omega_S^2\tau_e^2}\right] \qquad (2.7)$$

$$(T_{2M})^{-2} = \frac{\gamma_I^2 g^2 (S+1)\beta^2}{15\, r^6}\left[4\tau_c + \frac{3\tau_c}{1+\omega_I^2\tau_c^2} + \frac{13\tau_c}{1+\omega_S^2\tau_c^2}\right] + \frac{S(S+1)}{3}\left[\frac{A}{\hbar}\right]^2\cdot\left[\frac{\tau_e}{1+\omega_I^2\tau_c^2} + \tau_e\right] \qquad (2.8)$$

The first terms represent a dipole-dipole interaction between the electron spin, S, and the nuclear spin, I. The second term gives the scalar contribution characterized by τ_e.

The various correlation times which modulate such electron-nucleus interactions are defined as

$$\frac{1}{\tau_c} = \frac{1}{\tau_S} + \frac{1}{\tau_M} + \frac{1}{\tau_R} \qquad (2.9)$$

and,

$$\frac{1}{\tau_e} = \frac{1}{\tau_S} + \frac{1}{\tau_M} \qquad (2.10)$$

where τ_M, is the bound life-time of the nucleus,

τ_R, the rotational correlation time of the bound paramagnetic species,

τ_S, the electron-spin relaxation time.

Some of the other quantities which appear in equations 2.7, 2.8 are ω_S and ω_I, the electronic and nuclear Larmor frequencies; $(A/\hbar)$ is the electron nuclear hyperfine coupling constant measured in Hz. The other quantities have their usual meanings as defined previously (c.f. list of symbols).

2.3 *The Effect of Chemical Exchange on Paramagnetic Relaxation*

Having given an explicit expression for the paramagnetic relaxation rate above it is important to consider the effect of chemical exchange on the relaxation time.

The Solomon-Bloembergen equations (2.7 - 2.8) apply to the bound state. If chemical exchange between the paramagnetic species and the ligand is considered, it can be shown that the observed relaxation rate $(T_{1\ obs})^{-1}$ depends on the fraction of nuclei in the bound condition as well as the rate of chemical exchange between the bound and unbound condition [40,41]. In particular

$$\frac{1}{T_{1\ obs}} = \frac{1}{T_{1A}} + \frac{P_M q}{T_{1M} + \tau_M} \qquad (2.11)$$

where $(T_{1A})^{-1}$ is the relaxation rate of unbound ligand nuclei.

P_M is the mole fraction of bound nuclei,

q the number of ligands per metal bound,

τ_M is the life-time of the bound condition.

If $q = 1$ and $[L] >> [M]$, then the mole fraction $P_M = [M]/[M] + [L]$ may be approximated by $f = [M]/[L]$ and thus from equation (2.11) one may write for

the paramagnetic contribution to the observed relaxation rate,

$$\frac{1}{T_{1p}} = \frac{1}{T_{1\,obs}} - \frac{1}{T_{1A}} = \frac{f}{T_{1M} + \tau_M} \tag{2.12}$$

Similarly for $(T_{2\,obs})^{-1}$ one may write

$$\frac{1}{T_{2p}} = \frac{1}{T_{2\,obs}} - \frac{1}{T_{2A}} \tag{2.13a}$$

$$= \frac{f}{\tau_M} \frac{1/T_{2M}(1/T_{2M} + 1/\tau_M) + \Delta\omega^2_M}{(1/T_{2M} + 1/\tau_M)^2 + \Delta\omega^2_M} \tag{2.13b}$$

where $\Delta\omega_M$ is the chemical shift difference between the bound and unbound ligand resonances.

Inspection of equations (2.12) and (2.13) shows that there exist a number of limiting cases which correspond to slow, intermediate and fast exchange between the paramagnetic ion and ligand. In particular, in the fast exchange region equation (2.13b) reduces to

$$\frac{1}{T_{2p}} = \frac{f}{T_{2M}} \tag{2.14}$$

since $(1/T_{2M}\tau_M) >> (1/T_2{}^2{}_M)$ and $\Delta\omega^2{}_M$. Thus the observed spin-spin relaxation rate is the weighted average of the two environments under fast exchange conditions ($1/\tau_M$ is large). The observed resonance line width is thus controlled by $(T_{2p})^{-1}$. Similarly, the spin-lattice relaxation time induced by the paramagnetic species reduces to

$$\frac{1}{T_{1p}} = \frac{f}{T_{1M}} \tag{2.14}$$

It is evident that if explicit equations for $(T_{1M})^{-1}$ and $(T_{2M})^{-2}$ are available useful information might be extracted from a knowledge of $(T_{1p})^{-1}$ and $(T_{2p})^{-1}$. Inspection of the Solomon-Bloembergen equations (2.7 - 2.8) shows that in particular geometric information may be obtained concerning the distance between the paramagnetic centre and the ligand nuclei.

In the slow and intermediate exchange regions the paramagnetically induced relaxation enhancement depends on changes in precessional frequencies and, of course, on the rate of chemical exchange. These complications render it difficult, if not impossible to derive geometric information from paramagnetic rates, and are beyond the scope of this study.

2.4 *Classification of Paramagnetic Metal Ions as Shift and Relaxation Probes*

It may be recalled from equations (2.9) and (2.10) that the correlation times τ_c and τ_e are determined by the bound life-time, the rotational correlation time and the electron-spin relaxation time, τ_S.

Paramagnetic ions may be classed according to whether $(\tau_c)^{-1}$ is dominated by $(\tau_S)^{-1}$ or $(\tau_R)^{-1}$. Where $(\tau_c)^{-1}$ is dominated by $(\tau_R)^{-1}$, i.e the electron-spin correlation time is long ($\tau_S > \tau_R$), the value of $(T_{2M})^{-1}$ becomes large and thus the spectral lines are substantially broadened. These ions are grouped into class I, and include Mn(II), Gd(III), and Cu(II).

The metal ions of class 1 also have a large $(T_{1M})^{-1}$ value, which renders them efficient relaxation probes.

Ions of class 2 have short electron-spin relaxation times ($\tau_S \approx 10^{-12}$ - 10^{-13}S), thus $(\tau_c)^{-1}$ is dominated by $(\tau_S)^{-1}$. These ions do not induce much

line broadening and result in $(T_{1M})^{-1}$ values typically two orders of magnitude less than for class 1 ions. Consequently the hyperfine shift to line width ratio is favourable for class 2 ions such as Co(II), Ni(II), Fe(II), Fe(III) and most other lanthanide trivalent ions, to use these as shift probes.

2.5 *Paramagnetic Ions as Shift Probes*

The magnetic resonances of nuclei in paramagnetic complexes often show very different chemical shifts relative to their diamagnetic analogues. Class 2 paramagnetic species result in little resonance line broadening and thus the hyperfine shifts they induce become readily measurable.

Shifting of a resonance may arise from one or both of the following types of interaction.

(i) Contact or scalar shifts.

(ii) Pseudo-contact or dipolar shifts.

Contact shifts result from delocalization of electron spin density at the resonating nucleus. This effect, transmitted through chemical bonds, is analogous inter-nuclear J coupling and thus is expected to attenuate fairly rapidly with the number of intervening bonds. On the other hand, the pseudo-contact shifts originates from an anisotropic magnetic field produced by the unpaired electron spin density, which does not average to zero.

Contact shifts

This mode of shifting an n.m.r. line can be represented schematically in terms of the hyperfine coupling constant, A, (observable in the e.s.r. spectrum of the paramagnetic species) and the electron-spin relaxation rate $(\tau_S)^{-1}$ as in Figure 2.3 . Consider scalar coupling between a proton

and an electron. If $(\tau_S)^{-1} >> A$ ($\tau_S = 10^{-12} - 10^{-13}$S), then little line-broadening results making the ion a suitable shift probe.

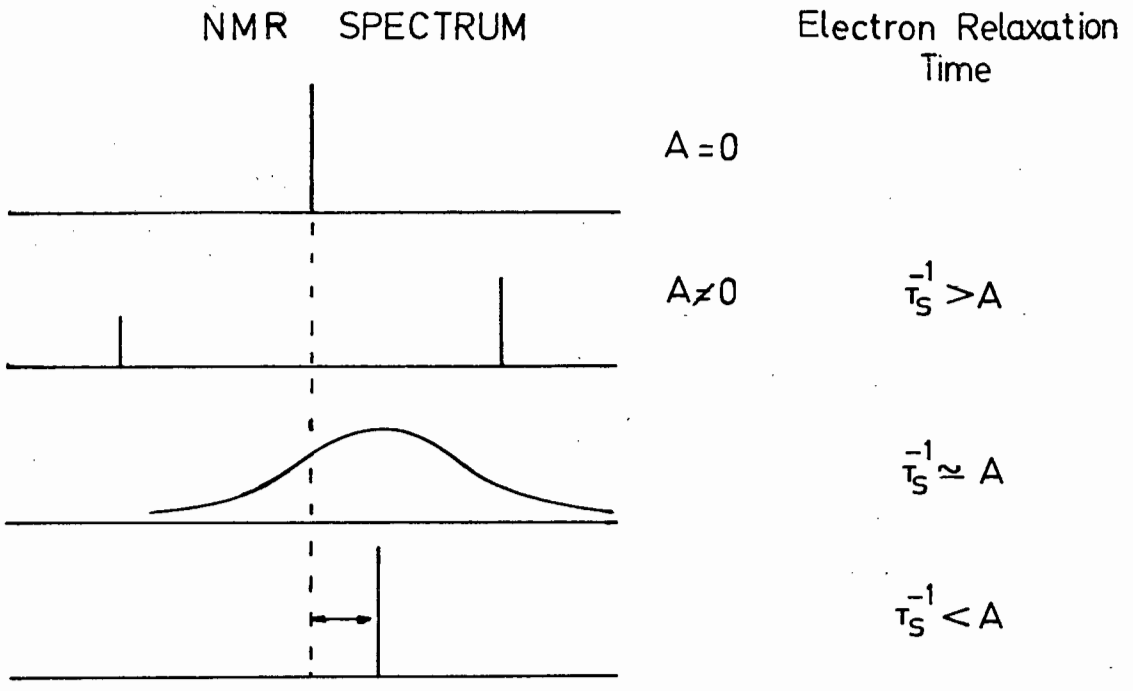

Figure 2.3: Schematic diagram to show paramagnetically induced shifts in the n.m.r. spectrum.

When τ_S is long enough for A to be resolved, the proton spectrum would result in two lines (of unequal intensity) separated by A MHz. If on the other hand τ_S is very short compared to A then a single line, the weighted mean of the two original resonances, is observed. This line is shifted from the uncoupled resonance by an amount that depends upon the electron spin quantum number S, the absolute temperature T, and the value for A. Bloembergen [42] has given an expression for this shift for the 1st-row transition metals,

$$\frac{\Delta\nu}{\nu_o} = -\frac{A}{\hbar}\,\frac{g\,\beta\,S(S+1)}{3kT\,\gamma_I} \qquad (2.16)$$

$\Delta\nu$ is the shift from the corresponding diamagnetic case, ν_o the irradiating frequency.

Of course the rate of chemical exchange$(\tau_M)^{-1}$ cannot be ignored. In general for a shift probe to be useful, $(\tau_M)^{-1}$ must be greater than A in addition to τ_S << A. If these conditions are complied with, then one would observe sharp resonances, shifted considerably from the diamagnetic complexes.

Pseudo-contact or dipolar shifts

If the g-factor for the paramagnetic ion is isotropic, then there is no dipolar electron nuclear interaction and the paramagnetic species induces Fermi contact shifts only. In many cases, however, the g-factor is anisotropic and the unpaired electron-spin nuclear dipolar interaction does not average to zero. In such cases pseudo-contact shifts (P.C.) are induced at the nucleus in question.

The magnitude and nature of this P.C. shift depends on (i) the principal molecular magnetic susceptibilities, χ, of the paramagnetic species (ii) the extent of spin-orbit coupling (given by quantum number J) and, (iii) the ligand field splitting of the ion's electronic levels. The nature of the P.C. shifts induced by the 1st-row transition metals is thus quite different from the P.C. contributions arising from the lanthanide ions. It also turns out that the P.C. shift is dependent upon the overal symmetry of the paramagnetic complex.

La Mar [43] has derived a general equation for evaluating the P.C. shift which represents an average over the possible molecular motions (assumed rapid on the n.m.r. time scale).

$$\frac{\Delta\nu_M}{\nu_o} = D\left\langle \frac{3\cos^2\theta - 1}{r^3} \right\rangle_{ave} + D'\left\langle \frac{\sin^2\theta \cos 2\Omega}{r^3} \right\rangle_{ave} \qquad (2.17)$$

The terms D and D' are temperature dependent constants for each system. θ is the angle between the principal symmetry axis (the $\bar{k}$ axis) of the complex and Ω the angle between the equatorial projection of $\bar{r}$ and the $\bar{i}$ axis. $\bar{r}$ is the inter-nuclear vector. A diagram will make this clearer (Fig 2.4).

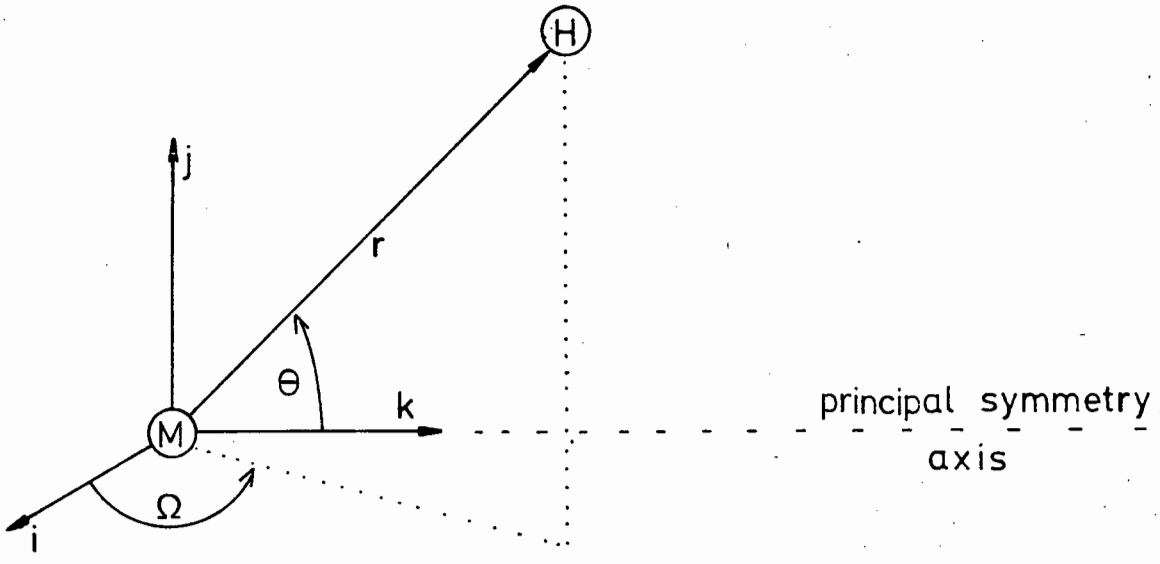

Figure 2.4: Diagram defining parameters of the pseudo-contact shift equation (2.17).

The exact nature of the constants D and D' is complex and a subject of continuous modification [44,45]. Bleaney [44] has shown that for the lanthanide ions the P.C. shift is predominant and that the Fermi contact contribution is negligible for nuclei far from the paramagnetic centre.

If axial symmetry can be assumed, then D' in equation (2.17) reduces to zero and the effective P.C. shift is given by the term

$$\frac{\Delta\nu_M}{\nu_o} = D\left\langle \frac{3\cos^2\theta - 1}{r^3} \right\rangle_{ave} \qquad (2.18)$$

The geometric value of equation (2.18) is self evident. If a knowledge of D is available along with an assumption that contact shifts are negligible, measurements of lanthanide induced shifts will give details of the conformation of the paramagnetic complex in solution.

Tha lanthanide ions have been studied in much detail with regard to their use as probes for molecular conformation [44-48]. The large number of conformational studies that have appeared support the contention that if applied with care, a good deal of information about molecular conformation may be obtained.

Bleaney [46] and Barry [47] have shown that for lanthanides the P.C. shift contribution is dominant and that isomorphous substitution of lanthanides allows the verification of (i) the predominantly P.C. nature of the shifts induced and (ii) that effective axial symmetry is present. In other words, if as many lanthanides as possible induce *comparable* shift ratios then criteria (i) and (ii) above must hold. In this case then equation (2.18) may be used to evaluate the term $(3\cos^2\theta - 1)/r^3$. Since evaluation of D is difficult, it is more usual to consider a shift ratio

$$R_i = \frac{\Delta\nu_i}{\Delta\nu_o} = \frac{\left\langle \frac{3\cos^2\theta_i - 1}{r_i^3} \right\rangle_{ave}}{\left\langle \frac{3\cos^2\theta_o - 1}{r_o^3} \right\rangle_{ave}} \qquad (2.19)$$

The shift ratio is simply obtained by normalizing any particular shift ($\Delta\nu_i$) onto a chosen shift induced in the same molecule ($\Delta\nu_o$). In this way D is eliminated, and one may then compare shift ratios induced by various lanthanide ions.

2.6 *The Determination of Conformation Using Lanthanide Shift and Relaxation Probes*

Reference to equations (2.7) and (2.8) shows that the value of $(T_{1M})^{-1}$ and $(T_{2M})^{-1}$ depends on r^{-6}. If it can be assumed that the scalar contribution to relaxation is negligible, one can calculate a ratio given by

$$\frac{(T_{jM})_i^{-1}}{(T_{jM})_o^{-1}} = \frac{r^{-6}}{r^{-6}} \qquad (2.20)$$

(j = 1,2)

Hence relative distance of a particular nucleus, i, from the Gd(III) ion can be obtained if a unique binding site for the gadolinium ion is known. In principle it is possible to obtain such distances even if there are more than one binding site. This requires a knowledge of the formation constants involved. Swift and Connick [49] as well as other workers [50] have shown that for Gd(III) the scalar contribution is indeed negligible for nuclei not directly bound to the paramagnetic centre, hence the use of equation (2.20) is justifiable.

From the knowledge of $(T_{1M})^{-1}$ one can therefore obtain relative values for the internuclear vector, $\bar{r}$. Combining the shift ratio function (2.19) with such relaxation data gives an effective method for determining the conformation of a suitable substrate molecule.

From a knowledge of the molecular structures, scale models may be constructed for the compound under investigation from which calculated shift and relaxation ratios may be obtained. These are then compared with the experimentally determined ratios. If agreement between observed and calculated ratios is good for all observable protons then one may accept the

results with confidence. Although computer search routines for all possible conformations are available [47] it is often more efficient to eliminate unrealistic conformations using some chemical intuition, and thus manual conformation searches become possible within reasonable time limits for small molecules.

In practice $(T_1)^{-1}$ is obtained from a plot of $\ln(A_\infty - A_\tau)$ against τ. This follows from a slightly recast form of the relevant Bloch equation (2.5),

$$\ln(A_\infty - A_\tau) = \ln 2A_\infty - \tau/T_1 \qquad (2.21)$$

In this equation A_∞ is the initial amplitude of the free induction decay, while A_τ is the value after a time delay τ following the 180^o pulse.

From values of $(T_1)^{-1}$ one may calculate the paramagnetically enhanced relaxation rate, $(T_{1p})^{-1}$, from

$$(T_{1p})^{-1} = (T_1)^{-1}_{obs} - (T_{1A})^{-1} \qquad (2.22)$$

$(T_{1A})^{-1}$ is the relaxation rate of the substrate protons in the absence of a relaxation probe.

Finally it follows from equation (2.15) that a plot of $(T_{1p})^{-1}$ against f should yield a straight line for each proton, with slope $(T_{1M})^{-1}$, and y-intercept at the origin. It may be recalled that this approach is valid only for the conditions of fast chemical exchange.

2.8 Scale Molecular Models and Calculations Involved

Drieding molecular models with a scale 2.54 cm per 10 nm were constructed for SAM and SAH. Crystallographically determined bond lengths as found for AMP, ATP, L-methionine and S-methyl-L-methionine hydrochloride [13,14,17,56] were compared with our Drieding model bond lengths. It was found that in all cases agreement between the experimental values and the model bond lengths was better than 0.01 nm. In searching for a conformation, interculear distances were generally determined to ±0.01nm while angles measured from the principal symmetry axis are estimated

accurate to ± 2^{o}.

In calculating the average distance of a methyl proton (or other magnetically equivalent protons) from the paramagnetic centre the relation

$$\frac{1}{r_{av}^{6}} = \frac{1}{n}\sum_{i=1}^{n}\frac{1}{r_{i}^{6}} \qquad (2.22)$$

was used. The value r_i correspond to individual proton-metal ion distances.

It is also possible to estimate the relative populations of the *syn* and *anti* conformers of the adenine moiety by means of $(T_{1M})^{-1}$ relaxation data. For this purpose a slightly modified form of equation (2.20) may be written:

$$(T_{1M})^{-1} = K\left[\frac{\tau_{anti}}{(r_{anti})_i^{6}} + \frac{1 - \tau_{anti}}{(r_{syn})_i^{6}}\right] \qquad (2.23)$$

Here, τ_{anti} is the fraction of time spent in the *anti* conformation with the corresponding distance $(r_{anti})_i$ from the metal to H_i.

2.9 Conformational Nomenclature

The possibility of rotation of the adenine moiety about the glycosyl bond N(9)-C(1') has already been referred to. Figure 1.3 shows the *syn* and *anti* conformations as defined by Donahue *et al* [9]. This rotation may be quantised in terms of a torsion angle ϕ_{CN}. By convention, ϕ_{CN} is measured as the angle between the plane of the purine base and the projection of the C(1')-O(1') bond. ϕ_{CN} is taken as positive for a clockwise rotation of the base looking from C(1') toward the N(9) atom. Refer to Figure 2.6. Nucleosides and nucleotides are defined as *anti*

if $\phi_{CN} = 0^{o} \pm 90^{o}$ while for the *syn* conformation $\phi_{CN} = 180^{o} \pm 90^{o}$.

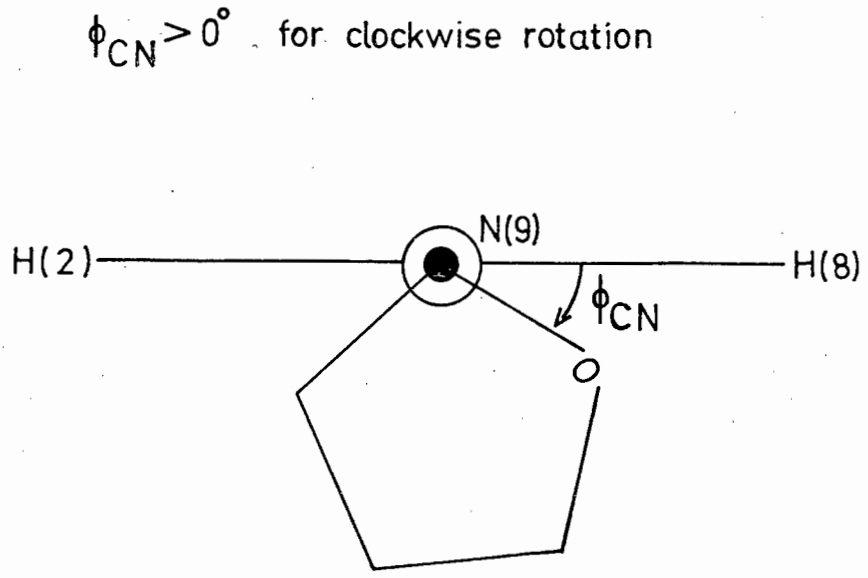

Figure 2.6: The definition of the glycosyl torsion angle ϕ_{CN}.

An alternative convention for the glycosyl torsion angle is often used [37]. This convention defines the torsion angle χ in a similar fashion as ϕ_{CN} but $\chi = -\phi_{CN}$.

Ribose conformation

The furanose ring may adopt a variety of puckered conformations. One way of describing these conformations is by a 'least-square plane' method in which a four/three atom plane is considered [37]. The four atom plane gives rise to an envelope (E) conformation, while the 3-atom plane results in a twist (T) pucker. The two most strongly favoured sugar puckers are the C(3')-*endo*(^{3}E) and C(2')-*endo*(^{2}E) types. Additionally two twist

conformations ${}^{3}_{2}T$ and ${}^{2}_{3}T$, designating the C(3')-*endo* / C(2')-*exo* and C(2')-*endo* / C(3')-*exo* forms are possible. Figure 2.7 shows these limiting furanose conformations.

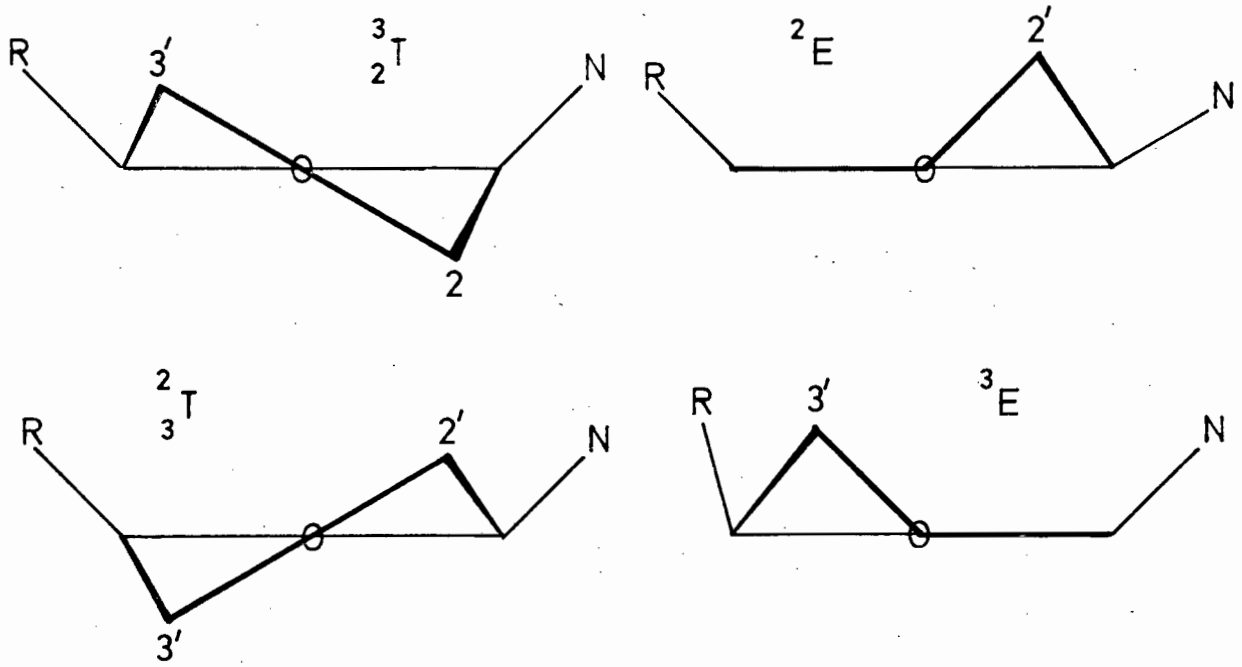

Figure 2.7: The ribose ring conformations.

An elegant description of the conformation of the sugar ring in nucleosides and nucleotides was developed by Altona and Sundaralingam [37,53]. This method is based on the concept of pseudorotation and each of the infinite number of possible furanose conformations is then characterized by a *phase angle* P(domain 0^{o}-360^{o}) and a *amplitude* of pucker τ_m (range $\overline{40}$ to 40). Both quantities are related to the five torsion angles of the furanose ring. One thus obtains a convenient way of defining the conformation of a ribose ring. The standard conformation for which $P = 0^{o}$ ($\tau_m = 40^{o}$) is taken to be the symmetrical ${}^{3}_{2}T$ pucker as illustrated in Figure 2.7. Conformations with $0^{o} < P < 36$ are referred to as N-type

while those in the 144^{o} to 180^{o} domain are the S-type conformation. The latter corresponds to the ${}^{2}_{3}T$ pucker.

Consideration of the exocyclic C(4') substituent shows that the $-CH_2R$ group is capable of rotation. This torsion angle, ψ, about the C(4')-C(5') bond is usually considered in terms of three possible minimum energy orientations [9]. These are for $\psi = 60^{o}$, 180^{o} and 300^{o} respectively, referred to as *gauche-gauche*, *gauche-trans* and *trans-gauche*. The angle ψ is defined by the clockwise rotation of the C(5')-R' plane relative to the C(4')-furanosyl-oxygen plane, about the C(4')-C(5') bond. These rotamers are shown by means of Newman projection in Figure 2.8.

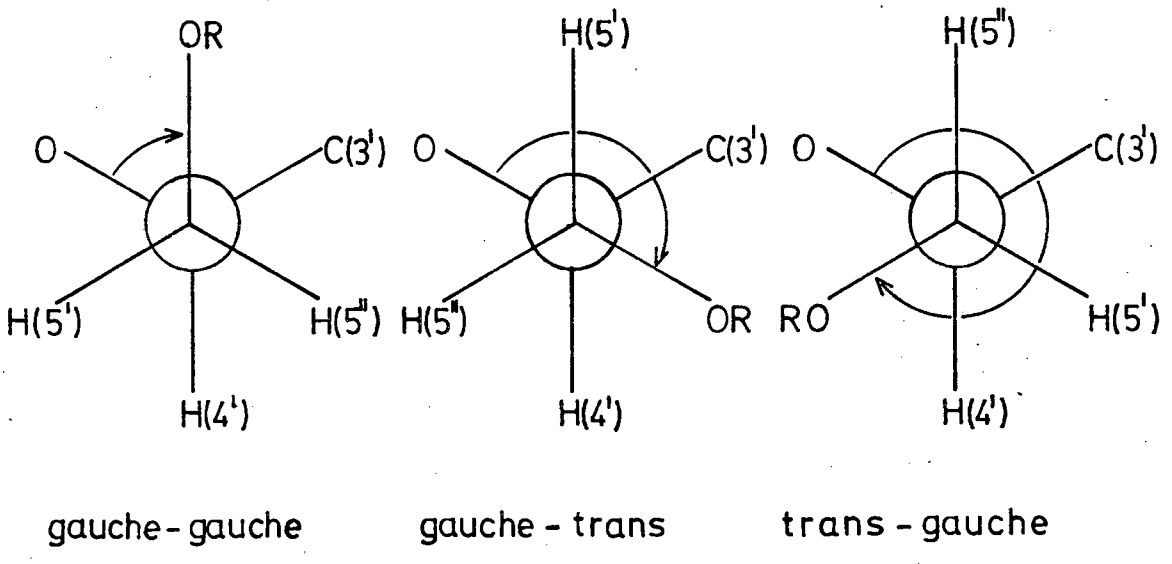

Figure 2.8: Possible rotamers about the C(4') - C(5') bond.

2.10 Preparation of $Ln(NO_3)_3.xH_2O$ Salts

Lanthanide oxides supplied by Rare Earth Products of 99.9% purity were dissolved in a slight excess of ANALAR grade HNO_3. The mixture was treated under reflux until clear, filtered and the acid lanthanide nitrate solution evaporated to dryness under reduced pressure. Addition of small portions of distilled water, followed by evaporation, was repeated until the pH of the lanthanide nitrate solution was *ca* 5.

In this way crystalline lanthanide nitrates of formula $Ln(NO_3)_3.xH_2O$ were obtained. Drying at 90°C under vacuum produced hygroscopic salts in various states of dehydration. Thus, where it was necessary to know the concentration of a $Ln(NO_3)_3$ solution, titration with standard ethylenediaminetetraacetic acid using xylenol orange as indicator proved satisfactory [51]. In general the value of x in the formation $Ln(NO_3)_3.xH_2O$ ranged from 2 to 6.

2.11 Preparation of $K[Ln(EDTA)(H_2O)_n]$ hydrates

10 mmol solid Ln_2O_3 was added to 50 cm^3 distilled water containing 25 mmol ethylenediamine-tetraacetic acid and 20 mmol KOH. The suspension was heated under reflux until a clear solution resulted. In most cases this occurred within a 0.5 to 3 hour period. The cool solution was filtered, the pH of the filtrate adjusted to *ca* 6.5 and excess water slowly evaporated until crystallisation occurred. Yields of between 60-90% were obtained. The salts were recrystallised from water, dried under vacuum, checked for purity by microanalysis as indicated in Table 2.1. Evidently these salts were almost completely anhydrous since crystals obtained from water contained from 4 to 6 water molecules.

Table 2.1: Microanalysis of $K[Ln(EDTA)(H_2O)_n]$ salts. (These salts were dried under vacuum prior to analysis).

$K[Ln(EDTA)(H_2O)_n].xH_2O$			FOUND			EXPECTED		
Ln	n	x	%C	%H	%N	%C	%H	%N
La	3	1	22.1	3.7	5.2	22.3	3.7	5.2
Pr	3	0	23.1	3.4	5.5	23.0	3.5	5.4
Eu	2	0	23.9	3.0	5.5	23.3	3.1	5.4
Gd	2	0	23.8	3.0	5.5	23.1	3.1	5.4
Dy	2	0	23.1	3.0	5.5	22.8	3.0	5.3
Ho	1	0	23.3	2.8	5.5	23.5	2.8	5.5
Er	1	0	23.4	2.8	5.4	23.4	2.7	5.5
Ub	1	0	23.3	2.8	5.4	23.2	2.7	5.4

2.12 Nuclear Magnetic Resonance Spectroscopy

Solutions of between 20 to 30 mM SAH and SAM were prepared with 99% ^2H_2O the pH adjusted with conc. ^2HCl or conc. NaO^2H solutions. The pH was measured using a Metrohm EA-125 microelectrode coupled to a Beckman Zero-matic SS-33 pH meter. The pH reading was corrected for an isotopic effect, by means of the relation actual pH = scale reading + 0.4. An uncertainty of ±0.1 pH unit is estimated. Weighed amounts of lanthanide nitrate and $K[Ln(EDTA)(H_2O)_n]$ salts were dissolved in known amount ^2H_2O. The solutions were saturated, while the pH was adjusted to *ca* 7.0 for the EDTA chelates and *ca* 5.5 for nitrate solutions.

^1H n.m.r. spectra were obtained using a Bruker WH -90DS spectrometer operating at 90 MHz in the Fourier Transformation mode. Spectra were measured at 308 K with sodium 3-trimethylsilyl propane-sulphonate (DSS) as internal reference. Measurements of the spin-lattice relaxation rate

were made using the 180^{o}-τ-90^{o} pulse sequence as described in section 2.7. Relaxation exhancements were measured as incremental amounts of K[Gd(EDTA)-$(H_2O)_2$] solution were added to the sample. At the end of each shift or relaxation experiment the pH was checked. Deviations of not greater than 0.2 pH unit from the initial pH value were observed.

Shift experiments were performed by adding µl amounts of the respective shift probe solution using Labora Mahnheim Capilettor micropipettes, to a aliquot of 0.5 cm^3 SAH or SAM solution.

250 MHz ^1H n.m.r. spectra were obtained on a Cameca 250 M Hz spectrometer at the Centre d' Etudes Nucleaires de Saclay in Gif-sur-Yvette, France where the simulated spectra were also produced.

PART I

CHAPTER III : RESULTS AND DISCUSSION

Lanthanide Shift and Relaxation Probes

RESULTS AND DISCUSSION

3.1 The ^1H n.m.r. spectra of S-adenosyl-L-methionine and S-adenosyl-L-homocysteine

S-adenosyl-L-homocysteine

The 90 and 250 M Hz spectra of SAH in ^2H_2O at pH 7.0 are shown in Figure 3.1. Included is the numbering scheme for SAH which is used throughout this work. At 90 M Hz the spectrum appears deceptively simple, coupling constants are poorly resolved and ribose proton resonances are partly obscured by the residual ^2HOH peak. The dramatic improvement of resolution at 250 M Hz is self evident.

Table 3.1 summarises the assignments for both SAH and SAM. In general for both these substances three regions of resonance are seen. The purine protons at low field, the ribose resonances in the 4 to 6 ppm range, while the homocysteine moiety protons resonate below 4 ppm relative to DSS. Assignments were based on proton-proton decoupling experiments. For example, irradiation with low R.F. power at the resonance centred at 2.14 ppm results in collapse of the triplet at 3.79 and 3.03 ppm to single peaks. From their relative intensities these were assigned to H(9') and H(5') , H(5") respectively.

The observations by Maeda [27] and Jardetzky [28] that H(8) in purine systems exchanges with deuterium, fascillitated assignment of the adenosyl protons. Heating SAH in ^2H_2O (pH 7.5) at 353 K for *ca* 2 hours resulted in an intensity drop of the resonance at 8.32 ppm of *ca* 50%. This was therefore assigned to H(8)

Table 3.1: The ^{1}H n.m.r. chemical shifts of SAH and SAM in $^{2}H_2O$ measured at 90 and 250 M Hz.

Conditions	Chemical Shifts / ppm relative to DSS											
	Purine[b]		Ribose[b]				Amino Acid[b]					
	H(2)	H(8)	H(1')	H(2')	H(3')	H(4')	H(5')	H(5'')	H(7'7'')	H(8'8'')	H(9')	Me
SAH, 90 M Hz pH 7.0	8.14	8.32	6.03	∿4.82	a	∿4.40	3.03		2.69	2.14	3.79	-
SAH 250 M Hz[c] pH∿6.5	8.26	8.35	6.08	4.86	4.43	4.34	3.07	3.00	2.71	2.14	3.82	-
SAM, 90 M Hz pH 7.0	8.26	8.26	6.08	∿4.93	a	a	3.93		3.53	2.31	3.77	2.95
SAM, 90 M Hz pH 3.4	8.37	8.37	6.12	∿4.84	a	a	3.92		3.54	2.34	3.78	2.95
SAM, 250 M Hz[c] pH∿3.0	8.49	8.47	6.19	4.90	4.65	4.63	4.06	3.97	3.60	2.41	3.61	3.02

a: obscured by residual ^{2}HOH resonance,
b: at 90 M Hz all shifts are ±0.002 ppm,
c: at 250 M Hz shifts were much more accurately measurable.

Figure 3.1: The numbering convention used and the 90 and 250 M Hz ^1H n.m.r. spectra of S-adenosyl-L-homocysteine.

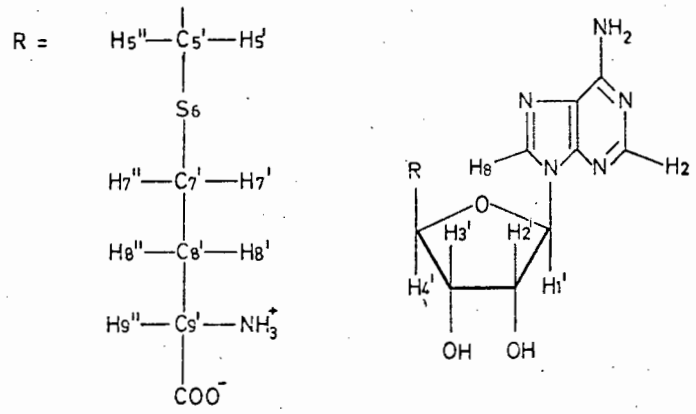

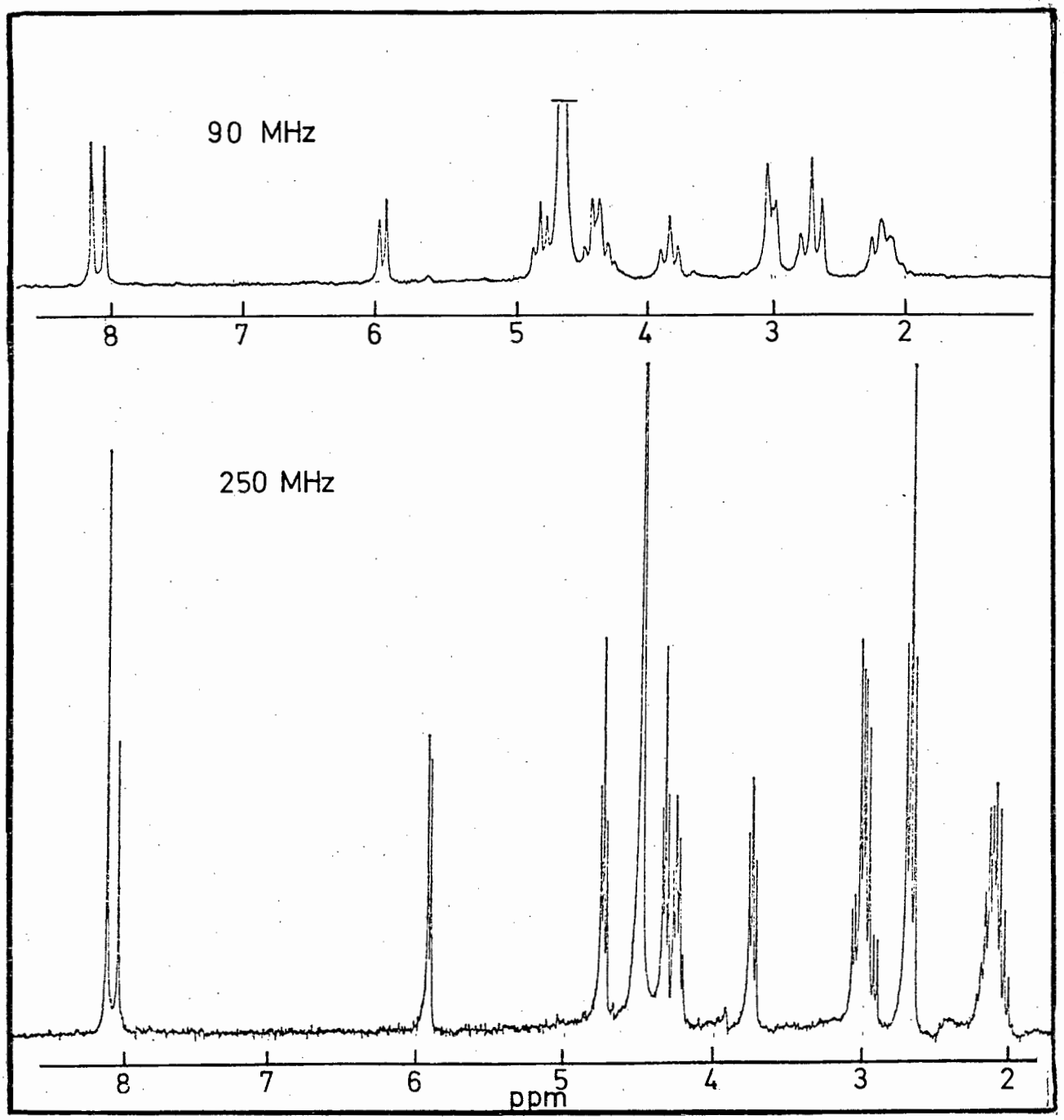

The ribose proton resonances were more readily assigned at 250 M Hz appart from the obvious H(1') resonance at 6.03 ppm. In general these were assigned by means of the coupling pattern observed and comparison with previously published work [37,67].

S-adenosyl-L-methionine

The 90 MHz spectrum as well as the numbering system employed in SAM, is shown in Figure 3.2. The spectra were recorded at pH 3.4 and 7.0. Evidently the solution is poor particularly so at pH 7.0. The work of Ramirez [15] suggests that SAM is expected to decompose rapidly in neutral to alkaline aqueous solution. Such behaviour is indeed observed as the pH exceeds 7.5 or if neutral solutions are kept for a few hours at room temperature.

In contrast to SAH, the H(2) and H(8) resonances are virtually coincident in the case of SAM and their chemical shift is pH dependent. This pH dependence may be understood in terms of protonation of the adenine moiety. The pK values of SAM and SAH have been measured previously [8]. The adenine pK value is estimated at 3.4 and 3.5 for SAM and SAH respectively, while the carboxyl and amino pK values are 1.8, 7.8 and 1.95, ≈9.2. Thus at pH 3.4, *ca* 50% of the adenine groups of SAM are expected to be protonated, while at pH 7.0 the adenine moiety is almost totally neutral. This explains the pH dependence of H(2) and H(8) in the case of SAM, while a similar trend is expected for SAH.

It should also be noted that for SAM, the sets of H(5'), H(5") and H(7'), H(7") protons are substantially deshielded relative to their corresponding resonance frequencies in the SAH. This is attributable to the electro-

Figure 3.2: The numbering convention used and the 90 M Hz ^{1}H n.m.r. spectrum of S-adenosyl-L-methionine.

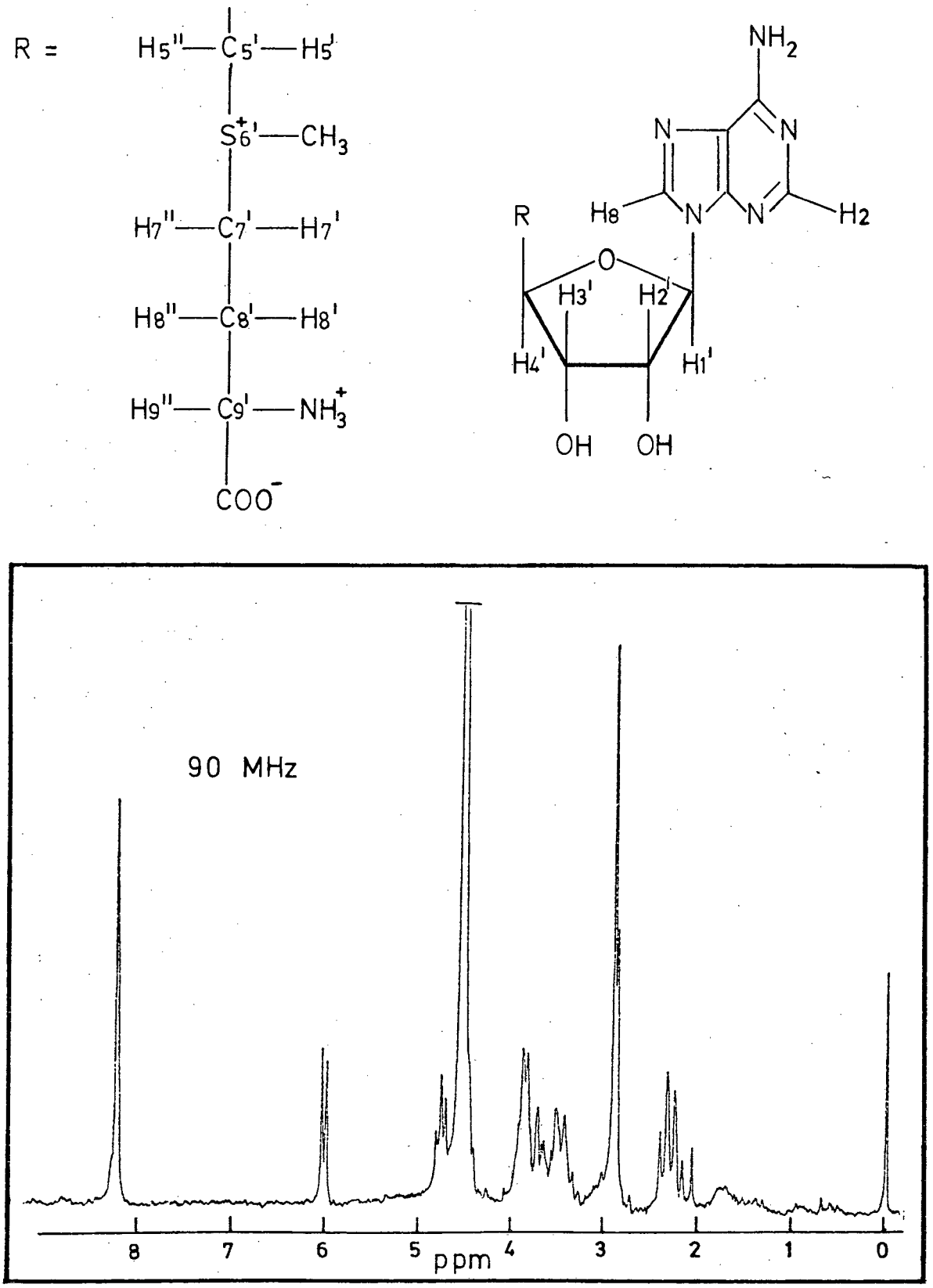

negativity of the positive sulphonium centre.

On the other hand the remaining resonance frequencies of SAM are approximately equal to the corresponding SAH values. Furthermore, the ribose, H(8'), H(8''), H(9') and methyl resonances of SAM are virtually pH independent in the range pH 3.4 - 7.0. Such behaviour is expected in view of the similar pK values of the amino acid terminus in both SAM and SAH. Also in both cases the zwitterionic forms of the amino acid moieties are expected to predominate in neutral to slightly acid solutions. The isoelectric point of methionine at 5.7 supports such a contention [29].

3.2 Gadolinium Induced Relaxation in S-adenosyl-L-homocysteine at 90 M Hz

Gadolinium does not measurably alter the chemical shifts of the SAH protons, but substantially shortens their respective relaxation times. Under conditions of fast chemical exchange the relaxation enhancement induced, $(T_{1M})^{-1}$, may be measured. Providing a unique, known metal binding site can be assumed, $(T_{1M})^{-1}$ data gives interpretable information about the molecular geometry of the metal complex. This follows from the proportionality of $(T_{1M})^{-1}$ to r^{-6}, where $\bar{r}$ is the internuclear metal to proton vector.

A second requirement for a successful conformational analysis is that the stoichiometry of the metal ligand complexes must be known. The case in which only a mononuclear 1:1 complex is formed is simplest to handle. In the present case a 1:1 complex is assumed, since only small amounts of gadolinium relative to SAH were required. Additionally, gadolinium was introduced as the potassium salt of $[Gd(EDTA)(H_2O)_3]^-$. Previous

workers have used lanthanoid EDTA chelates to ensure effective 1:1 stoichiometry [34,38].

It is difficult to obtain absolute values for the internuclear vector, r, as this requires a knowledge of the molecular correlation time τ_c. It is more usual to consider relaxation ratios from which relative internuclear distances may be obtained by means of equation (2.20).

It has been shown that $[Ln(EDTA)(H_2O)_n]^-$ anions form only 1:1 complexes with carboxylic acids [34]. Further, the known preference of the hard lanthanide ions for chelating oxygen ligands [35] renders it safe to consider that the carboxyl moiety of the methionine chain of SAH is the predominant binding site of the $[Gd(EDTA)(H_2O)_3]^-$ anion.

Incremental additions of a 5 mM solution of $K[Gd(EDTA)(H_2O)_3]$ at pH 7.0 to a 17 mM solution of SAH resulted in proton relaxation enhancement data given in Table 3.2. These data were obtained as outlined in section 2.7.

Figure 3.3 shows a linear plot of $(T_{1p})^{-1}$ against f, the gradient of each line giving a particular value of $(T_{1M})^{-1}$. It should be noted that the reference, DSS, also shows a slightly increased relaxation rate, in the presence of gadolinium. This is presumably due to outer-sphere relaxation and/or bulk magnetic susceptibility changes. $(T_{1M})^{-1}$ values given in Table 3.2 have been 'corrected' for such effects by substraction of the $(T_{1M})^{-1}_{reference}$ term which was always smaller than 10% of any $(T_{1M})^{-1}$.

Using a chemically reasonable Ln-O distance of 0.25 ± 0.01 nm, based upon crystallographic data [30-33], Dreiding scale models produced an average

Figure 3.3: A linear plot of $(T_{1p})^{-1}$ against f for gadolinium induced spin-lattice relaxation data for 17 mM SAH at pH 7.0 (308K).

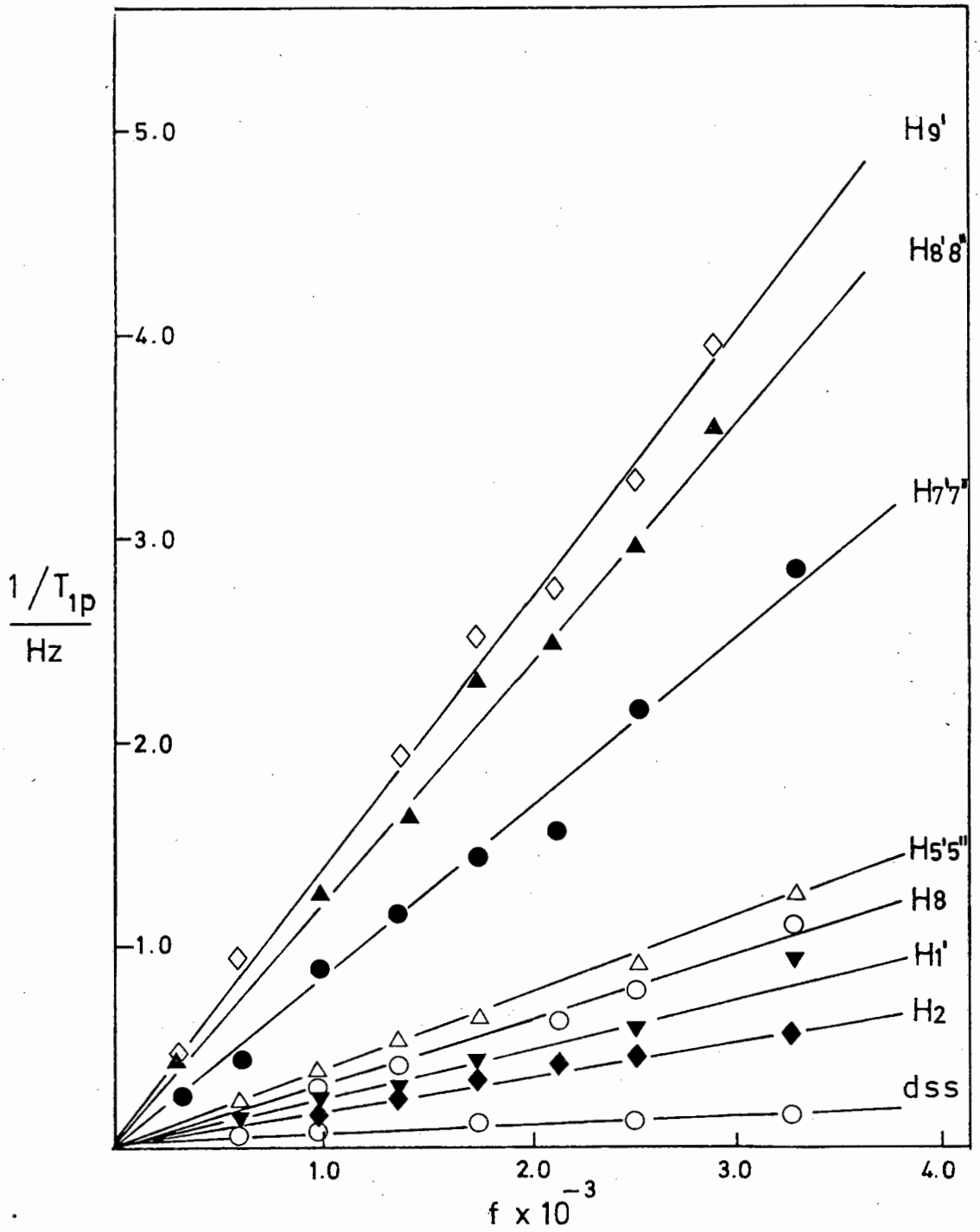

Table 3.2: Gadolinium induced spin-lattice relaxation data for 17 mM SAH at pH 7.0 (308K).

Parameter	H(9')	H(8',H8'')	H(7',7'')	H(5',5'')	H(1')	H(8)	H(2)
(T_{1M}^{-1})/Hz	1255	1081	262	675	217	293	209
$[T_{1M})_{H(9')}/(T_{1M})_{Hi}]^{-\frac{1}{6}}$	1.00	0.98	0.77	0.90	0.74	0.79	0.77
$(r_{H(9')}/r_{Hi})_{calc}$	1.00	0.98	0.77	0.91	0.74	0.80[a]	0.75[a]
$(r_{Hi})_{calc}$/nm	0.48	0.49	0.62	0.53	0.65	0.60[a]	0.64[a]

a: based upon a 75% *anti* conformation of the adenine moiety.

Gd to H(9') distance of 0.48 ± 0.02 nm. This distance is fixed in the metal complex of SAH, and thus all relaxation data are normalized on $(T_{1M})^{-1}_{H(9')}$. Similarly, the relative internuclear distances were calculated using equation (2.20) for any possible conformation. If the ratios $(r_{H(9')}/r_i)_{calc}$ for various r_i values (corresponding to the metal-proton i internuclear distances) are equal to the experimentally determined relxation ratios, $[T_{1M})_{H(9')}/(T_{1M})_{Hi}]^{-\frac{1}{6}}$, then the model conformation used to obtain $(r_{H(9')}/r_i)_{calc}$, may be considered a representation of the metal-bound solution conformation of SAH. Table 3.2 lists the values of r_i for which best agreement between the calculated internuclear distance ratio and experimentally found $[(T_{1M})_{H(9')}/(T_{1M})_{Hi}]^{-\frac{1}{6}}$ ratio is obtained.

Inspection of the r_i values in table 3.2 shows that H(9') and the two methylene protons H(8'), H(8'') are almost equidistant from the metal ion. The same is true for the H(7'), H(7'') and H(1') protons being situated at 0.62 nm and 0.65 nm respectively, from the metal ion. Unfortunately no data for any

other ribose protons could be obtained due to their close proximity to the comparatively large ^{2}HOH resonance.

The purine protons H(8) and H(2) could not be interpreted by a single orientation of the purine moiety with respect to the metal ion center. The $(T_{1M})^{-1}$ data was however interpreted by considering a dynamic equilibrium between the *syn* and *anti* orientations of the purine ring. Such an equilibrium has been used previously to understand relaxation behaviour of a number of simple nucleotides [36]. Application of equation (2.23) yielded time average values of $r_{H(8)}$ and $r_{H(2)}$ based upon a 75% *anti* time average conformation.

Since no relaxation data is available for the ribose protons H(2'), H(3') and H(4') the question of what conformation the ribose ring assumes cannot be satisfactorily answered. The rigid nucleotide concept favours strongly only two ribose ring conformational states, *viz.* the C(3')-*endo* (^{3}E) or the C(2')-*endo* (^{2}E) state [37]. It is clear that interconversion between these two extremes may result in a variety of intermediate ribose nuclear conformations. It is therefore not unreasonable to consider the solution conformation to be neither purely ^{3}E nor purely ^{2}E, but may be best described as a rapid equilibrium $^{2}E \rightleftharpoons {}^{3}E$. Nevertheless, it was found that with the purine ring in the *anti* conformation, the best agreement between calculated distance ratio and observed relaxation ratio is obtained with the ribose ring in the ^{3}E pucker. The limitations of the relaxation data in determining a more detailed ribose ring conformation were overcome by means of coupling constant data from ^{1}H n.m.r. spectra observed at 250 M Hz. These results will be presented at a later stage in this work.

3.3 Lanthanide Induced Shifts at 90 M Hz and the Conformation of S-adenosyl-L-homocysteine

Titration of a 25 mM solution of SAH in 0.2 M aqueous $La(NO_3)_3$ at pH 6.5 with 1 M $Pr(NO_3)_3$ gave rise to reproducible shifts in the resonances of the ^1H n.m.r. spectrum of SAH. A plot of these shifts as a function of the mole ratio, f (Pr^{3+}:SAH), is shown in Fig. 3.4. It is evident that the shifts tend to level off as f exceeds unity, suggesting that only 1:1 Pr^{3+} SAH complexes are formed and that La^{3+} is in effective competition with Pr^{3+} with regard to binding SAH.

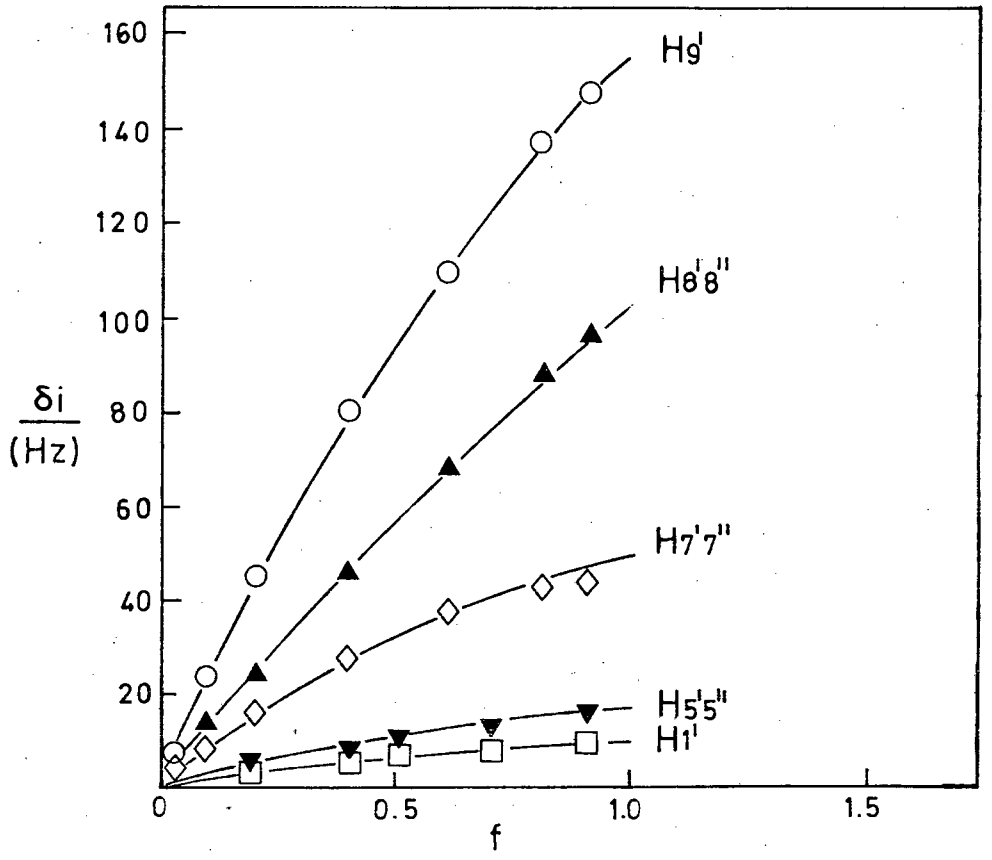

Figure 3.4: A plot of shifts induced by Pr^{3+} in SAH.

It was however decided to use the $K[Ln(EDTA)(H_2O)_n]$ (n = 2,3) salts as shift probes in preference to the aquo Ln(III) ions, exploiting the following advantages:

(i) Above pH 6 Ln(III) ions are known to participate in hydrolysis reactions, resulting in $Ln(OH)_3$ precipitates (log K_{so} = -19.0 for lanthanum to log K_{so} = -23.7 for lutetium). [35,38,39]

(ii) It has been shown that the $[Ln(EDTA)(H_2O)_n]^-$ anion binds deprotonated carboxylic acid groups forming only 1:1 complexes [34,38].

(iii) The pH range in which the EDTA chelates are useful shift probes is approximately 3-8.

(iv) Using 0.2 M $La(NO_3)_3$ as a source of 'background' La^{3+} ion to inhibit higher order metal-SAH complexes results in a solution of ionic strength of *ca* 1.2. To be able to compare shift and relaxation data, it is desirable to maintain as uniform a set of conditions as possible. Furthermore since the formation constants of the Ln^{3+} ions/SAH system are unknown it is impossible to state categorically that only 1:1 complexes are formed even in the presence of the high buffering concentration of La^{3+}.

Titrating 26 mM SAH solutions with a saturated neutral solution of the salt, $K[Ln(EDTA)(H_2O)_n]$ (n = 2,3) where Ln = Pr, Dy, Er and Yb results in the shift ratios tabulated in Table 3.3. The shifts are all normalised onto the H(9') resonance (which shifted most). For comparison with the shifts induced by the praseodymium ion (Fig. 3.4), the shifts induced by the chelate $[Pr(EDTA)(H_2O)_3]^-$ are shown in Fig. 3.5.

In addition to the paramagnetic lanthanide shift induced, further diamagnetic shifts may be induced at a particular proton. The magnitude of this diamagnetic contribution generally alternates rapidly with increased distance

Table 3.3: Observed lanthanide induced shifts normalized on H(9') for SAH (26 mM) in ^2H_2O at pH 7.0 and 308 K.

Observed proton(s)	Lanthanide shift ratios extrapolated to infinite dilution Pr/La[a]	Pr(EDTA)	Dy(EDTA)	Er(EDTA	Yb(EDTA)
H(9')	1.00	1.00	1.00	1.00	1.00
H(8') H(8'')	0.58	0.58	0.58	0.62	0.56
H(7') H(7'')	0.34	0.37	0.44	0.38	0.38
H(5') H(5'')	0.18	0.12	0.24	0.18	0.15
H(1')	0.02	0	-0.03	-0.03	-0.12
H(4')	b	0.15	b	b	b
H(2) obsd.	0.03	c	-0.05	-0.01	-0.08
H(8) obsd.	0.03	c	-0.03	-0.10	-0.14

a: Titration in the presence of 0.2 M $La(NO_3)_3$.

b: Not resolved from residual ^2HOH resonance.

c: Unreliable data through interference from Pr(EDTA) resonance.

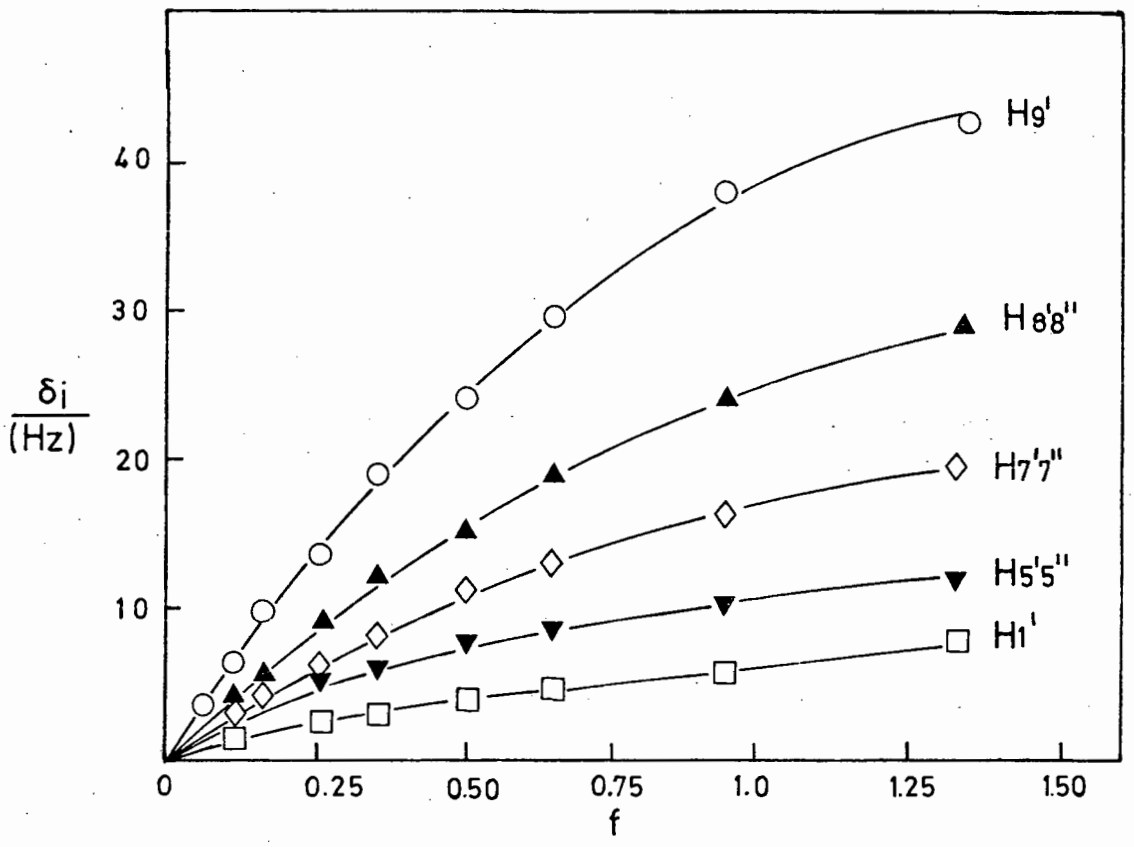

Figure 3.5: A plot of shifts induced by $[Pr(EDTA)]^-$ in SAH.

from the metal ion and is generally small. It may however be estimated from the resonance shifts that $[La(EDTA)(H_2O)_3]^-$ induces. In all cases these were found to be negligibly small, but in the event of these being significant, the paramagnetic shift induced may be approximated by means of the relation $\delta_{para} = \delta_{obs} - \delta_{dia}$.

Reference to table 3.3 shows that for the purine and ribose protons generally very small shifts are induced. This implies that protons H(8), H(2), and H(1') (as well as other ribose protons H(2'), H(3'), H(4') are either very far from the paramagnetic centre or they lie on or near

the surface of a cone which subtends an angle of $54^{o}44'$ with the principal magnetic symmetry axis. This follows by inspection of equation (2.18) which tends to zero as $r \to \infty$ or as $\theta \to 54^{o}44'$.

The gadolinium relaxation data clearly precludes any assertion that the lanthanide nucleus lies a very large distance from the adenosyl and ribosyl protons. This fact considerably restricts the locus of the paramagnetic centre relative to the protons of SAH.

Isomorphous substitution of various lanthanide shift probes should result in shift ratios independent of the particular lanthanide ion *only* if two conditions are satisfied:

(i) the shift is pseudo-contact in origin (i.e. contact contributions are negligible).

(ii) the symmetry of the complexed lanthanide ion is effectively axial.

The excellent agreement between the various shift ratios as given in Table 3.3 convincingly support the conclusion that both criteria (i) and (ii) are satisfied for at least Pr, Dy, Er and Yb. Unfortunately very small shifts as well as severe line broadening limited the shift experiments to the four lanthanides already mentioned. Ideally as many as possible lanthanides should be used to test for the validity of the conditions outlined above.

Based upon the gadolinium relaxation data, the lanthanide nucleus was 'placed' such that the carboxyl group of SAH occupied two of the remaining coordination sites of the lanthanide EDTA chelate. It may be recalled that the mean Ln-O distance used previously was 0.25 ± 0.01 nm, and

consequently the Ln-H(9') distance is fixed at 0.48 ± 0.01 nm. This allows relative shift ratios to be calculated using equation (2.19) for the various possible conformations. Relaxation data indicate that H(8') and H(8'') lie close to the paramagnetic centre. For this to be compatible with their observed shift data the effective magnetic symmetry axis must lie along the C(10')-C(9') bond, bisecting the $\hat{OCO}$ angle of the carboxyl moiety. This is illustrated in Fig. 3.6.

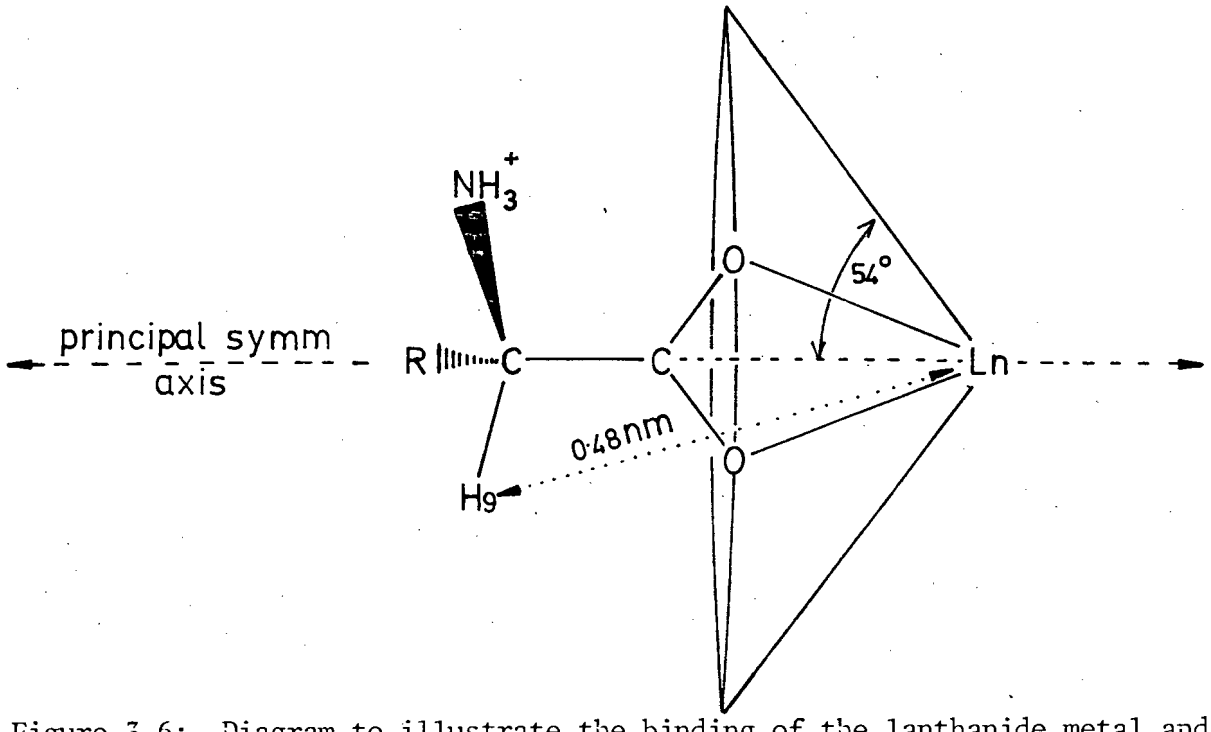

Figure 3.6: Diagram to illustrate the binding of the lanthanide metal and the direction of the principal symmetry axis.

In searching for the 'best-fit' conformation the objective was to minimise the difference between the observed, R_{obs}, and calculated shift ratios, R_{calc}, whence the parameters θ_i and r_i for the i-th proton were obtained.

The various staggered rotamers about the C(9')-C(8') bond were first considered. The agreement between R_{obs}- and R_{calc} was thus optimized taking

into account the relaxation data. Next the possible rotamers about the C(8') - C(7') bond were examined and, in turn, the possible configurations about the S(6') - C(5') bond. In this way the conformation of the homocysteine chain of SAH was established.

The next step was to relate the homocysteine moiety with the adenosyl portion of the molecule. Unfortunately the shift data for the ribose protons H(2'), H(3') and partly H(4') is incomplete (because of a large residual ^{2}HOH solvent resonance and small absolute shifts induced). The shift and relaxation data for H(1') and the purine protons, H(2) and H(8) made it possible to establish a unique locus for the paramagnetic ion and thus define the average solution conformation of SAH. Relaxation rates for H(2) and H(8) (c.f. Table 3.2) indicate a dynamic equilibrium between the *syn* and *anti* orientations of the purine system. The *anti* conformation is favoured by 75 ± 10%. The shift data is found to be compatible with this distribution between the *syn* and *anti* configurations. It appears that H(2) and H(8), in both the *syn* and *anti* orientations of the base, lie near the surface of the 54^{o} 44' cone. This is reflected in the small shifts as well as the fluctuation in sign of the induced shift ('inside' the cone all protons are shifted in the same relative direction i.e. up-field or downfield, while those protons 'outside' the cone are shifted in the opposite direction to those 'inside'). The best agreement between R_{obs} and R_{calc} for the purine protons as well as for H(1') resulted from a ^{3}E ribose pucker conformation in which the base lies *anti* with $\phi_{CN} = -45^{o}$. When considering the *syn* purine orientation the best results were obtained with the furanose ring in approximately an ^{2}E conformation while $\phi_{CN} = 130^{o}$. However due to the insensitivity of these shifts to changes in Θ_i and r_i, the detailed conformation of the ribose ring could

not be verified, and 250 M Hz coupling constant data was resorted to.

Table 3.4 lists the values of θ_i and r_i for which best agreement between R_{calc} and R_{obs} is found. These parameters thus define the average solution conformation of SAH bound to a $[Ln(EDTA)]^-$ chelate. Comparison

Table 3.4: The observed and calculated shift ratios for SAH and the corresponding θ_i and r_i values

Observed proton(s)	Average observed Ln(EDTA) shift ratio[a]	r_i calc./mm	θ_i calc./ degrees	Calc. shift ratio
H(9')	1.00	0.48	11	1.00
H(8')	0.59	0.51	25	0.62[b]
H(8'')		0.51	25	
H(7')	0.39	0.68	10	0.34[b]
H(7'')		0.71	14	
H(5')	0.17	0.62	39	0.18[b]
H(5'')		0.76	40	
H(1')	-0.06	0.67	60	-0.05
H(4')	0.15	0.74	36	0.13
H(2)	-0.05			
anti		0.68	83	
syn		0.79	60	
75% anti[c]				-0.08
H(8)	-0.09			
anti		0.63	59	
syn		0.57	71	
75% anti[c]				-0.13

a: average from data in table 3.3. b: Average for pairs of geminal protons.
c: Anti $\phi_{CN} = -45^o$, syn $\phi_{CN} = +130^o$.

of the relative internuclear distances predicted by the Gd(III) relaxation enhancement and the corresponding shift data shows that overall agreement between experimental and predicted shift ratios is excellent.

Fig. 3.7 shows a computer generated diagram depicting the conformation of SAH for which the θ_i and r_i values have been defined in Table 3.4. Only the *anti*/^{3}E conformation is shown.

Examination of the conformation obtained shows that SAH is not extended, but that the methionine moiety is in such a position that interaction between the EDTA chelate and the purine ring cannot be ruled out. Such interactions might well take the form of hydrogen bonding between the amine group of the purine ring and a carboxylate oxygen atom of EDTA; alternatively there may simply be an electrostatic interaction between a partially protonated purine ring (pK of base = 3.5) [8] and the negative charge of the lanthanide EDTA chelate.

In any event, it appears that the torsion angle $\phi_{C(4')-C(5')}$ lies predominantly in the *trans-gauche* range with an angle of *ca* 300^o. The C(3')-C(4')-C(5')-S atoms thus lie approximately on a plane.

Consideration of the rest of the homocysteine chain shows that the torsion angle $\phi_{C(7')-C(8')}$ is such that a staggered rotamer, in which H(7'')H(7') and H(8')H(8'') are *anti* with respect to each other, is favoured. A staggered conformation about the C(8') and C(9') bonds is also observed such that the atoms C(7')-C(8') C(9')-C(10') lie approximately on a plane. Such staggering is not entirely unexpected in view of a crystal structure determination of L-methionine [56]. The unit cell of a crystal of L-methionine

Figure 3.7: The proposed conformation of the S-adenosyl-L-homocysteine [Ln(EDTA)] complex.

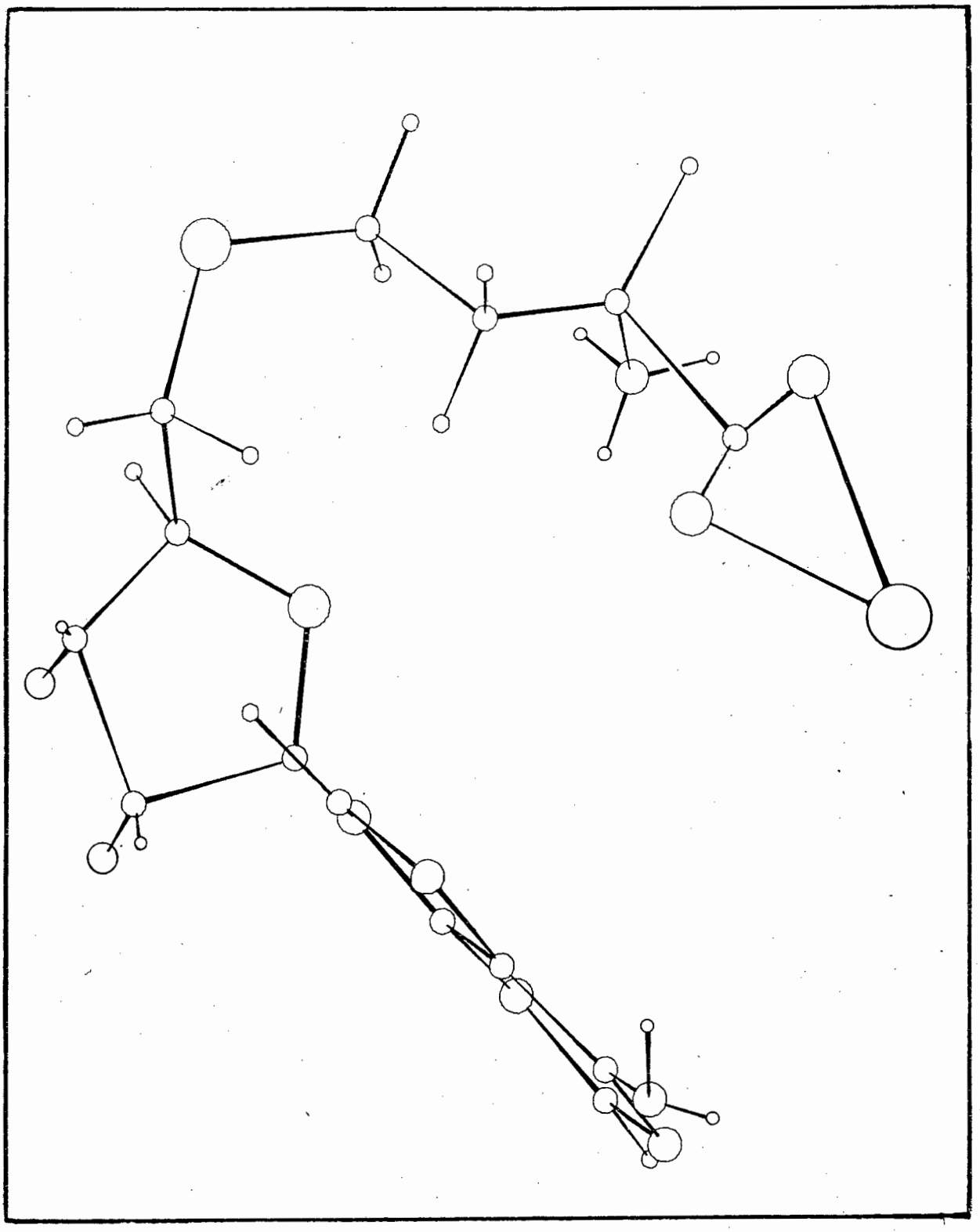

was found to contain two independent molecules A and B, in which A was completely extended with a *trans* conformation about C(1)-C(2), C(2)-C(3) and C(3)-S bonds (numbering the carboxyl carbon atom C(1), and so on). The B molecule of L-methionine was found to assume a *trans*, *gauche* and *gauche* conformation for the corresponding bonds of molecule A.

Comparing the homocysteine moiety of SAH to molecule A of L-methionine it may be seen that two differences in conformation occur (i) the torsion angle about the C(5')-S(6') bond in SAH is estimated to be 120 ± 10° in contrast to the corresponding vaue of 174.2° in L-methionine and (ii) in L-methionine the atoms N(1), C(2), C(3) and C(4) form a plane, while in SAH the carboxyl atom, C(10'), has taken the place of the nitrogen atom in the plane so defined. Refer to Figure 3.8.

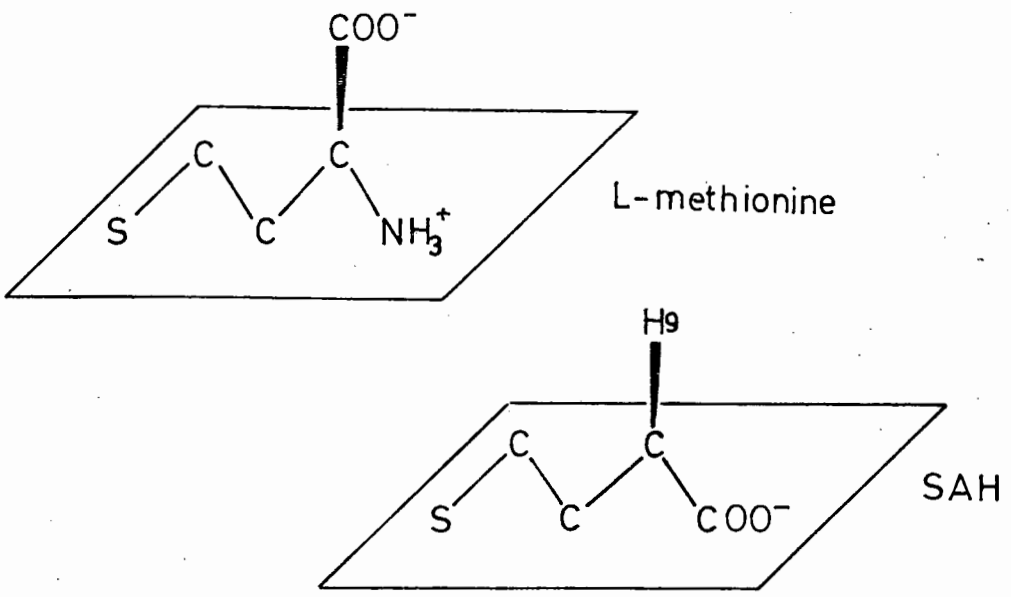

Figure 3.8: A comparison of the conformations of L-methionine (after [56]) and SAH as deduced in this work.

3.4 Some Preliminary Observations on the Effect of Shift Reagents on S-adenosyl-L-methionine

It will be recalled that in the case of SAH, the primary binding site of a lanthanide cation was found to be the carboxyl moiety. This was found to be so irrespective of whether an aquated ion or an EDTA chelate was used; ostensibly the latter binds less strongly to the carboxyl group.

Preliminary titrations of solutions of SAM with solutions of dysprosium and praseodymium nitrate produced negligible shifting of all resonances, but served only to cause further loss of overall resolution. The pH of the solution did not seem to affect these observations. Such results point to a blocking of the carboxyl group to lanthanide ion coordination. In view of the comparable carboxyl acidities of SAH and SAM, the absence of binding of a hard lanthanoid cation to SAM is surprising. Considering the structure of SAM, it becomes tempting to postulate some form of *intramolecular* interaction, so rendering the carboxyl moiety unavailable for coordination. Mudd and Klee [8] have suggested that there are ample possibilities for hydrogen-bond formation in which the COO^- and ribosyl hydroxy groups might be involved. In view of the similarity of the carboxyl pK values of SAH and SAM however, these authors considered strong electrostatic interactions between the cationic sulphonium centre and the anionic carboxyl group highly unlikely.

On the other hand, Mazza *et al* [17] have shown that van der Waal's potential energy calculations favour a cyclic conformation of S-methyl-L-methionine. The calculations point to a pseudo-ring formation in which coulombic interactions between the carboxyl group and sulphonium moiety is postulated. Such a cyclic conformation would serve to explain the rapid degradation of

SMM salts in alkaline solutions as observed by Ramirez [15].

In the light of the above, it may be expedient to compare the pK values of SAH and SAM here briefly. Table 3.4 shows pK values as measured by Mudd *et al* [8].

Table 3.4: pK values for SAM, SAH and their methyl analogues (after Mudd [8]).

Compound	pK values		
	-COOH	$-NH_2$	adenine
S-adenosyl-L-methionine	1.8	7.8	3.4
S-adenosyl-L-homocysteine	1.95	a	3.5
L-methionine	2.2	9.2	-
S-methyl-L-methionine	1.9	7.9	-

a : not measured (all values ± 0.1).

It is not unreasonable to expect the amino pK of SAH to be close to 9.2. The difference in pK is remarkable, especially considering the similarity of the other pK values. It may be seen that the charged sulphonium group in SAM (and S-methyl-L-methionine) is 4 bonds separated from the amino acid terminus. The increased electronegativity of the sulphur atom is observed to affect significantly only the two immediately adjacent groups of atoms as seen from the ^1H n.m.r. chemical shifts of SAM and SAH. (Table 3.1). Only H(7'), (7'') and H(5'), (5'') are deshielded in SAM relative to SAH. The H(9') proton resonates at a very similar frequency in both SAM and SAH. It is thus difficult to account for the relatively large difference

in amino pK values in terms of inductive effects.

The low bascity of SAM amino group may be accounted for by postulating an electrostatic interaction between the COO^- and S^+ moieties. Such an interaction is expected to predominate above pH 3. At the lower end of this range all the amine groups would be protonated, while a significant fraction of the carboxyl moieties would also be protonated. This state of affairs would tend to disfavour the postulated coulombic interaction between the S^+ and COO^- groups. On the other hand, as the pH is raised one might expect the interaction to become increasingly predominant and reach a maximum above the isoelectric point of the amino acid terminus of SAM. A balance between attractive forces of the two oppositely charged poles and repulsion between the anionic poles (S^+ and NH_3^+) would thus determine the extent of postulated electrostatic interaction. By such a mechanism one might expect an early deprotonation in SAM as compared with SAH. These conclusions are at variance with those of Mudd and Klee [8] who considered the "relatively normal" pK values of the carboxyl group as evidence against cyclic electrostatic interactions of S^+ and COO^-. However, at the pH where the COO^- pK values are measured, such electrostatic interactions are expected to be least favourable, and thus not expected to be reflected significantly in the COO^- pK values. It is misleading to consider the above variations in the pK values in isolation and caution must be excercised in infering conformational data from such measurements.

The above arguement must not be regarded as an *a priori* proof of the postulated electrostatic interactions in molecules like SAM, but rather as possible consequences of such interactions if these can be shown to exist. In any event, the important point is that SAM does not show any

affinity to bind lanthanide anions, but as might be expected, cations such as $[Fe(CN)_6]^{3-}$ and $[Ln(EDTA)(H_2O)_n]^-$ do affect the chemical shifts of SAM proton resonances significantly. Such interactions are postulated to occur by an ion-pairing mechanism.

Reuben and Elgavish [52] have observed ion-pairing interaction between substituted ammonium cations and lanthanide EDTA chelates and noted in general a capacity of the $[Ln(EDTA)(H_2O)_n]^-$ anions to serve as shift reagents for organic cations in solution.

3.5 Gadolinium Induced Relaxation in S-adenosyl-L-methionine at 90 M Hz.

Reference to Figure 3.2 shows that at both pH 3.4 and 7.0 the H(2) and H(8) resonances of SAM are virtually coincident. To achieve meaningful relaxation data for these two protons it was necessary to separate these resonances by means of a suitable shift reagent. It was found that the most effective paramagnetic reagent was potassium ferricyanide. The symmetrical $[Fe(CN)_6]^{3-}$ anion is expected to ion pair fairly strongly with positively charged centres on SAM. It may be recalled that Fe(III) is a class 2 paramagnetic ion and thus does not significantly broaden the line widths. Figure 3.9 shows the 90 M Hz spectrum of SAM with varying amounts of 1M $K_3[Fe(CN)_6]$ ^2H_2O solution. Evidently satisfactory separation of the overlapping H(2) and H(8) resonances is achieved, with little line broadening. A slight simplification of the overlap in the 3-4 ppm range is also observed, the optimum concentration of ferricyanide being *ca* 7 mM.

In order to assign the two separated low field resonances, solutions at

Figure 3.2: The 90 M Hz ^{1}H n.m.r. spectra of SAM with varying amounts of 1 M $K_3[Fe(CN)_6]$ in $^{2}H_2O$.

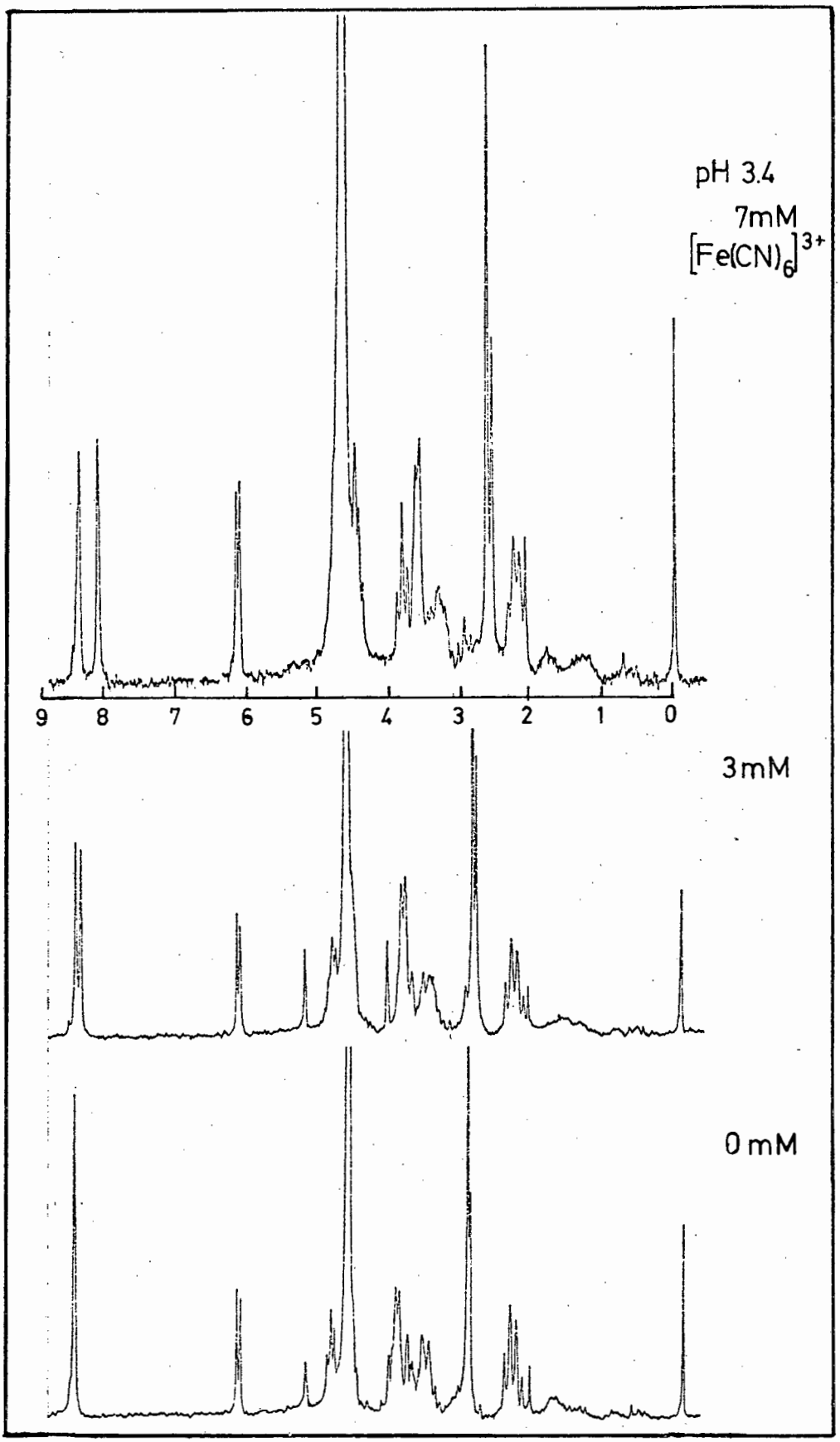

pH 7 and 3.4 were kept at 335 K for several hours. The lowest field resonance decreased in relative intensity, and was accordingly assigned to H(8).

The $(T_{1M})^{-1}$ relaxation rates of SAM were thus measured by titration with $K[Gd(EDTA)(H_2O)_3]$ in the usual fashion at pH = 3.4, and are summarized in Table 3.5. Because SAM is much more stable at low pH, relaxation experiments were carried out only at pH 3.4. Since these experiments are time consuming, significant decomposition is thus avoided. Shift experiments were however carried out at pH 3.4 and pH 7.0, (see below).

Table 3.5: Relaxation data of the protons of 25 mM SAM at pH 3.4 (308K) in the presence of 7 mM $[Fe(CN)_6]^{3-}$

Parameter	H(9')	H(8',8'')	H(7',7'')	H(5',5'')	CH_3	H(1')	H(8)	H(2)
$(T_{1M})^{-1}$/Hz	595	918	1630	400	517	156	335	215
$[(T_{1M})_{H(9')}/(T_{1M})_{Hi}]^{-\frac{1}{6}}$	1.00	1.07	1.18	0.94	0.98	0.80	0.91[a]	0.84[a]
$(r_{(H9')}/r_{Hi})_{calc}$	1.00	1.04	1.13	1.04	0.86	0.79	0.91[a]	0.91[a]
$r_{Hi\ calc}$/nm	0.75	0.72[b]	0.66[b]	0.72[b]	0.87	0.95	0.82	0.82

a average values based upon 60% *anti* conformation,

b average values for pairs of protons not independently resolvable at 90 M Hz.

Since it is not possible to assume a well defined binding site in the case of SAM, the task of interpreting the relaxation data given in Table 3.5 was formidable. It is observed that the H(7',7'') set of methylene protons

relax most rapidly in the presence of $[Gd(EDTA)(H_2O)_3]^-$. This in itself rules out any direct coordination of the carboxyl group (compare SAH relaxation data, Table 3.2). In order to obtain conformational information from the $(T_{1M})^{-1}$ data, the relaxation rates were normalized onto the $(T_{1M})^{-1}$ value for H(9'), and the $[(T_{1M})_{H(9')}/(T_{1M})_i]^{-\frac{1}{6}}$ ratio computed. For any value of the internuclear metal to H(9') vector, one may then calculate relative distances to all observed protons. To simplify matters a Drieding model of SAM was placed in a similar conformation to that found for SAH as a first approximation. A further postulate that the carboxyl moiety lies near the charged sulphonium centre was made. An appropriate Drieding for the $[Gd(EDTA)(H_2O)_3]^-$ chelate was then 'placed' in the most likely ion-pairing site. This site was chosen so that the locus of the metal ion was such as to produce best agreement between calculated and observed relaxation ratios.

Three possible ion-pairing sites were considered (i) the sulphonium centre (ii) the protonated amino group and (iii) the protonated adenine moiety. At pH 3.4 the adenine moiety is expected to be *ca* 50% protonated, while the fraction of amino groups protonated, is unity. The carboxyl groups are considered to be almost completely deprotonated. It is believed that N(1) is the predominant protonation site in the adenine moiety [57]. Inspection of the relative relaxation rates for the various protons of SAM in Table 3.5 shows that H(2) and H(8) relax relatively slowly in the presence of $[Gd(EDTA)(H_2O)_3]^-$. Furthermore, the methionine chain protons relax much more rapidly, suggesting a greater relative proximity of these protons to the paramagnetic centre. On this basis, as well as control shift experiments (see below), ion pairing with the protonated adenine moiety is considered negligible.

A tedious search finally produced a metal locus which yielded values of $(r_{H(9')}/r_{Hi})_{calc}$ most consistent with the experimental relaxation ratios (c.f. Table 3.5). Considering the magnitude of the problem, the agreement so found is gratifying. Although agreement is not perfect, it is believed to be good if it is remembered that no fixed coordination site of metal is postulated. The largest difference between experimental and calculated relaxation ratios is *ca* 12.5%, which means an uncertainty of about 1 in 8 nm in internuclear distance for the metal to the S-methyl group protons.

It is found that the gadolinium nucleus lies approximately equidistant from the sulphonium and protonated amino poles, *ca* 7.5 nm from H(9'), above the proposed cyclic ring formed by the methionine moiety. The conformation of this ring is found to be the chair conformer, with the amino group equatorially placed. Figure 3.10 shows such interactions diagramatically.

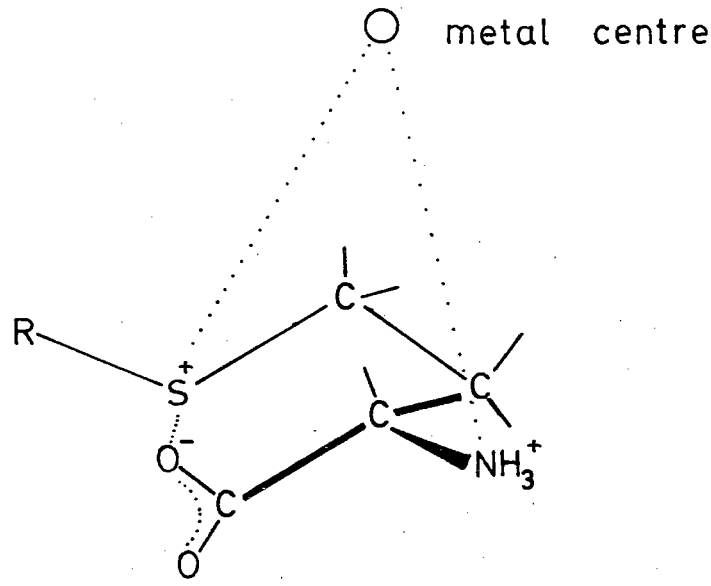

Figure 3.10: Diagramatic representation of the locus of the metal with respect to the proposed pseudo-cyclic conformation of SAM.

It cannot be established whether the gadolinium chelate ion-pairs with only the sulphonium or amino pole, or whether a rapid equilibrium between these two sites exists. Nevertheless the experimental relaxation data can only be accounted for if the metal is placed as described above, and one postulates a 'cyclization' of the methionine moiety. In this conformation the similarity of relaxation of H(2) and H(8) are considered to suggest that no unique conformation about the glycosidic C(1')-N(9) bond exists, but that a rapid equilibrium between *syn*/^{2}E and *anti*/^{3}E exists. Application of equation (2.23) favours the *anti* conformation over the *syn* by 6:4. This estimate must however be considered in the light of the uncertainty of the locus of the gadolinium nucleus. The most favourable torsion angle, ϕ_{CN}, is found to be *anti* - 25^o and *syn* 145^o.

The question the ribose ring conformation is difficult to settle based only on the above relaxation data, since as in the case of SAH, the ribose protons were severely obscured by the redual solvent resonance. The experimental and calculated relaxation ratios of H(1') show good agreement if the ^{3}E ribose pucker is used for the *anti* base position while the ^{2}E pucker is suggested if the base is *syn*. However, consideration of the proposed model shows that the relative H(1') distances for the ^{3}E and ^{2}E puckers is not very different, and thus using only relaxation data for H(1') does not reliably estimate the ribose ring conformation. This must be established by other means and an attempt has been made to utilize 250 M Hz ^{1}H n.m.r. data, from which geminal and vicinal coupling constants can be measured. These results will be presented below.

3.6 Lanthanide Induced Shifts at 90 M Hz and the Conformation of S-adenosyl-L-methionine

Titration with various $[Ln(EDTA)(H_2O)_n]^-$ cations showed that small but reproducible shifts were induced for SAM at both pH 3.4 and 7.0. Unfortunately the small absolute shifts induced, as well as severe loss of resolution (due to some unavoidable broadening induced by lanthanides) limited reliable shift results to only Pr, Dy, and Yb. These shift results are presented in Table 3.6, while the shifts induced by $[Dy(EDTA)(H_2O)_3]^-$ are plotted against f in Figure 3.11.

It may be observed that overall agreement between shifts induced is poor, particularly if $[Pr(EDTA)(H_2O)_3]^-$ data is compared with $[Yb(EDTA)(H_2O)_2]^-$. Additionally, data at pH 3.4 is not in all cases identical with that obtained at pH 7.0, although pH dependent differences are more marked only for thepurine proton resonances. Such behaviour supports the postulate that no clearly defined binding site between shift reagent and substrate exists.

In postulating an ion-pair formation one might expect changes in the steric requirements and mode of coordination of the various lanthanide EDTA chelates to affect the nature of an ion-pair interaction. The well documented 'lanthanide contraction' as one passes through the series of lanthanide ions from La to Yb would suggest that such changes occur [35,39]. Crystallographic structure determinations of some salts of lanthanide EDTA chelates show that $[La(EDTA)(H_2O)_3]^-$ anions are nine-coordinate [53] while the heavier lanthanide chelates are expected to be eight-coordinate. It has been found recently in our laboratories that $Cs[Yb(EDTA)(H_2O)_2]$ is indeed eight-coordinate [54]. Reuben and

Table 3.6: Lanthanide shifts normalized on H(8',8'') for 25 mM SAM in ^2H_2O at 308 K.

Protons	Lanthanide shift ratios extrapolated to infinite dilution					
	Pr (EDTA)		Dy (EDTA)		Yb (EDTA)	
pH:	3.4	7.0	3.4	7.0	3.4	7.0
H(9')	~1.2	-	~1.2	1.45	1.35	1.40
H(8') H(8'')	1.00	-	1.00	1.00	1.00	1.00
H(7') H(7'')	0.15	-	0.80	0.60	0.41	0.53
CH_3	0.48	-	0.43	0.40	0.59	0.25
H(5') H(5'')	~0	-	0.55	0.42	0.21	0.30
H(1')	0.25	-	0.19	0.20	~0	~0
H(8)	0.90[a]	-	0.45	0.15	0.40	~0
H(2)	0.20	-	0.18	~0	~0	~0

a: uncertain due to interference from Pr(EDTA) resonance

b: small shifts, tending to fluctuate about zero.

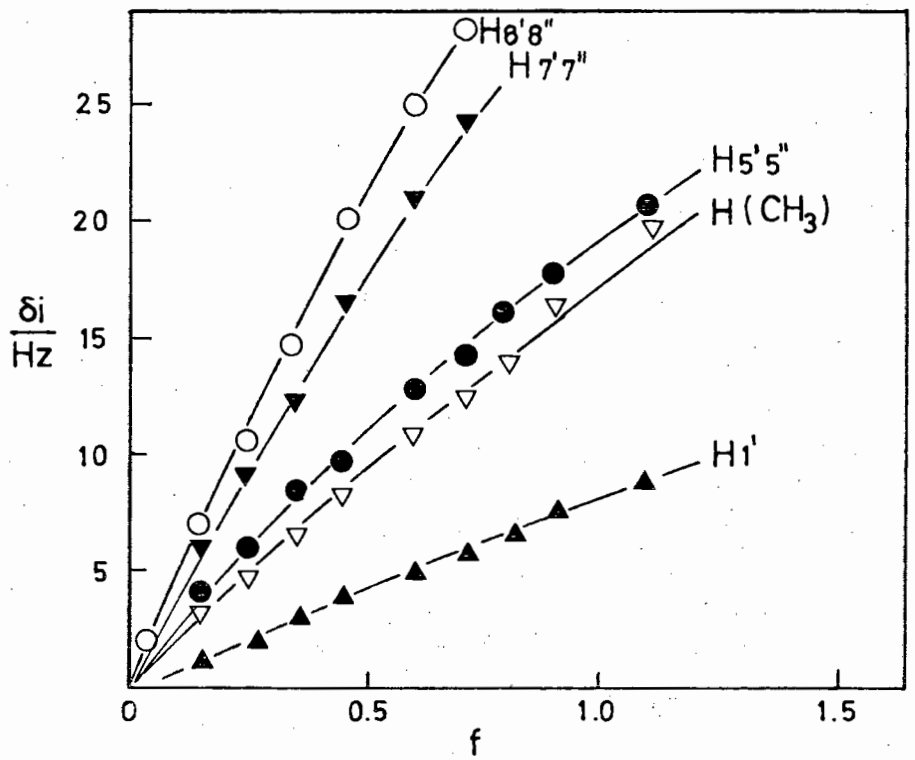

Figure 3.11: A plot of the shifts induced by $[Dy(EDTA)]^-$ in SAM (pH 3.4).

Elgavish have also suggested structural changes in the lanthanide chelates passing from La to Lu occur. These authors have suggested that ion-pairing for the 'lighter' lanthanide chelates with cationic species may take place *via* an un-coordinated EDTA acetate group, while for the heavier lanthanide chelates (Dy-Yb) this mechanism is ruled out [34,52]. Further evidence for structural changes along the lanthanide series has been put forward by Sherry and Pascual [55]. These authors suggest that the mode of coordination of lanthanide ion to carboxyl groups changes from monodentate for the ions $Pr^{3+} \rightarrow Tb^{3+}$ to bidentate in $Dy^{3+} \rightarrow Yb^{3+}$.

In view of such structural changes, the poor agreement of the shifts induced in SAM by various lanthanide EDTA chelates is perhaps not unexpected. Unfortunately, this makes the task of interpreting any shift data obtained by means of ion-pairing extremely difficult, while the resulting 'conformation' if it can be obtained, must be viewed with great caution.

Consideration of shift data requires a knowledge of the principle magnetic symmetry axis as discussed in section 3.3 above. It attempting to interpret the shifts induced by $K[Dy(EDTA)(H_2O)_3]$ at pH 3.4, it was assumed that the $[Dy(EDTA)(H_2O)_3]^-$ anion occupies approximately the same relative position with respect to SAM as does $[Gd(EDTA)(H_2O)_3]^-$. In view of the same sign of all shifts induced by $[Dy(EDTA)(H_2O_3]^-$ (c.f. Table 3.6), it is then reasonable to take the effective magnetic symmetry axis such that all protons lie within the limiting cone of $54^o\ 44'$. This results in the effective symmetry axis to point toward the pseudo-ring postulated for the methionine chain of SAM. A laborious

search yielded calculated shift ratios in reasonable agreement with the experimentally observed ones. In this case the symmetry axis lies just outside the pseudo-ring's C(8')-C(9') bond. The dysprosium nucleus is placed approximately equidistant from the sulphonium and amino cationic poles 0.76 nm from H(9'). The calculated shifts are compared with the experimental $[Dy(EDTA)(H_2O)_3]^-$ shifts in Table 3.7. Listed also are various angles and relative internuclear distances.

Table 3.7: Observed and calculated shift ratios for $[Dy(EDTA)]^-$ induced shifts in SAM at pH 3.4.

Parameter	H(9')	H(8'8'')	H(7'7'')	CH_3	H(5'5'')	H(1')	H(8)	H(2)
Observed shift ratio	1.2	1.00	0.80	0.43	0.55	0.19	0.45	0.18
Calculated shift ratio	1.12	1.00[a]	0.76[a]	0.49	0.41[a]	0.21	0.49[b]	0.17[b]
$(\phi_i)_{calc.}$	2	20	31	27	44	38	30(anti) 54(syn)	70 18
$(r_i)_{calc.}$	0.76	0.74	0.73	0.88	0.69	1.0	0.81 0.84	0.84 0.81

a: average for geminal protons

b: based on 60% *anti* conformation, $\phi_{CN} = -25^o$. (ϕ_{CN}, *syn* $= +145^o$)

It might be expected that the dysprosium EDTA chelate interacts to some extent with a partially protonated adenine moiety at pH 3.4. However as already indicated by relaxation data, this interaction cannot be significant. Two factors are considered to further support this contention *viz* (i) control shift experiments with adenosine and $[Dy(EDTA)(H_2O)_3]^-$ at pH 3.4 showed no significant shifts in the H(2) and H(8)

resonances

(ii) the reasonable similarity between shift data for SAM at pH 3.4 and 7.0.

On the other hand, examination of shift data in Table 3.7 shows that agreement between shift ratios for H(8) and H(2) at pH 3.7 and 7.0 is not good, although ratios for the methionine and observable ribose protons agree reasonably well at these two pH values. The reason for this is not entirely clear but an acceptable explanation might be that at pH 7.0 the *syn/anti* ratio for the adenine moiety is significantly different from the 2:3 ratio estimated at pH 3.4. This difference might arise out of some weak charge interaction between a protonated purine group and the negatively charged dysprosium chelate afterall. Such an interaction would be expected to disturb the *syn/anti* ratio significantly and hence affect the respective shift ratios for H(2) and H(8).

Taken together with relaxation data, the $K(Dy(EDTA)(H_2O)_3]$ shift results at pH 3.4, yielded an overall conformation for SAM as depicted in Figure 3.12. The conformation proposed has the following general features:

(a) The methionine side forms a non-rigid pseudo-ring *via* ion pairing between the S^+ and COO^- poles.

(b) The $[Ln(EDTA)(H_2O)_n]^-$ chelate forms an ion-pair such that it is approximately equidistant from S^+ and NH_3^+.

(c) The adenosyl moiety is best described by a rapid equilibrium between the *anti*/^{3}E and *syn*/^{2}E conformers. The former conformer is favoured by *ca* 60%, although this distribution appears to be pH dependent.

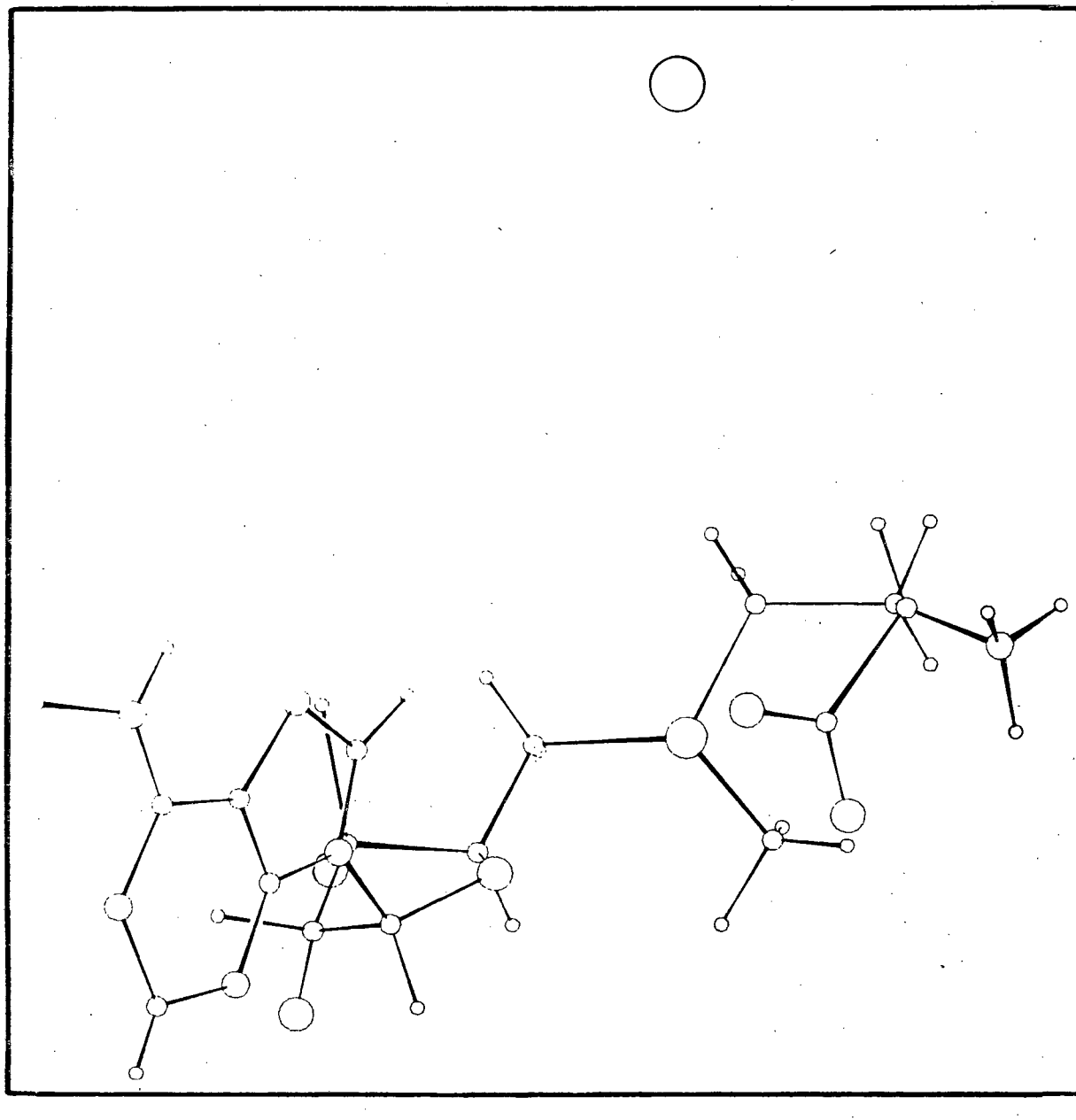

Figure 3.12: The proposed conformation of the S-adenosyl-L-methionine molecule.

PART I

CHAPTER IV : RESULTS, DISCUSSION AND CONCLUSIONS

250 M Hz ^{1}H N.M.R. Data

4.1 Introduction

Although numerous reports on the use of lanthanide shift and relaxation probes have appeared in the literature [21,36,38,45-48], the initial enthusiasm about exclusive use of such probes for conformation analysis has become tempered by reports that "fitting of the LIS and broadening $(T_2)^{-1}$ data alone is not a sufficient criterion for a conformational solution; solutions must also be compatible with the coupling constant information" [58]. Williams has shown that lanthanide data is compatible with coupling constant results if shift and relaxation information is considered in terms of an equilibrium between different conformations [59]. In the present case the observed shift and relaxation data obtained for SAH and SAM are incomplete for the ribose ring protons, leaving the ring conformation poorly defined in the first instance.

It therefore seemed desirable to examine the ^1H n.m.r. spectra for SAH and SAM in more detail, with a view to obtaining suitable coupling constant for the ribose moiety. It has been shown that the ribose conformation can be extracted from the $J_{1'2'}$, $J_{2'3'}$ and $J_{3'4'}$ coupling constants [60]. Further the $J_{4'5'}/J_{4'5''}$ set of couplings gives information about the exocyclic rotamer population about the C(4')-C(5') bond. This follows from the well known Karplus equation, which relates a vicinal coupling constant, $^3J_{HH}$, to the torsion angle, ϕ_{HH}, formed by the vicinal C-H vectors [61,62]. Figure 4.1 shows such a relation schematically.

In the case of a pentose ring Altona and Sundaralingam have observed that the $^3J_{HH}$ couplings "cannot assume random values, independent of each other, but must obey interrelationships governed by the law of pseudorotation" [60,63]. These authors have shown that there exists two predominant

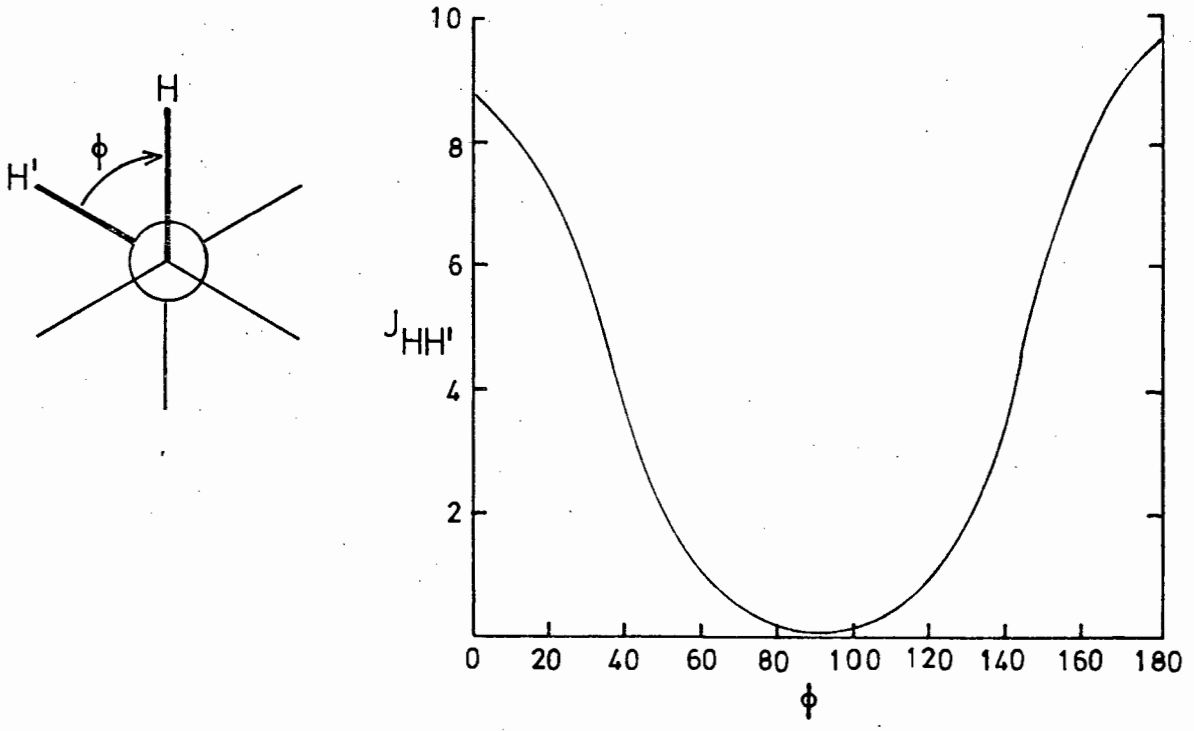

Figure 4.1: The dependence of vicinal coupling constants on the angle ϕ as predicted by the Karplus equation.

ribose puckers, each characterized by a narrow range of the phase angle of pseudorotation [37,60]. These two classes of pucker are labelled type-N (C(2')-exo, C(3')-endo) and type-S (C(2')-endo, (C(3')-exo) corresponding to the ^{3}E (and $_{2}^{3}T$) and ^{2}E ($_{3}^{2}T$) conformers (c.f. section 2.9).

Altona and Sundavalingam have proposed a modified version of the Karplus equation,

$$J_{HH} = A\cos^{2}\phi_{HH} - B\cos\phi_{HH} + C \qquad (4.1)$$

to describe the relation between J_{HH} and ϕ_{HH} in pentose rings [63]. In this equation A,B and C are regarded as geometry dependent, adjustable parameters for $0 \leq \phi \leq 180^{o}$. Equation (4.1) may be used to extract conformational information for pentose rings that show the following generalizations:

(i) $^{N}J_{1'2'} = {}^{S}J_{3'4'} \simeq 0$ Hz.

(ii) $^{S}J_{1'2'} = {}^{N}J_{3'4'} \simeq 10$ Hz.

(iii) $(J_{1'2'} + J_{3'4'}) \simeq$ constant > 9 Hz.

It must be remembered that the experimentally observed couplings reflect not one static pucker, but a dynamic conformational equilibrium, albeit between presumably two, overwhelmingly predominant puckers, *viz.* the N and S type [37,63]. If it is accepted that only these two puckers contribute significantly to the observed $^{3}J_{HH}$ couplings then it is possible to determine the relative fraction of N and S conformers by means of the linear relationship

$$J_{obs} = X_N \, {}^{N}J_{ij} + X_S \, {}^{S}J_{ij} \qquad (4.2)$$

where the mole fractions, $\Sigma X_i = 1$, and $^{N}J_{ij}$, $^{S}J_{ij}$ are the coupling constants due to the N and S puckers respectively. It must be emphasized that this approach is valid for only those pentose systems that obey the generalizations (i), (ii) and (iii) given above.

Methods have been devised to determine the equilibrium distribution of N and S puckers in terms of the phase angle of pseudorotation, P, and the corresponding 'amplitude' of pucker τ_m [63,65,66]. The simplest procedure has been advanced by Guschlbauer and Tran-Dinh Son [66], which does not involve elaborate computation. These authors have computed coupling constants for all possible ribose conformations for $P = 0^{o}$ to $P = 360^{o}$, $\tau_m = 30^{o}$ to $\tau_m = 50^{o}$ and plotted these parameters as functions of the $J_{2'3'}$ and $(J_{1'2'} + J_{3'4'})$ coupling constants. Hence, with any set of *observed* coupling constants, one may resolve these into a set of ^{N}J and ^{S}J values, which have been calculated from the parameters P and τ_m. By means of

equation (4.2) it becomes possible to estimate the mole fraction N and S-type pentose pucker.

4.2 The Conformation of the Ribose Ring in S-adenosyl-L-homocysteine as Determined from J_{HH} Coupling Constants

The 250 M Hz proton spectrum of SAH has already been described in section 3.1. At this field strength the coupling constants could be easily measured. These constants, measured from a 1.3 mM aqueous solution of SAH at 304 K and pH 7.0 are collected in Table 4.1.

Table 4.1: Coupling constants of the ribose moiety protons of SAH.

Coupling constants J_{ij}/Hz						
1'2'	2'3'	3'4'	4'5'	4'5''	5'5''	$J_{1'2'} + J_{3'4'}$
5.0	5.5	4.4	5.2	6.7	-14.0	9.4

These constants are estimated accurate to ± 0.3 Hz. Coupling constants were measured from an expanded 250 M Hz spectrum shown in Figure 4.2. The assignments were confirmed by computer simulation of the observed spectrum utilizing the observed chemical shifts and coupling constants. The agreement between simulated and experimental spectrum is excellent, imparting confidence to the coupling constant values so obtained.

Conformation of Ribose Moiety

The phase angle of pseudorotation, P and corresponding τ_m was obtained from plots of $J_{2'3'}$ against $J_{1'2'} + J_{3'4'}$ as computed by Guschlbauer [65].

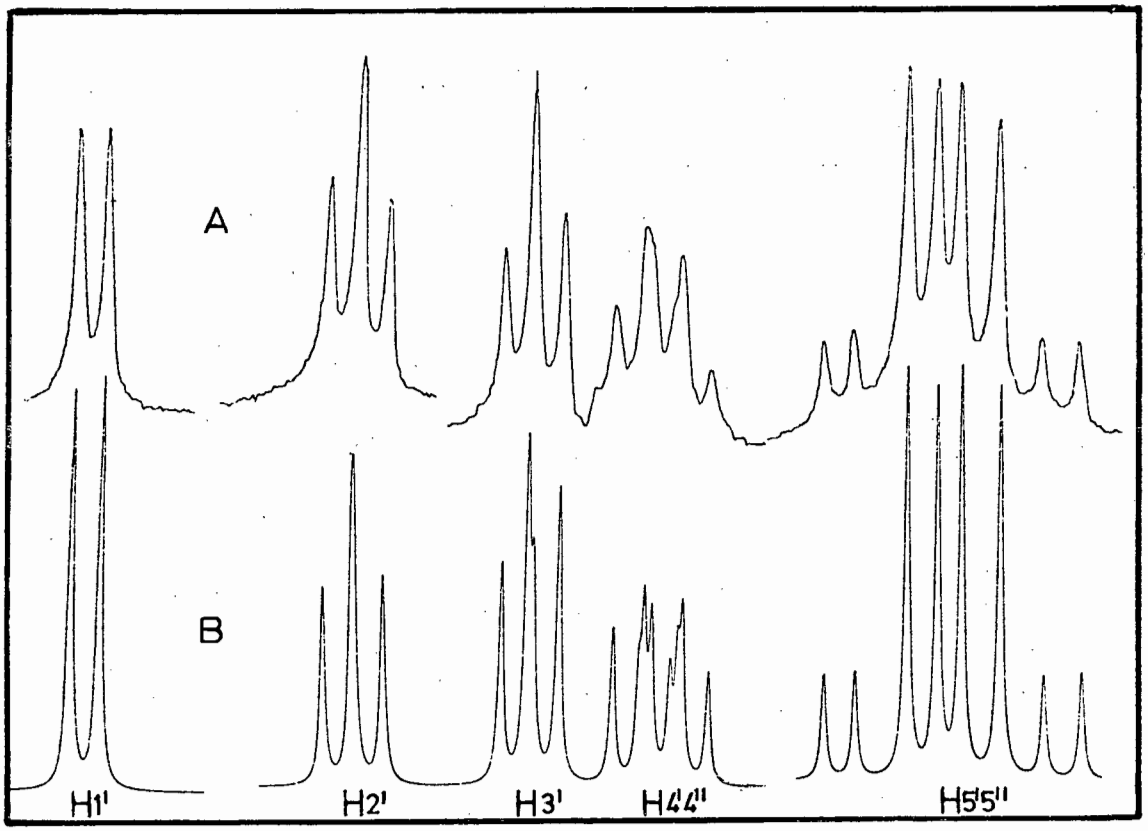

Figure 4.2: The 250 M Hz (A) observed and (B) computed spectrum of SAH

These parameters, as well as the fraction of N and S conformer calculated from equation (4.2) are tabulated in Table 4.2.

Table 4.2: Conformational parameters of the ribose moiety of SAH, with estimated fraction N and S pucker

	τ_m	N_P	S_P	$N_{J_{calc}}$	$S_{J_{calc}}$	%N	%S
1:	40.5°	16°	164°	~0.1	10.1	43	50
2:	43.5°	29°	151°	~0.25	9.8	44	50

$N_{J_{calc}} = {}^{N}J_{1'2'} = {}^{S}J_{3'4'}$ computed from τ_m, P.

$S_{J_{calc}} = {}^{S}J_{1'2'} = {}^{N}J_{3'4'}$ computed from τ_m, P.

1: using A = 10.5, B = 1.2, C = 0

2: using A = 9.8, B = 0.9, C = 0.

The %N and %S conformer do not total 100% as might have been expected. The root of this discrepancy may lie in (i) the change of electronegativity as O(5') is replaced by S(5') and (ii) the fact that only two conformations (S and N) are considered to exist. Previous workers have advocated a correction of the observed $^{3}J_{HH}$ value for electronegativity effects [64,65]. However, present knowledge of bond lengths and angles for molecules in solution does not warrant the application of such correction. It seems more likely that the observed J_{HH} couplings do reflect a small (6-7%) fraction of other possible puckers not accounted for in equation (4.2). Evans and Sarma have concluded, after a detailed error analysis of the Altona-Sundaralingam approach, that it is necessary to assume an uncertainty of 10% in the computed fractions of S and N ribose puckers [66]. If such an error margin is accepted, then the discrepancy observed in %N + %S not totalling exactly 100% is not serious. It is therefore reasonable to conclude that the ribose ring in SAH under the above conditions exists in a dynamic equilibrium between roughly equal fractions of N and S-type conformers.

The ribose ring need not necessarily determine the base orientation about the C(1') - N(9) bond, although a correlation between the ribose pucker conformation and the torsion angle, ϕ_{CN}, has been noted [37,63]. For purine nucleotides there is a clear preference for an *anti*/N-type pucker conformation, while for the S-type both the *syn* and *anti* purine orientations seem to be isoenergetic [63]. Hence if the S-type ribose pucker exists in significant proportions, it might be expected to observe a considerable fraction of the *syn* base orientation in purine nucleotide conformations. Finally, it should be noted that the N-type ribose conformer favours a range in ϕ_{CN} from 0^{o} to -40^{o}, while the S-type ribose ring favours a more

negative glycosidic torsion angle -40^{o} to -80^{o}. These trends have been established by examination of a large number of solid state studies [37].

The question of how the lanthanide shift and relaxation results for SAH compare with data obtained from coupling constant analysis will now be discussed. Relaxation data indicate that the adenosyl moiety exists in dynamic equilibrium between *syn* and *anti* orientations, such that the *anti* conformer is favoured by 75 ± 10%, $\phi_{CN} = -45^{o}$ while for *syn*, $\phi_{CN} = 130^{o}$. It may be recalled that in calculating shift and relaxation ratios, the ribose ring was 'placed' into the ^{3}E pucker (corresponding to N-type in terms of Altona-Sundaralingam rotation) with the base *anti*. This conformation produced good agreement between experimental and calculated ratios. (Similarly, for the 25% *syn* orientation, the ribose ring was 'placed' into approximately ^{2}E pucker). Consequently, for want of more detailed shift and relaxation information on the ribose protons, the ribose pucker was "linked" to the *anti* adenosyl orientation, and to a first approximation a 75 ± 10% ^{3}E ribose conformer was implicated. This conclusion, however, must clearly be revised in the light of the $^{3}J_{HH}$ coupling constant analysis.

On the whole though, the lanthanide data is not at variance with the results from the coupling constant analysis. The estimate of 75 ± 10% *anti* fits the roughly equal fractions of ^{3}E and ^{2}E ribose conformers, if viewed in the light of remarks concerning the *anti*/^{3}E preference. Similarly $\phi_{CN} = -45^{o}$ is compatible with the distribution of ribose conformations. Qualitatively, a slightly greater % S pucker (^{2}E) would be expected to result in an even more negative ϕ_{CN}.

Conformation about the Backbone C(4') - C(5') Angle, ψ.

Consideration of the possible rotamers about the exocyclic C(4') - C(5') bond, and the relevant coupling constants, is expected to give information about which of the possible *gg*, *gt* or *tg* rotamers (ψ = 60°, 180°, and 300°) is preferred, if any (see section 2.9). Examination of $J_{4'5'}$ and $J_{4'5''}$ in Table 4.1 shows these values to be fairly large in comparison with couplings measured for molecules such as N^6-methyladenyl-uridine (m^6ApU) and adenyl-uridine (ApU). These dinucleoside monophosphates have been shown to be considerably stacked in aqueous solution, leading to a 80 - 90% *gg* rotamer population [67], estimated by the method of Wood *et al* [68,69]. The relation

$$f_{gg} \simeq \frac{13 - (J_{4'5'} + J_{4'5''})}{10} \qquad (4.3)$$

where f_{gg} is the fraction *gg* rotamer population has been used for this purpose. Table 4.3 compares some of Altona's results with the data obtained for SAH.

Table 4.3: Coupling constant data and fraction *gauche-gauche* conformation about C(4') - C(5') bond.

J/Hz	SAH[b]	ApU[a]	m^6ApU[a]	m^6ApU[a]
$J_{4'5'}$	5.2 adenylyl	2.3	2.3	2.2
	uridyl	2.9	1.9	2.0
$J_{4'5''}$	6.7	3.3	3.0	3.3
		2.9	2.0	2.2
$J_{4'5'} + J_{4'5''}$	11.9	5.6	5.3	5.5
		5.8	3.9	4.2
f_{gg}	0.11	0.74	0.77	0.75
		0.72	0.91	0.88

a : data from ref [67], 50 mM at 293 K
b : this work, 1.3 mM at 304 K.

It is clear from Table 4.3 that the fraction *gg* rotamer for SAH is very small if not negligible. It must be remembered that equation (4.3) represented only an estimate of f_{gg}. In any event the unusually large $J_{4'5'}$ and $J_{4'5''}$ coupling constants underline the fact that the *gt* and *tg* rotamers are predominant in SAH. Additionally these values are not very different suggesting that neither *gt* nor *tg* is favoured to any large extent. This conclusion is in good agreement with the shift and relaxation data predicted conformation. Figure 4.3 shows the predominant rotamer about the C(4') - C(5') bond.

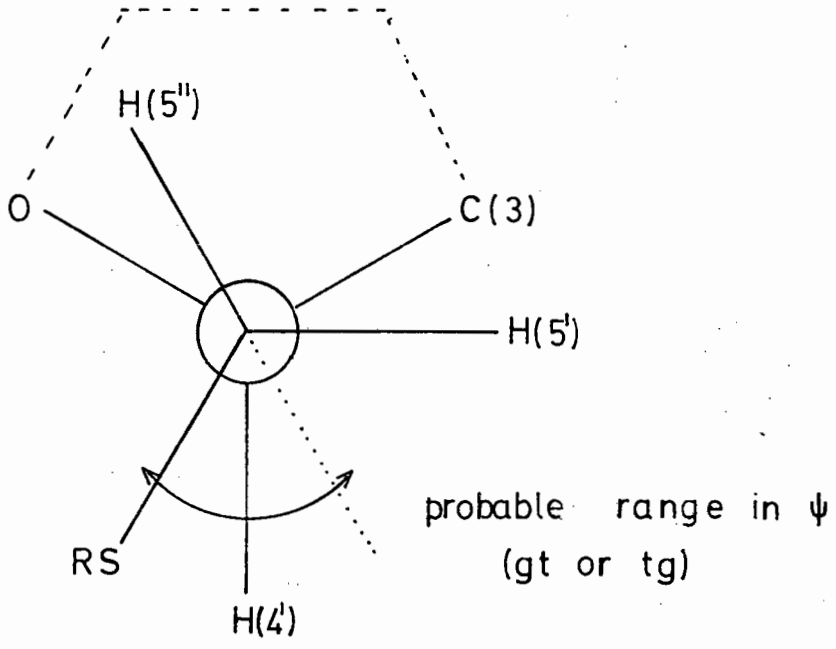

Figure 4.3: The predominant rotamer about the C(4') - C(5') bond.

4.3 The Conformation of the Ribose Ring in S-adenosyl-L-methionine

Measurement of the vicinal coupling constants for SAM were performed exactly as for SAH in the previous section. These results are tabulated in Table 4.4.

Table 4.4: Coupling constants of the ribose moiety protons of 5 mM SAM at pH 3.5, 304 K.

Coupling Constants J_{ij}/Hz						
1'2'	2'3'	3'4'	4'5'	4'5"	5'5"	$J_{1'2'} + J_{3'4'}$
4.4	4.6	5.0	9.0	7.5	-13.6	9.4

These constants are estimated accurate to ± 0.3 Hz.

Comparison of these values with those listed in table 4.1 underline a difference in the two conformations in question. It is clear that in the case of SAM the positive sulphonium centre is expected to affect the ribose coupling constants as a result of the fairly high electronegativity of the S^+ group. The correction for this electronegativity effect is small [65] and electronegativity alone cannot account for the difference in the overall pattern of vicinal couplings in SAM compared to SAH.

Conformation of Ribose Moiety

Table 4.5 summarizes the conformational parameters calculated for SAM, which were obtained exactly as for SAH previously. It is clear from Table 4.5 that SAM seems to favour the N-type pucker by *ca* 10% over that of SAH, but that the two ribose conformers S and N are again found in roughly equal proportion. It is also interesting that in this case the

Table 4.5: Conformational parameters of the ribose pucker of SAM, and estimated fraction N and S puckers.

	τ_m	N_P	S_P	$N_{J_{calc}}$	$S_{J_{calc}}$	%N	%S
1:	44.3°	-8°	188°	∿0	9.2	54%	48%
2:	43.5°	9°	171°	∿0	9.4	53%	47%

$^{N}J_{calc} = {}^{N}J_{1'2'} = {}^{S}J_{3'4'}$ computed from τ_m, P.

$^{S}J_{calc} = {}^{S}J_{1'2'} = {}^{N}J_{3'4'}$ computed from τ_m, P.

1: using A = 10.5, B = 1.2, C = 0

2: using A = 5.8, B = 0.9, C = 0.

%N and S does total (even slightly exceed) 100%. Nevertheless, no significance can be attached to this fact in view of the claimed uncertainty in the fraction N and S conformers so calculated [66].

Lanthanide shift and relaxation data, although of poor quality for SAM, predicted a *syn/anti* ratio of *ca* 2:3 where for the *anti* base orientation, $\phi_{CN} = -25°$ while for *syn* $\phi_{CN} = 145°$. These results are again not at variance with the ribose conformations predicted by the coupling constant analysis. The preference for the N ribose pucker, for instance, does imply that a glycosidic torsion angle should be biased toward the range 0° to -40°. The relatively low value for ϕ_{CN} (-25°) predicted by lanthanide probes is in keeping with a predominance of N-type ribose pucker. However, comparing the lanthanide shift and relaxation results must be

done with caution, since the possibility of an interaction with the adenine group (at pH 3. , largely protonated) and the negatively charged lanthanide EDTA chelate cannot be ruled out. Such an interaction might alter the *syn/anti* ratio to some extent.

Conformation about the Backbone C(4') - C(5') Angle

The $J_{4'5'}$ and $J_{4'5''}$ coupling constants in SAM are most interesting. Reference to Table 4.4 shows these vicinal coupling constants to be abnormally large, even larger in fact than those for SAH. This difference may reflect (i) a relatively large electronegativity effect in passing from S to S^+ and (ii) an unusual conformation about the C(4') - C(5') bond, i.e. a large value of ψ. With regard to the electronegativity effect, the corrected $J_{4'5'}$ and $J_{4'5''}$ values would be expected to be slightly smaller than those in Table 4.4, but even if there were a 10-fold change in the electronegativity in passing from S to S^+, the difference in coupling constants should not be more than *ca* 1 Hz. It is therefore reasonable to expect that an unusual conformation about the C(4') - C(5') bond must be responsible for the values of 9.0 Hz and 7.5 Hz for $J_{4'5'}$ and $J_{4'5''}$ respectively.

Evidently equation (4.3) cannot be applied to estimate the fraction *gg* rotamer (for which $\psi = 60^{\circ}$). It would predict a negative f_{gg}! This state of affairs is taken to mean that the torsion angle, ψ, is always large meaning that only *gt* and *tg* rotamers are favoured. The large $J_{4'5'}$ and $J_{4'5''}$ coupling constants suggest strongly that ψ is in the region of 270°, such that almost the optimum Karplus angle (for maximum coupling) between H(4') and both H(5') and H(5'') is achieved. Such a conclusion is entirely compatible with results from lanthanide shift and relaxation

experiments. Reference to Figure 3.12 shows that such unusual $J_{4'5''}$ and $J_{4'5'}$ coupling constants were expected.

Obviously, from these results it is not possible to deduce any conformational information about the methionine chain, but the fair agreement between coupling and shift and relaxation data does impart confidence to the conformation predicted by lanthanide probes. Unfortunately it was not possible to extend this Karplus equation type analysis to the methionine fragment protons H(7'), H(7''), H(8'), H(8'') and H(9') in the case of either SAH or SAM. The methylene protons appear to be magnetically equivalent and are not separately assignable.

4.4 General Discussion and Conclusions

The conformational analysis of the two title compounds, SAH and SAM, was fraught with numerous difficulties, some of which could not be satisfactory resolved. Recalling the objectives of this work (c.f. section 1.4), it is reasonable to conclude that the conformations determined by means of lanthanide shift and relaxation probes represent at best an average conformation of these two molecules, with probably some degree of freedom. In combination with coupling constant data it is believed that a semiquantitative picture of the conformations of SAH and SAM has been established. The answer to the question concerning the similarity or difference in the conformations of SAH and SAM, must of course depend on the accuracy with which the SAM and SAH conformations have been defined.

The average solution conformation of SAH is believed to have been demonstrated with considerable certainty. This follows from the good lanthanide

shift and relaxation data, as well as its consistency with the coupling constant data predictions. On the other hand the conformation of SAM remains less accurately defined. There can be no reasonable doubt however, that in slightly acid solution the conformation of SAM is not similar to SAH. In particular, the methionine moiety in SAM is blocked to coordination by the lanthanide metal ions. Substantial evidence exists that the mechanism of such blocking is likely to be a intramolecular ion-pairing effect between an anionic sulphonium and cationic carboxyl group. Not only do van der Waal's potential energy calculations favour such an interaction in the case of S-methyl-L-methionine [17] but so does the observed degradation behaviour of SMM salts suggest such an intramolecular interaction [15]. The present shift and relaxation results for SAM are not compatible with any conformation in which no such pseudo-cyclic conformation is postulated. It is gratifying to observe unusual $J_{4'5'}$ and $J_{4'5''}$ coupling constants, conclusions of which are consistent with the proposed conformation of SAM.

In conclusion it may be advantageious to summarize the general features of the SAH and SAM conformations below.

S-adenosyl-L-homocysteine

The conformation of SAH is concluded to have the following general features in dilute neutral aqueous solution:

(i) The ribose pucker is found to assume roughly equal fractions of N and S conformers. In this case the S conformer seems somewhat favoured.

(ii) The purine moiety is best considered in terms of a *syn/anti* equilibrium in the ratio of about 1:4. The glycosidic torsion angle is estimated to be $\simeq -45^{o}$ (*anti*) and $\simeq 130^{o}$.

(iii) The *gt* and *tg* rotamers about the C(4')-C(5') bond are predominantly favoured while a small contribution of *ca* 10% *gg* conformer is indicated by the $J_{4'5'}$ and $J_{4'5''}$ coupling constants.

(iv) The homocysteine fragment exists in fairly extended form, with the rotamers about the S(6') - C(7'), C(7') - C(8') and C(8') - C(9') bonds may be approximately described as *gauche*, *trans*, and *trans* (with respect to the NH_3^+ and C(7') groups). The lanthanide ion binds to the carboxyl moiety (see Figure 3.6).

S-adenosyl-L-methionine

At a pH ≃ 3.5 the SAM conformation is proposed to exhibit the following features.

(i) The ribose pucker exists in fast equilibrium between roughly equal populations of $N(^3E)$ and $S(^2E)$ conformations. The $N(^3E)$ pucker is slightly favoured.

(ii) The adenosyl moiety exists in fast exchange between the *anti* and *syn* orientations, such that ϕ_{CN} $\simeq -25^o$ and $\simeq 145^o$ while the *anti/syn* ratio is about 2:3.

(iii) The torsion angle, ψ, is large, indicating a predominance of *gt* and *tg* rotamer populations about the C(4') - C(5') bond (the *gg* conformation is considered negligible).

(iv) The COO^- and S^+ groups are considered to interact electrostatically so forming a relatively flexible pseudo six-membered ring occupying predominantly a chair conformation.

APPENDIX

Coordinates for SAH and SAM conformations as used in the generation of Figures 3.6 and 3.12.

(fractional coordinates)

SAH	x	y	z
C(1')	0.59	0.46	0.56
C(2')	0.62	0.35	0.58
C(3')	0.51	0.31	0.60
C(4')	0.44	0.38	0.56
C(5')	0.36	0.37	0.66
O(1')	0.49	0.47	0.56
H(1')	0.62	0.49	0.49
H(4')	0.40	0.35	0.50
H(5')	0.39	0.43	0.71
H(5'')	0.37	0.31	0.70
S(6')	0.25	0.40	0.62
C(7')	0.24	0.51	0.57
C(8')	0.30	0.59	0.64
C(9')	0.29	0.68	0.61
C(10')	0.38	0.76	0.65
O(10')	0.34	0.81	0.66
O(10'')	0.43	0.73	0.71
H(7')	0.27	0.52	0.49
H(7'')	0.17	0.52	0.57
H(8')	0.37	0.56	0.63
H(8'')	0.27	0.59	0.71
H(9')	0.20	0.73	0.59
NH_3^+(N)	0.34	0.69	0.52
N(1)	0.85	0.71	0.66
C(2)	0.82	0.67	0.57
N(3)	0.75	0.61	0.55
C(4)	0.70	0.56	0.64
C(5)	0.73	0.60	0.73
C(6)	0.80	0.67	0.74
N(7)	0.67	0.55	0.79
C(8)	0.62	0.49	0.74
N(9)	0.63	0.50	0.64
H(2)	0.86	0.70	0.51
H(8)	0.56	0.43	0.77
NH_2	0.82	0.70	0.83
Ln	0.50	0.87	0.74

SAM	x	y	z		x	y	z
C(1')	0.36	0.33	0.14	C(4)	0.26	0.24	0.27
C(2')	0.29	0.39	0.07	C(5)	0.23	0.26	0.36
C(3')	0.32	0.49	0.07	C(6)	0.17	0.19	0.41
C(4')	0.43	0.48	0.07	N(7)	0.28	0.35	0.38
C(5')	0.48	0.57	0.11	C(8)	0.33	0.39	0.29
O(1')	0.44	0.39	0.14	N(9)	0.31	0.31	0.24
H(1')	0.38	0.26	0.10	H(2)	0.15	0.04	0.24
H(2')	0.21	0.38	0.10	H(8)	0.38	0.45	0.29
H(3')	0.30	0.53	0.19	NH_2(N)	0.14	0.21	0.50
H(4')	0.46	0.46	0.0				
H(5')	0.44	0.59	0.16				
H(5'')	0.48	0.62	0.05				
S(6')	0.60	0.54	0.14				
Methyl							
C(6')	0.67	0.52	0.04				
H	0.63	0.45	0.0				
H	0.68	0.58	0.00				
H	0.73	0.49	0.04				
C(7')	0.66	0.64	0.20				
C(8')	0.77	0.63	0.21				
C(9')	0.78	0.54	0.30				
C(10')	0.71	0.45	0.25				
O(10')	0.73	0.41	0.19				
O(10'')	0.65	0.43	0.29				
H(7')	0.62	0.66	0.27				
H(7'')	0.64	0.71	0.16				
H(8')	0.80	0.69	0.25				
H(8'')	0.80	0.61	0.16				
H(9')	0.76	0.56	0.38				
NH_3^+(N)	0.86	0.51	0.29				
N(1)	0.13	0.11	0.38				
C(2)	0.16	0.10	0.27				
N(3)	0.23	0.16	0.23				

REFERENCES

1. Du Vigneaud, V., "A Trial of Research", Cornell Univ. Press, Ithaca, N.Y., (1952).
2. Mudd, S.H. and Cantoni, G.L., in "Comprehensive Biochemistry", Vol. 15, 1, (1964).
3. Cantoni, G.L., *J. Amer. Chem. Soc.*, 74, 2942, (1952).
4. Mudd, S.H., and Mann, J.D., *J. Biol. Chem.*, 238, 2164, (1963).
5. Lehninger, A.L., in "Biochemistry", Worth Publishers, New York, 1972.
6. Durell, J., Rawitscher, M. and Sturtervant, J.M., *Biochim. Biophys. Acta*, 56, 552, (1962).
7. Mudd, S.H., Klee, W.A. and Ross, P.D., *Biochemistry*, 5, 1653, (1966).
8. Mudd, S.H. and Klee, W.A., *Biochemistry*, 6 (4), 988, (1967).
9. Donohue, J. and Trueblood, K.N., *J. Mol. Biol.*, 2, 363, (1960).
10. Shefter, E. and Trueblood, K.N., *Acta Crystallogr.*, 18, 1067, (1965).
11. Follmann, H. and Gremels, G., *Eur. J. Biochem.*, 47, 187, (1974).
12. Follmann, H., Kuntz, I. and Zacharias, W., *Eur. J. Biochem.*, 58, 31, (1975).
13. Kraut, J. and Jensen, L.H., *Acta Cryst.*, 16, 79, (1963).
14. Kenhard, O., Isaacs, N.W., Motherwell, W.D.S., Coppola, J.C., Wampler, D.L., Larson, A.C. and Watson, D.G., *Proc. R. Soc. Lond. A.*, 325, 401, (1971).
15. Ramirez, F., Finnan, J.L. and Carlson, M., *J. Org. Chem.*, 38 (15), 2597, (1973).
16. March, J., in "Advanced Organic Chemistry: Reactions Mechanisms and Structure", McGraw-Hill, New York, 263, (1968).
17. Del Re, G., Gavuzzo, E., Giglio, E., Lelj, F., Mazza, F. and Zappia, V., *Acta Cryst.*, B33, 3289, (1977).
18. Cornforth, J.W., Reichard, S.A., Talalay, P., Carrell, H.L. and Glusker, J.P., *J. Amer. Chem. Soc.*, 99 (22), 7292, (1977).
19. Pople, J.A., Schneider, W.G. and Bernstein, H.J., "High-resolution Nuclear Magnetic Resonance", McGraw Hill, New York, 1959.
20. Emsley, J., Feeney, J. and Sutcliffe, L., "High Resolution Nuclear Magnetic Resonance Spectroscopy", Vol. 1,2, Pergamon Press, London, 1967.
21. Dwek, R., in "Nuclear Magnetic Resonance (N.M.R.) in Biochemistry", Claredon Press, Oxford, (1973).
22. James, T.L. in "Nuclear Magnetic Resonance in Biochemistry", Academic Press, New York, (1975).
23. Shaw, D., in Fourier Transform N.M.R. Spectroscopy" Elsevier, Amsterdam, (1976).
24. Farrar, T.C. and Becker, E.D., in "Pulse and Fourier Transform N.M.R.", Academic Press, New York, 1971.

25. Bloch, F., *Phys. Rev.*, 70, 460, (1946).

26. Bloch, F., Hansen, W.W. and Packard, M., *Phys. Rev.*, 70, 474, (1946).

27. Maeda, M., Saneyoshi, M. and Kawazoe, Y., *Chem. Pharm. Bull.*, 19, 1641, (1971).

28. Bullock, F.J. and Jardetzky, O., *J. Org. Chem.*, 29, 1988, (1964).

29. Finar, I.L., "Organic Chemistry", 2, (4th Ed.), Longmans, 1968.

30. Hoard, J.L., Lind, M.D., Byungkook, Lee, *J. Amer. Chem. Soc.*, 87 (7), 1612, 1965.

31. K.W. Bagnall ed., "Lanthanides and Actinides" MTP, Vol. 7, Butterworths 1972.

32. Nosterova, Ya. M., *et al.*, *J. Structural Chemistry*, 13, 739, (1972).

33. Albertson, J., *Acta. Chem. Scand. (A)*, 28, 347, (1974).

34. Rueben, J. and Elgavish, G.A., *J. Am. Chem. Soc.*, 98, 4755, (1976).

35. Cotton, F.A. and Wilkinson, G., "Advanced Inorganic Chemistry", 3rd Edition, John Wiley, New York, 1972.

36. Fazakerley, G.V., Russel, J.C. and Wolfe, M.A., *Eur. J. Chem.*, 76, 601, (1977).

37. Sundaralingam, M., in "Structure and Conformation of Nucleic Acids and Conformation of Nucleic Acids and Protein-Nucleic Acid Interactions", University Park Press, Baltimore, p. 487, (1975).

38. Williams, R.J.P., Dobson, C.M. and Xavier, A.V., *J. Chem. Soc. Dalton*, 1762, (1974).

39. Topp, N.E., in "The Chemistry of the Rare-Earth Elements", Topics in Inorganic and General Chemistry, No. 4, Elsevier, (1965).

40. Swift, T.J. and Connick, R.E., *J. Chem. Phys.*, 37, 307, (1962).

41. Luz, Z. and Meilboom, S., *J. Chem. Phys.*, 40, 2686, (1964).

42. Bloembergen, N., *J. Phys. Chem.*, 27, 595, (1957).

43. LaMar, G.N., Horrocks, W. de W. and Allen, L.C., *J. Chem. Phys.*, 41, 2126, (1964).

44. Bleany, B., *J. Mag. Res.*, 8, 91, (1972).

45. Horrocks, W. de W., Snipe, J.P. and Sudnick, D., in "Nuclear Magnetic Resonance Shift Reagents", Academic Press, New York, (1973).

46. Bleaney, B., Dobson, C.M., Levine, B.A., Williams, R.J.P. and Xavier, A.V., *Chem. Commun.*, 791, (1974).

47. Barry, C.D., Glasel, J.A., Williams, R.J.P. and Xavier, A.V., *J. Mol. Biol.*, 84, 471, (1974).

48. De Boer, J.W.M., De Boer, E., Sakkers, P.J.D. and Hilbers, C.W., *J. Mag. Res.*, 25, 455-476, (1977).

49. Swift, T.J. and Connick, R.E., *J. Chem. Phys.*, 37, 307, (1962).

50. Shulman, R., Sternlicht, H. and Wyluda, B., *J. Chem. Phys.*, 43, 3116, (1965).

51. Schwatzenbach, G. and Flascka, H. in "Complexiometric Titrations", 2nd Edition, Methuen & Co., London, 1969.

52. Reuben, J. and Elgavish, G.A., *J. Amer. Chem. Soc.*, 99 (6), 1762, (1977).

53. Hoard, J.L., Lind, M.D. and Byungkook, L., *J. Amer. Chem. Soc.*, 87, 1611, (1965).

54. Nassimbeni, L.R., Wright, M.R.W., van Niekerk, J.C. and McCallum, P.A., *Acta. Cryst.*, (1979) in press.

55. Sherry, A.D. and Pascual, E., *J. Amer. Chem. Soc.*, 99 (18), 5871, (1977).

56. Torri, K. and Iitaka, Y., *Acta Cryst.*, B29, 2799, (1973).

57. Izatt, R.M., Christensen, J.J. and Rytting, J.H., *Chemical Reviews*, 71 (5), 439, (1971).

58. Birdsall, B., Birdsall, N.J.M., Feeney, J. and Thornton, J., *J. Amer. Chem. Soc.*, 97 (10), 2845, (1975).

59. Geraldes, C.F.G.C. and Williams, R.J.P., *Eur. J. Biochem.*, 85, 471, (1978).

60. Altona C and Sundaralingam, M., *J. Amer. Chem. Soc.*, 94 (23), 8205, (1972).

61. Karplus, M., *J. Amer. Chem. Soc.*, 85, 2870, (1963).

62. Karplus, M., *J. Chem. Phys.*, 30, 11, (1959).

63. Altona, C. and Sundaralingam, M., *J. Amer. Chem. Soc.*, 95 (7), 2333, (1973).

64. Davies, D.B. and Danyluk, S.S., *Biochemistry*, 13, 4417, (1974).

65. Güschlbauer, W. and Tran-Dinh Son, *Nucl.Acid.Res., Specl.Publ.* S85-88 (1975)

66. Lee, C.H. and Sarma, R.H., in "Structure and Conformation of Nucleic Acids and Protein-Nucleic Acid Interactions", Edited by M. Sundaralingam and S.T. Rao, University Park Press, Baltimore, p. 631, (1975).

67. Altona, C. *ibid*, p. 613, (1975).

68. Wood, D.J., Mynott, R.J., Hruska, F.E. and Sarma, R.H., *FEBS Letters*, 34, 323, (1973).

69. Wood, D.J., Hruska, F.E., Mynott, R.J. and Sarma, R.H., *J. Can. Chem.*, 51, 2571, (1973).

PART II

CHAPTER I : INTRODUCTION

INTRODUCTION

The interaction of metal species with nucleic acids and derivatives of these acids has stimulated great interest in the chemistry of such processes. The report by Rosenberg that some Pt(II) compounds show potent antitumor activity [1-3] and the subsequent discovery that nucleic acids are probably the prime site of action of such antineoplastic drugs [4,5], has contributed greatly to renewed interest in the coordination chemistry of platinum and related metals.

The subject of metal interactions with nucleic acids and their derivatives is vast, and a number of comprehensive reviews have appeared. The literature on metal binding that has been reviewed up to 1971 [6,7,8], makes little reference to the platinum group metals. However, Marzilli has compiled a much needed review of the subject and the interaction of platinum(II) and palladium(II) features predominantly [9].

This work is devoted to the study of some platinum(II) interactions with simple nucleosides and model systems thereof.

1.1 The Binding of Platinum(II) to Nucleosides and Nucleotides and Some Model Systems - A literature review

Following reports by Rosenberg on the antineoplastic activity of *cis*-$[Pt(amine)_2Cl_2]$ type complexes, but the apparent inactivity of the corresponding *trans*-analogues [3], the first attempt to rationalize the nature and sites of Pt(II) binding to nucleic acid bases involved U.V. spectroscopy [10]. Binding sites such as N(7) in guanosine and $NH_2(6)$, N(7)

chelation in adenosine were suggested, but more direct methods were required. Figure 1.1 shows the structure of and numbering convention used in common purine and pyrimidine nucleosides. On the other hand, there have been many studies involving the interaction of Pt(II) species with nucleic acids, specifically DNA and RNA [11-18]. Controversy exists as to the exact nature of Pt(II) binding to these nucleic acids. There is evidence for interstrand cross-linking [13], while the renaturing effects of *cis* and *trans* platinum(II) and (IV) compounds on calf thymus DNA suggests that cross-linking is not the primary mechanism of action of the anti-tumor platinum drugs [16]. In addition, there is evidence that the *cis*$[Pt(NH_3)_2Cl_2]$ drug bind preferentially to guanosine/cytosine rich DNA [14].

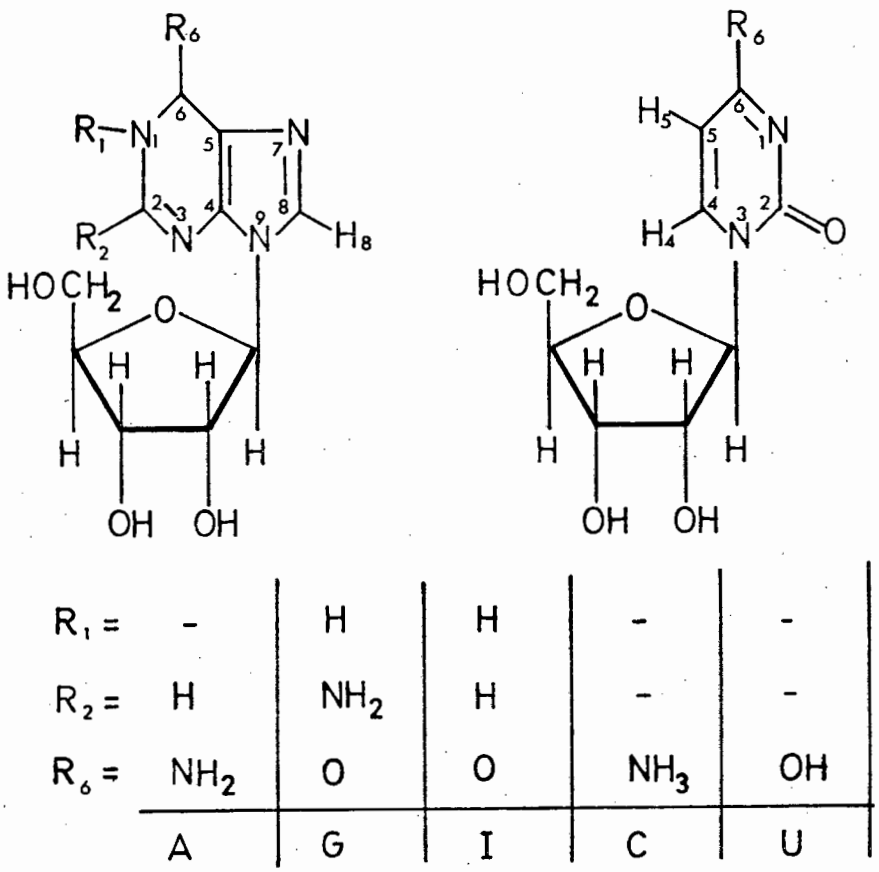

R_1 =	-	H	H	-	-
R_2 =	H	NH_2	H	-	-
R_6 =	NH_2	O	O	NH_3	OH
	A	G	I	C	U

Figure 1.1: The structure of and numbering convention used in common purine and pyrimidine nucleosides.

^{1}H n.m.r. studies have been applied successfully in determining the binding sites of Pt(II) to simple nucleosides. Several bis(nucleoside) complexes of Pt(II) have been prepared and investigated by ^{1}H n.m.r. [19-22]. In the case of guanosine, inosine and xanthosine the binding site of Pt(II) was found to be N(7), while in adenosine both N(1) and N(7) were postulated binding sites. The extent of binding of Pt(II) to N(1) and N(7) in adenosine was found dependent on the Pt:nucleoside ratio [20,21,22]. Pt(II) binding studies have been extended to nucleotides, but essentially the same mode of binding as for the corresponding nucleosides were invoked. There have been no reports of possible Pt(II) phosphate interaction in solution [23].

Palladium(II) has often been used as a model for the binding of Pt(II) in view of their similar chemistry [22,24,25,26]. Palladium complexes themselves have not been reported to show any significant antitumor activity. Use of Pd(II) as a model for Pt(II) has been primarily justified by the fact that Pd(II) reacts much more rapidly (several orders of magnitude) with nucleosides and their analogues [24,25]. Martin *et al* used ^{13}C n.m.r. to investigate the mode of binding of Pd(II) to cytidine, thymidine, uridine and guanosine. Assignment of binding sites was achieved by comparing complexation shifts induced with corresponding protonation shifts. Ettore *et al* has reported studies of the interaction of Pt(II) and Pd(II) with cytosine investigated by means of ^{1}H and ^{13}C n.m.r. [27]. These authors used DMSO as solvent and did not report any ^{195}Pt-^{13}C coupling constants. Other studies involving the interaction of Pd(II) with adenosine in DMSO solution have been reported, assigning binding sites of Pd(II) to N(1) and N(7) in adenosine [28]. In the case of guanosine in aqueous solution, definitive

evidence of O_6N_6 chelation of Pd(II) has been claimed [29].

In extensive studies involving Raman, ^1H and to a lesser extent ^{13}C n.m.r. spectroscopy Tobias *et al* have investigated the interaction of *cis*-diamine platinum(II) and ethylenediamine platinum(II) with inosine, guanosine, cytidine adenosine and uridine monophosphates as a function of the metal:ligand ratio and the pH [30-33].

Kong *et al* have investigated the interaction of *cis*-$[Pt(DMSO)_2Cl_2]$ with purine nucleosides in DMSO and have reported the formation of *trans*-$[Pt(DMSO)(N)Cl_2]$ which later isomerized to the *cis* isomer. The predominant binding site of Pt(II) was found to be N(7) [34]. These conclusions were reached by means of mainly ^{195}Pt-^1H coupling constants.

The interaction of Pt(II) with pyrimidine bases and nucleosides has been subject to much discussion, since aqueous solutions of complexes of Pt(II) and uracil, poly(U), thymine and other pyrimidine heterocycles are found to turn blue [9,31,35]. The exact nature of these 'platinum pyrimidine blues' remains unsettled although there is evidence that at least dinuclear complexes are involved which are paramagnetic [35]. These compounds are generally difficult to prepare and a lack of reproducability of method adds to the problem of characterizing their structure in detail.

Finally it should be mentioned that a number of crystallographic studies have been reported in which the molecular structures of *cis*-$[(NH_3)_2Pt(guanosine)]^{2+}$, *cis*-$[Pt(en)\ 5'\text{-CMP}\ ]_2$ and *cis*-$[Pt\ en(5'\text{-IMP})_2]^{2-}$ have been determined [36]. The structure of *cis*-$[Pt(en)5'\text{-CMP}\ ]_2$ is

particularly interesting since it represents an example of phosphate binding to platinum [37]. Furthermore the structural properties of relatively complex nonstoichiometric compound involving Pt(II) bound to inosine 5'-monophosphate has been reported in which binding of Pt(II) is via N(7), while the coordination geometry of platinum(II) is essentially normal square planar [38].

On consideration of the numerous studies involving the interaction of platinum with nucleosides, nucleotides and model systems, it is evident that nuclear magnetic resonance studies have ranked highly in the assignment of binding sites in solution. Of particular use has been the 34% abundant platinum-195 nucleus which has nuclear spin $\frac{1}{2}$. The resultant spin-coupling to other easily observable (spin $\frac{1}{2}$) nuclei has been of great value in understanding the chemistry of such systems. Additionally platinum often forms non-labile bonds with other atoms such as C, N, O, P and others [26], which renders such systems ideally suitable for nuclear magnetic resonance studies. In this light it is perhaps surprising that not more other than proton nuclear magnetic resonance studies have been undertaken. Those reports of the use of ^{13}C n.m.r. have not recorded any ^{195}Pt-^{13}C coupling constants [22,27,31]. Martin *et al* have published a ^{13}C n.m.r. investigation of some platinum pyridine and bipyridyl complexes [39]. Only $^{3}J_{^{195}Pt-^{13}C}$ coupling constants were reported (42-43 Hz) for the pyridine complexes, while for bipyridine ^{2}J (30-34 Hz) and ^{3}J (30-33 Hz) coupling constants were observed. These authors concluded that a lack of easy discrimination among two and three bond coupling "may hinder their diagnostic use in identifying carbons in some types of aromatic ligands". Subsequently, Vrieze has reported an investigation of the bonding properties of

trans-[$PtCl_2XY$] where X = C_2H_2, CO and Y = 4-substituted pyridines [40]. In this report ^2J (~11 - 14 Hz), ^3J (~32 - 34 Hz) and ^4J (~6 - 8 Hz) platinum-195 to carbon-13 couplings were reported. Recently a ^1H n.m.r. study of platinum N-methylimidazole complexes appeared, but the authors encountered solubility problems and were unable to record ^{13}C n.m.r. spectra [41].

Finally, attention must be drawn to the fact that ^{13}C n.m.r. assignments based purely on 'complexation shifts' should always be treated with circumspect following reports that both anions and cations produced complicated shift trends in the ^{13}C resonances of molecules such as cytidine and guanosine in DMSO solution [42]. Diamagnetic shifts due to Mg^{2+}, Ca^{2+}, Sr^{2+} and Ba^{2+} are expected, but the observation that the chlorides, bromides and iodides of these cations all result in substantially different shifts is at first quite unexpected.

1.2 Objectives of Research

It is apparent from the previous section that there is a considerable lack of ^{13}C n.m.r. data about platinum(II) complexes involving coordination through nitrogen. The potential use of ^{15}N and ^{13}C n.m.r. is relatively easy to see for molecules such as the purine and pyrimidine nucleosides considering their structure. ^1H n.m.r. spectroscopy is limited by a lack of protons in many cases. Additionally $J_{^{195}Pt-^1H}$ coupling constants are often too small to be resolved. The ^{13}C nucleus resonates over a range of *ca* 600 ppm and $^1J_{^{195}Pt-^{13}C}$ coupling constants can be as large as 600 Hz. Such considerations render the additional time that is generally needed to obtain suitable ^{13}C n.m.r. parameters often well spent

in view of additional structural information that may be forthcoming.

The objectives of this work may be stated as follows:

(i) The preparation of simple nitrogen 5- and 6-membered heterocycle platinum(II) complexes as models for the interaction of Pt(II) with nucleic acids. These include complexes of imidazoles, substituted pyridines, and pyrimidines.

(ii) The examination of ^{1}H and particularly ^{13}C n.m.r. shift and coupling parameters of these model compounds.

(iii) The preparation and examination of some platinum(II) nucleoside complexes by means of ^{1}H and ^{13}C n.m.r. with the view to obtaining definitive ^{13}C spectral parameters.

PART II

CHAPTER II : THEORY AND METHODS

THEORY

The general principles of the magnetic resonance experiment have already been referred to in the first part of this work. These principles are similar for all nuclei with spin $\frac{1}{2}$ and will not be discussed in any detail here (see reference [19-24] in part I of this work). As a result of differing gyromagnetic ratios for spin $\frac{1}{2}$ nuclei and often low natural isotopic abundance, most other than ^{1}H nuclei have a much lower sensitivity at natural abundance. Consequently the development of direct observations of these nuclei depended largely on the availability of more powerful instrumentation, the most dramatic development having been the development of pulsed Fourier Transformation methods. (References [23,24] part I). A brief discussion of some aspects peculiar to ^{13}C n.m.r. will be presented here. More comprehensive accounts of the subject may be obtained in text-books by Stothers [43], Axenrod and Webb [44] and Levy [45]. An excellent account of some experimental Fourier Transform n.m.r. procedures is given by Müllen and Pregosin [46].

2.1 Carbon-13 N.M.R. Spectroscopy

In a given sample of carbon containing material, the natural abundance of the ^{13}C isotope is *ca* 1.1%, the remaining carbon being the ^{12}C isotope. Only the ^{13}C nucleus has spin quantum number $\frac{1}{2}$. Table 2.1 compares some properties of the ^{13}C nucleus with the ^{1}H nucleus. It is evident from table 2.1 that the inherent sensitivity of the ^{13}C nucleus is much lower than for ^{1}H, and when the isotopic abundance is taken into account it becomes much more difficult to observe a ^{13}C n.m.r. spectrum of reasonable signal to noise (S/N) ratio. However as a result of vast

Table 2.1: A comparison of some properties of the ^{1}H and ^{13}C nuclei.

Property	^{1}H	^{13}C
Natural Abundance	99.98%	1.108%
C yromagnetic ratio/M Hz Tesla^{-1}	10.705	42.577
Resonance frequency/M Hz (at 2.114 Tesla)	90.00	22.63
Relative sensitivity (S)*	1.00	1.59×10^{-2}
Sensitivity at natural abundance	1.00	1.72×10^{-4}
Typical T_1/sec	up to 10	1 - 100

* at constant field for equal number of nuclei.

improvements in instrumentation, ^{13}C n.m.r. spectroscopy has become routinely available in laboratories. This is primarily as a result of various techniques which may be employed to improve the gain in sensitivity of between 10^4-10^6. Most commonly, for ^{13}C n.m.r. spectroscopy at natural abundance the following gains are achievable:

(1) Pulsed Fourier methods, gain *ca* 25 (gain = $\sqrt{R/\Delta\nu_{\frac{1}{2}}}$ where R is the range of chemical shift and $\Delta\nu_{\frac{1}{2}}$ is the typical line width in Hz).

(2) Larger sample tubes, e.g. 10 mm tubes result in gain *ca* 4 (gain $\propto$ radius^2).

(3) Spectral accumulation, gain $\propto \sqrt{\text{time}}$ (e.g. 24h represents a gain of *ca* 37).

(4) Double resonance, results in gain of *ca* 2 if multiplets collapse (due to $^{13}C\{^{1}H\}$ decoupling). A further maximum gain of *ca* 2.9 is achievable due to the Nuclear Overhauser effect (see below).

Taken together these gain improvements compensate greatly for the low sensitivity of the ^{13}C nucleus so that the advantages of ^{13}C n.m.r. over ^{1}H n.m.r. may more often than not be readily exploited.

At this point, some aspects of the relaxation behaviour of the ^{13}C nucleus may be pertinent. The basic principles and definitions of spin-lattice (T_1)/spin-spin (T_2) relaxation times have already been given in part I, section 2.1 of this work. A principle source of ^{13}C relaxation lies in intramolecular dipole-dipole interactions between carbon and neighbouring protons. It will be recalled from section 2.1 (part I), that the fluctuating magnetic field $\bar{B}_{loc}$ depends inversely on r^3 and directly on θ, the internuclear vector and angle between this vector and the external field respectively. One or more protons directly attached to the carbon-13 atom in question thus provide an efficient means of relaxing the ^{13}C nucleus. These predictions are experimentally well substantiated by the observation that typical T_1 values are generally in the order of primary > secondary > quaternary (with no hydrogen atoms attached) carbon atoms [47,48].

There are a number of other relaxation mechanisms that contribute to the overall T_1 relaxation times of ^{13}C nuclei. Experimentally however, it has been found that most ^{13}C nuclei in organic molecules are predominantly, if not exclusively, relaxed by the dipole-dipole mechanism. The remaining

relaxation mechanism have been mentioned previously, but at the risk of repetition of (ii) the spin-rotation (iii) the chemical shift anisotropy (iv) the scalar coupling and (v) the quadrupolar relaxation mechanisms.

A knowledge of the T_1 relaxation time is important not only in the assignment of ^{13}C resonances but has important practical implications, particularly if efficient use of the spectrometer is desired.

2.2 Some Double Resonance Techniques and the Nuclear Overhauser Effect

Double resonance techniques play an extremely important role in most n.m.r. spectroscopy. One of the fundamental aspects of spectrometer operation in which the magnetic field is stablized, involves a double resonance experiment. Suppose the sample is irradiated with two frequencies ν_1 and ν_2, then two resonance conditions will be satisfied at constant B_o. If one of these resonances is monitored, one effectively also monitors B_o. Thus if drifting in B_o occurs, then this may be detected by a drift in the signal ν_2, which may be set up to cause a small 'correction current' to be applied to the magnet control circuitry thus returning the magnetic field to its original B_o value.

Hence drifting in B_o is effectively corrected by means of 'locking' the spectrometer onto a particular resonance frequency in the sample. Locking results in a much more stable and homogeneous magnetic field, a necessary prerequisite for the observation of sharp resonance lines in high resolution n.m.r. experiments. Commonly the spectrometer 'locks' onto a deuterium signal present in the molecules of solvent.

Decoupling Techniques

In the observation of ^{13}C magnetic resonance the ^{13}C nucleus is nearly always coupled to protons. These proton coupled spectra are often very complex, while a loss in sensitivity of between 3-6 commonly occurs. The use of spin decoupling techniques often greatly simplifies the ^{13}C n.m.r. spectrum, as well as resulting in an overall gain in sensitivity. Suppose a ^{13}C signal is spin coupled to a proton, resulting in a doublet of coupling constant, J_{CH}. If the region in which the proton resonates is irradiated with frequency, ν_2 transitions so induced affect the ^{13}C part of the spectrum in a manner that depends on the exact value of ν_2 and its 'power'. The power is measured in terms of the associated magnetic field so induced, $\gamma B_2/2\pi$, while the effect on the ^{13}C spectrum depends on relative values of $\gamma B_2/2\pi$ and J_{CH}. In general, these double resonance experiments are described by the symbolism $^{13}C\{^1H\}$, where the brackets denote the nucleus perturbed and ^{13}C the nucleus observed. The various decoupling experiments are generally classified according to the value of $\gamma B_2/2\pi$ as follows:

1)	$\gamma B_2/2\pi >> J_{CH}$	spin decoupling, causing collapse of multiplets connected to or close to ν_2
2)	$\gamma B_2/2\pi \simeq J_{CH}$	selected spin decoupling
3)	$\gamma B_2/2\pi \simeq \Delta\nu_{\frac{1}{2}}$	spin tickling experiment ($\Delta\nu_{\frac{1}{2}}$ line width at half height)
4)	$\gamma B_2/2\pi << J_{CH}$	measurement of Nuclear Overhauser Effect, (proton resonance saturated).

To effect complete decoupling of a ^{13}C spectrum, experimental problems in irradiating a large frequency range simultaneously are overcome by a technique in which the decoupling field is applied pseudo-randomly using a pulse-shift generator, which generates all the necessary frequencies from a single continuously generated frequency. This procedure is called

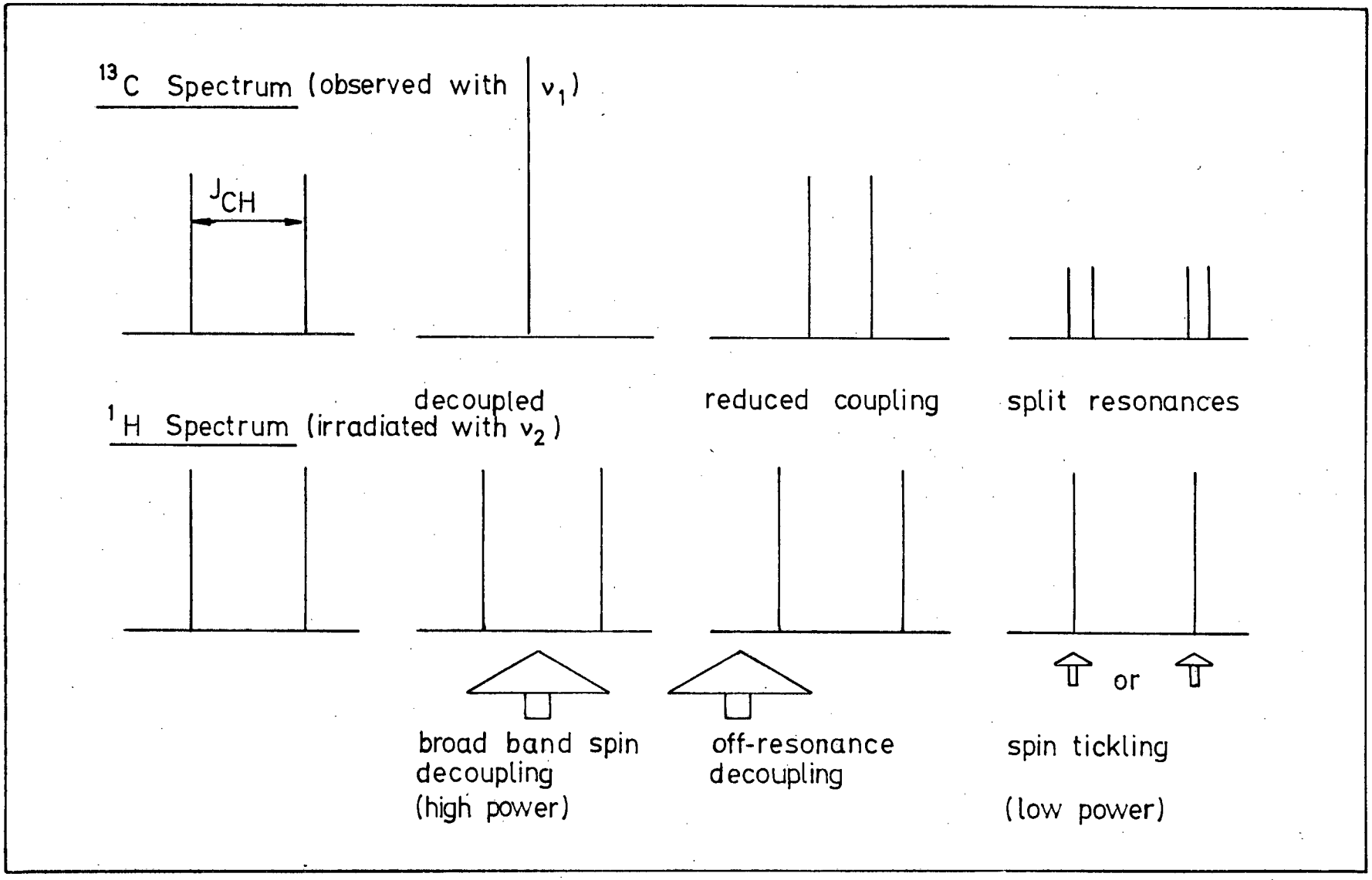

Figure 2.1: A schematic representation of some double resonance techniques

broadband decoupling and results in complete proton decoupling of a ^{13}C spectrum if the irradiation frequency ν_2 is placed in the centre of the proton spectrum. A useful alternative is the so called "off-resonance" broadband decoupling in which ν_2 is placed somewhere "off centre" of the proton spectrum. This mode of decoupling removes all long range $^{n}J_{CH}$ (n>1) coupling, and reduces the value of $^{1}J_{CH}$ somewhat. Consequently one can easily distinguish between methine (CH), methylene (CH_2) and quaternary carbon atoms, greatly assisting assignment of ^{13}C spectra. Figure 2.1 shows some double resonance techniques schematically.

Nuclear Overhauser Enhancement [49]

The Nuclear Overhauser Enhancement (NOE) results in a signal intensity improvement of a ^{13}C resonance under conditions of broadband $^{13}C\{^{1}H\}$ decoupling. This signal enhancement originates in changes in the spin populations of the energy levels of such a system, and is operative if predominantly dipole-dipole spin-lattice relaxation takes place between the two nuclei; all other relaxation mechanisms tend to oppose it. Figure 2.2 shows the energy level diagram of a CH resonance system, in which the relative populations of levels 1-4 are given by n_1-n_4 respectively. The transition probabilities are labelled W_1^C and W_1^H, representing single quantum transitions between the various levels. In addition W_0 and W_2 represent a zero quantum transition (adiabatic energy exchange) and a two quantum transition respectively. The latter probability has been shown to depend solely on a dipole-dipole spin-lattice relaxation (T_1^{DD}) mechanism.

Under conditions of a decoupling experiment the populations n_1 and n_3 are increased at the expense of n_2 and n_4 since the irradiation of the ^{1}H

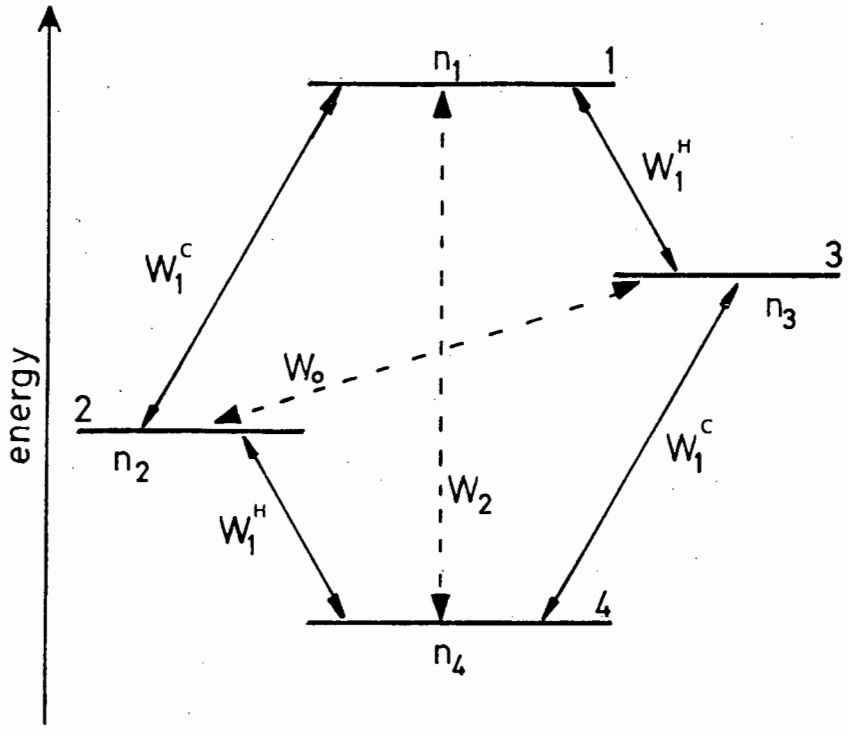

Figure 2.2: The energy level diagram of an AX spin system showing transition possibilities.

spectrum would saturate the transitions 2 ↔ 1 and 4 ↔ 3. However due to (T_1^{DD}) processes the probability W_2 would tend to increase the population n_4 at the expense of n_1 (this follows from the fact that $W_2 = 3(5T_1^{DD})^{-1}$. A greater net difference results between the lower and higher energy levels for the ^{13}C nucleus than the equilibrium (undecoupled condition) Boltzman distribution requires. Hence a signal enhancement is observed. It may be shown that if only (T_1^{DD}) processes occur then the nuclear Overhauser enhancement is given by:

$$NOE = 1 + \frac{W_2 - W_0}{2W_1^C + W_2 + W_0}\left[\frac{\gamma_H}{\gamma_C}\right] \qquad (2.1)$$

Under conditions of extreme line narrowing (applicable in most solutions of small molecules), this signal enhancement reduces to

$$NOE = 1 + \frac{\gamma H}{2\gamma_C} \qquad (2.2)$$

For a ^{13}C nucleus coupled to a proton the maximum NOE = 2.988. Such an enhancement has indeed been observed for a molecule like formic acid [46,49]. It should be noted that although the (T_1^{DD}) relaxation processes are dependent upon the internuclear distance, r, the NOE is not.

2.3 Some Aspects of Chemical Shifts and Spin-Spin Coupling

Detailed discussion of the origins and theories of chemical shifts and spin-spin couplings are well beyond the scope of this work. Recently substantial reviews of the subject have appeared [50,51]. In this section only a brief resumé of the terms in which shifts and coupling constants may be understood will be presented.

Chemical Shifts [43,50]

To achieve resonance condition any nucleus i requires a magnetic field B_i, which at a particular irradiating frequency $\neq B_o$. This is given by

$$B_i = B_o (1 - \sigma_i) \qquad (2.3)$$

where σ_i is the screening constant, which is a function of the chemical environment of the nucleus in question. In general σ_i is considered to be composed of a number of separate terms. The total screening constant is considered as a sum of 'local' terms. Hence

$$\sigma = \sigma_d + \sigma_p + \sigma' \qquad (2.4)$$

Here σ_d is the *diamagnetic shielding constant* which is generally positive, dependent upon the field induced electron circulation at the nucleus. For ^{13}C nuclei σ_d represents generally a small (few ppm) contribution to the overall shielding experienced. Electron withdrawing or donating groups in a molecule may be naïvely considered to effect σ_d by distorting the symmetrical electron distribution at the nucleus.

The *paramagnetic* term σ_p originates in the mixing of ground and excited electronic states induced by the external magnetic field. It cannot be adequately represented in classical terms rendering its evaluation complex, but σ_p is generally negative, resulting in low field shifts. *s*-electrons cannot contribute to it since they have zero orbital angular momentum but *p*- and *d*-electrons contribute strongly to σ_p, since their distribution is anisotropic. In general σ_p is the dominant contribution to chemical shifts of nuclei other than ^1H and is much larger (100 - 10000 ppm) than σ_d. σ_p depends primarily on three factors (for ^{13}C nuclei):

(i) the average excitation energy, ΔE, which replaces the unknown energies of all the excited states.

(ii) the atomic 2*p*-orbital dimensions, $\sigma_p \propto \langle r^{-3} \rangle_{2p}$

(iii) a term dependent on the charge densities of the 2*p* orbitals and the bond order of the bonds to the nucleus in question by the other atoms. (This term appears only to be significant if *both* σ and π bonds exist between the atoms in question [43].)

The third contribution to the chemical shift, σ', comprises only neighbour atom effects as (i) the anisotropy effect of groups such as phenyl, carboxy, alkenyl and alkynyl groups (very significant in ^1H n.m.r.), (ii) electric field effects (due to the presence of strongly polar groups), (iii) unpaired electron effects (such as the presence of a free radical or paramagnetic ion) and (iv) solvent effects. In general however, these effects are fairly small compared to the σ_p and σ_d contributions to the overall shift of a ^{13}C nucleus.

Spin-Spin Coupling

Two nuclei N and N', both of spin quantum number $\frac{1}{2}$, possess magnetic moments which may interact as magnetic dipoles. Such interaction is

understood in terms of the classical $(3\cos^2\theta-1)/r^3$ expression, where θ is the angle between their internuclear vector and the external magnetic field B_o. This interaction is termed the direct dipole-dipole interaction, applicable generally only in the solid or 'partially orientated' state of molecules containing the nuclei N and N'. In solution where rapid tumbling of molecules occurs, this direct dipole-dipole interaction averages to zero. It is generally observed that a further so-called indirect spin coupling interaction takes place. This indirect interaction is believed to be transmitted *via* magnetic polarization of electrons, to the respective nuclei. Spin-spin coupling constants are characterized by two important features, their sign and magnitude. Spin coupling constants are regarded as positive if the interaction leads to a lower energy state involving anti-parallel spins; on the other hand, if the lowest energy state involves parallel magnetic moments, then the coupling constant is regarded as negative. It should be noted however that the resulting spectrum is not dependent on the sign of J but depends only on $|J|$; two lines occur if $|J|>0$ if only a two spin system AX is considered. Figure 2.3 shows energy level diagrams for a two spin system coupled and uncoupled.

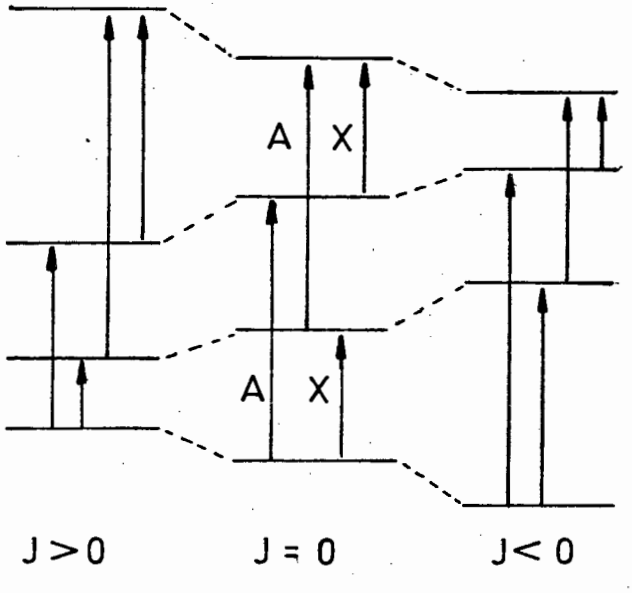

Figure 2.3: Energy level diagram for a two spin system coupled and uncoupled.

In general *absolute* sign determinations are very difficult to make, while *relative* signs generally involve the presence of a third I>0 nucleus. The spectra observed in practice are however unaffected by sign changes.

According to current theories concerning the nature of the indirect spin coupling, the observed (field independent) coupling constant is composed of three terms. Thus

$$J_{NN'} = J^{1a}_{NN'} + J^{1b}_{NN'} + J^{2}_{NN'} + J^{3}_{NN'} \qquad (2.5)$$

where $J_{NN'}$ is the indirect coupling constant between two nuclei N and N' measured in Hz. More generally, a reduced coupling constant $K_{NN'}$ may be defined such that it is independent of the gyromagnetic ratios of the participating nuclei. Hence

$$K_{NN'} = \frac{2\pi}{h} \gamma_N \gamma_{N'} J_{NN'} \qquad (2.6)$$

This definition is introduced for the sake of simplicity in the theoretical calculations and need not be discussed any further here.

The various terms contributing to the coupling constant $J_{NN'}$ as set out in equation (2.5) arise as follows:

(i) $J^{1}_{NN'}$, the orbital-dipole contribution, arises from the interaction of orbital electronic currents with the nuclear moments. Each nuclear moment induces electronic currents in the orbitals, which in turn induce secondary magnetic fields affecting the other nucleus. (This contribution consists of two terms J^{1a} and J^{1b}).

(ii) The second term $J^2_{NN'}$, is due to a dipole-dipole interaction between the nuclear and electronic magnetic moments. This term applies to electron density *outside* the nucleus, i.e. those electrons that have no finite probability of being at the nucleus. Thus only *p*- and *d*-electron density contributes to this term. It might therefore be expected that coupling which involves π bonds to contribute significantly to the observed coupling constant *via* this term.

(iii) The third term in equation (2.5) is generally considered the most important coupling mechanism. This contribution is known as the Fermi-contact term and involves the interaction of nuclear and electronic magnetic moments *at* the nucleus. Hence only *s*-electrons can contribute to this term, and it might be expected that the *s*-character of the bonding orbitals (between two coupling nuclei) would be reflected in the coupling constant observed. Numerous such correlations have been observed, for instance between J_{CH} and C-H internuclear distances or the bond type between two carbon atoms and J_{CC} values [43, and references therein]. These correlations are nevertheless only gross effects, since many more subtle effects occur that are much less readily understood.

What appears to have been firmly established is that the Fermi-contact term is seen to dominate at least one bond coupling constants, $^1J_{CX}$. To give an example as to the extent of such dominance, Table 2.2 gives some results obtained by SCF perturbation theory calculations of $^1J_{CX}$ coupling constants [51]. It may be seen that in all cases the Fermi-contact term appears to be dominant. Further, if $^1J_{CX}$ coupling to heavy

Table 2.2 : Some calculated and experimental coupling constants from reference [51].

Molecule	Calculated J_{CX}/Hz				Observed J_{CX}
	Fermi-Contact	Orbital-Dipole	Spin-Dipole	Total	
$C_6H_5C^*{\equiv}C^*H$	134.41	22.01	8.04	164.46	175.9
$NC^*{-}C_6{}^*H_5$	77.94	-2.38	0.46	76.02	80.3
$H_2C^*{=}C^*HCN$	69.99	-18.39	3.91	55.18	70.6
C_6H_6	64.34	-12.83	1.59	53.10	57.0
$B^*{-}(C^*H_3)_3$	42.2	-	-	42.2	46.7
$C^*H_3{-}N^*H_2$	-4.6	-	-	-4.6	±7
$F^*{-}C^*H_2CN$	-173.29	-31.42	+35.59	-169.12	-172

* indicates the nuclei coupled.

metals is considered using only the Fermi-contact term, then the agreement between experimental and calculated coupling constants compels one to admit Fermi-contact dominance [52].

Substituent effects on $^1J_{CX}$

Consideration of the contact term shows that for two nuclei joined by a σ bond show a coupling constant such that

$$J_{CX} \propto h\gamma_C\gamma_X\alpha_C{}^2\alpha_X{}^2\ \psi_C{}^2(0)\psi_X{}^2(0)\Delta E^{-1} \qquad (2.7)$$

where α^2 is the *s* character of the bonding orbital

$\psi^2(0)$ is the spin density of the nucleus of the valence *s* electrons

ΔE^{-1} is the average excitation energy.

Qualitatively speaking $^1J_{CX}$ depends primarily upon the hybridisation of the

bond between the coupled nuclei, as well as the residual electron density at the nucleus. An electronegative substituent is seen to alter the *s* character of the bond between the coupling nuclei. In general it has been observed that the larger the electronegativity, the larger $^1J_{CH}$ (for example, $^1J_{CH}$ = 125 Hz in methane but 149 Hz in methyl fluoride). In addition to changes in the hybridisation induced by electronegative substituents, a bond polarisation also takes place. The electron withdrawing group is expected to reduce the electron density at the carbon nucleus, resulting in an increased effective nuclear charge. This in general leads to an increase in $\psi_c^2(0)$ and thus ^1J. Which of these two effects is dominant is not clear since they both operate in a similar sense, but the important point is that both changes in the bond order as well as electron density at the coupled nuclei are operative [43].

Substituents have been empirically classified in terms of an inductive electron withdrawing/releasing effect characterised by a σ_I parameter and a resonance parameter R^n (which can be similarly electron releasing or withdrawing). Table 2.3 summarises these effects in terms of modified Swain-Lupton substituent constants [53,54].

Table 2.3: Swain-Lupton substituent constants from reference [54].

Substituent	σ_I	R^n	Substituent	σ_I	R^n
$N(CH_3)_3^+$	1.00	0	OCH_3	0.27	-0.40
±	0.50	-0.42	CN	0.56	0.05
Cl	0.46	-0.28	NO_2	0.65	0.03
Br	0.44	-0.24	NH_2	0.12	-0.38
I	0.39	-0.16	$COCH_3$	0.28	0.18
CH_3	-0.04	-0.06	CO_2CH_3	0.30	0.09

A considerable number of empirical correlations between ^{13}C shieldings and to a lesser extent coupling constants have been demonstrated in terms of such substituent constants [43,53,54,55]. The theoretical framework for such effects is however very complex and only in its embryonic stages but some of the underlying principles involved have recently been reviewed [55]. Further discussion on the theoretical aspects of substituent effects on spin coupling constants and chemical shifts will nevertheless be out of context here.

METHODS

2.4 Some Practical Aspects of ^{13}C n.m.r. Spectroscopy

It may be pertinent at this stage to mention some aspects concerning spectrometer operation involved in ^{13}C n.m.r. spectroscopy. The discussion here will be limited to Fourier Transform methods and no attempt will be made to cover the subject comprehensively, since excellent textbooks are available in this regard [46, and references 23, 24 in part I of this work].

In order to obtain ^{13}C spectra efficiently it is necessary to optimize factors such as (i) the spectral width and offset to be used, (ii) the pulse width, (iii) selection of memory size (which determines the acquisition time), (iv) the selection of the decoupling mode, (v) the delay before the next cycle starts, (vi) the number of transients required for an acceptable S/N ratio and (vii) mathematical manipulation of the data to improve S/N or resolution. In practice the most critical parameters to optimize are the pulse width and cycle repetition time. This is because in any given sample the various T_1 relaxation times are often very different for each type of carbon atom that may be present. If, for a repetitive experiment, the initial pulse angle is too large (say 60^{o}-90^{o}), while the acquisition time, t_{acq} is short, then all carbon resonances with relatively long T_1 values will become saturated with a consequent dramatic reduction of the signal intensity. Since in general most ^{13}C spectra are recorded over *ca* 6000 Hz at 8K memory storage size (8192 data points), t_{acq} is 0.682 seconds. This is far too short to allow adequate relaxation of typical tertiary aromatic carbons (which have T_1 values from 20-100 sec [46]). In such circumstance it is more profitable to use a much smaller pulse angle

(say 30^0-45^o) and place a delay between each subsequent experiment. If the longest T_1 values are known it is possible to use the theoretical optimum Ernst angle, given by

$$\cos \alpha_E = \exp [-(T_p/T_1)] \qquad (2.8)$$

T_p is the total cycle time for one experiment

T_1 is the longest T_1 value present.

The uncertainty in T_1 values may however, often prevent optimum conditions to be established at the first attempt.

A very effective way of reducing the spin-lattice relaxation time of all the carbon atoms present lies in the use of paramagnetic ions. These are generally introduced in the form of an inert complex, such that molecular association between molecules is negligible. The most commonly employed 'shiftless relaxation reagents' are tris(acetylacetonato)-chromium(III) or the corresponding Fe(III) compound [46]. In this work both $Cr(acac)_3$, soluble in organic media, and a water soluble gadolinium triethylenetetraaminehexaacetate, Gd(TTHA) [56], have both been used successfully. In general these relaxation reagents allowed the use of pulse angles up to 50^o and t_{acq} = 0.682 sec. This amounted to halving total accumulation time to *ca* 3.8 h for a typical 20000 transient accumulation. Normally the data was multiplied by an exponential S/N enhancement factor such that LB = 1, i.e. an artificial line broadening of *ca* 1 Hz resulted.

2.5 Experimental Procedure

^{13}C n.m.r. spectra were obtained on a Brucker WH-DS90 spectrometer operating at 22.63 M Hz (2.118 Tesla), using 10 mm sample tubes. In general always internal lock and reference substances were used; normally

a 50% mixture of the $^2H_2O/H_2O$ solvent system was employed. In the case of carbon containing solvents, purely deuterated solvent was used to minimize the solvent resonance peak. In aqueous media p-dioxane was the preferred internal reference substance. Shifts are quoted relative to TMS converted using the relations [43]:

$$\begin{aligned} \delta(TMS) &= \delta_{diox} - 67.7 \text{ ppm} \\ \delta(TMS) &= \delta_{DMSO} - 40.4 \text{ ppm} \end{aligned} \qquad (2.9)$$

Depending upon the solubility of the various complexes studied, between 5000 and 70000 transients were generally found necessary. As already mentioned shiftless relaxation reagents were employed in most cases at a 0.05 M concentration level. Consequently a 45^o-50^o pulse was used at a cycle repetition time equal to the acquisition time. Unless otherwise stated all spectra were measured at ambient temperature, *ca* 303 K. Chemical shifts are estimated correct to ±0.1 ppm, while coupling constants are estimated accurate to ± 1 Hz.

^1H n.m.r. spectra were obtained on a CW Varian XL-100 100 M Hz spectrometer, chemical shifts are quoted relative to TMS or DSS and are considered accurate to ± 0.05 ppm, while coupling constants are estimated to ± 0.5 Hz.

Imidazoles, pyrimidines, 3-substituted pyridimes and nucleosides that were commercially available (ICN, K and K laboratories, Sigma Chemical Company, Aldrich Chemicals and Merck) were used without further purification. $K_2[PtCl_4]$ was supplied by Johnson Mathey (London), while in general high quality standard laboratory reagents were used.

Microanalysis (%C, %N, %H) was performed at the University of Cape Town

Microanalysis Laboratory. All compounds were analysed for purity in this way and in general a deviation of 0.5%C, N and 0.25% H from expected values proved to be acceptable for the purposes of this work, since no significant impurities could be detected by either ^{1}H or ^{13}C n.m.r. spectroscopy.

2.6 Preparation of cis-$[Pt(NH_3)_2Cl_2]$

A slight variation of the published method of preparation [57] produced a better yield. A solution of 100 mmol (41.5g) $K_2[PtCl_4]$ in 500 cm^3 water containing 25 cm^3 conc. HCl was treated with 30g NH_4Cl, followed by the dropwise addition of *ca* 100 cm^3 3M aqueous ammonia until the solution was neutral to litmus. A further 200 mmol NH_3(aq) (67.5 cm^3 3M solution) was then added, the mixture stirred for 3h at room temperature. On refrigeration for 48 h the precipitate was filtered off and redissolved in 850 cm^3 0.1 M HCl. Filtration of the hot yellow solution conveniently separates insoluble green tetraamineplatinum(II) tetrachloroplatinate(II). Cooling the filtrate affords 21.5 g yellow needles (70 % yield), which were shown to be the *cis-*$[Pt(NH_3)Cl_2]$ by the Kurnakov test [58] (yellow tetrakis(thiourea)platinum(II) needles were formed). Microanalysis data is collected in Table 3.4.

2.7 Preparation of cis-$[Pt(NH_3)_2(X)_2]Cl_2$ *where X = imidazoles, nucleosides*

Typically a 2 mmol (600 mg) portion of *cis-*$[Pt(NH_3)_2Cl_2]$ dissolved in 50 cm^3 H_2O was warmed to *ca* 335 K, while stirring the solution magnetically. A 4.01 mmol portion of the imidazole or nucleoside dissolved in a

minimum of water was added to the yellow solution of *cis*-$[Pt(NH_3)_2Cl_2]$. The mixture, protected from light, was stirred for a further 2 h at 335 K, at which time the yellow colour had generally been discharged. Furthermore, conductivity measurements showed no further significant increase in solution conductance. This was taken to indicate the reaction end-point.

Isolation procedure depended on the nature of the various compounds produced. In general for the nucleoside complexes, which are much less water soluble than the imidazole compounds, the solution volume was simply reduced upon which white to cream coloured precipitates were formed. This was washed with 5 cm^3 portions of cold water, ethanol, collected, recrystallized from water-ethanol mixtures and dried.

The imidazole complexes were much more water soluble and were consequently isolated and purified as follows. The complex solution was evaporated to dryness under vacuum using a Buchi Rotorvapor apparatus. This was followed by anhydrous diethyl ether extraction of any uncoordinated imidazole, and recrystallization from ethanol/acetone/diethylether mixtures. It was found convenient to collect the imidazole complexes in an anhydrous N_2 atmosphere, as these tend to be hygroscopic and often form a 'syrup' by just sucking air through them.

After drying at *ca* 335 K under vacuum in a desiccator, the compounds were checked for purity by microanalysis (see Table 2.4).

2.8 Preparation of cis-[Pt(Nucleoside)$_2$Cl$_2$] where nucleoside = inosine and guanosine

These complexes were prepared according to the procedure of Theophanide [59]. Briefly, 500 mg $K_2[PtCl_4]$ dissolved in 5 cm^3 H_2O was added to 10 cm^3 of an aqueous solution of *ca* 1.7 g NaCl and a stoichiometric quantity of inosine or guanosine. On standing for 3 days in the dark, the water was evaporated.

Dimethylformamide (5cm^3) dissolved the complex thus separating the NaCl. An excess ethanol added to the DMF solution precipitated the complex, which was washed several times with ethanol, dried and microanalysed. Yields were *ca* 90% in both cases. Found for inosine 3.1 % H, 28.0 % C, 12.7 % N, while *cis*-[Pt(inosine)$_2$Cl$_2$] requires 3.0 % H, 29.9 % C, 13.9 % N. Found for guanosine 3.1 % H, 28.1 % C, 16.0 % N, and *cis*-[Pt(guanosine)$_2$Cl$_2$] 3.1 % H, 28.8 % C and 16.8 % N.

Preparation of *cis*-[Pt(DMSO)$_2$Cl$_2$]

To 3 mmol (1.25 g) $K_2[PtCl_4]$ dissolved in 10 cm^3 water, 9 mmol (700 mg) dimethylsulphoxide (DMSO) in 2cm^3 H_2O were added. The solution rapidly changed colour from red to yellow, and on standing for 3 days in the dark, yellow needles were collected by filtration, washed with two 5 cm^3 portions water and dried (yield was 87%). Microanalysis gave 2.9 % C, 11.5 % H while $PtC_4H_{12}O_2S_2Cl_2$ requires 2.9 % C, 11.4 % H.

2.9 Preparation of cis-[Pt(NH$_3$)(H$_2$O)$_2$](ClO$_4$)$_2$

A stoichiometric quantity $AgClO_4$ was added to a 10 mmol (3.0g) portion $[Pt(NH_3)_2Cl_2]$ dissolved in 100 cm^3 water, protected from light. The

mixture was stirred for 2 h at *ca* 353 K, cooled and filtered through fine Whatman No. 542 paper. The colloidal filtrate was then centrifuged at 20000 r.p.m. for 20 mins. The clear, pale yellow solution was finally filtered through a small quantity of active charcoal to remove last traces of solid AgCl.

Evaporation of excess water under reduced pressure yielded yellow, hygroscopic *cis*-$[Pt(NH_3)_2(H_2O)_2](ClO_4)_2$. This substance was stored under N_2 below 273 K, in view of a tendency to decompose if kept otherwise (material blackens).

2.10 Preparation of cis-$[Pt(NH_3)_2(X)_2](ClO_4)_2$ where X = 3-substituted pyridines, some pyrimidines, and selected nucleosides

A 1 mmol portion *cis*-$[Pt(NH_3)_2(H_2O)_2](ClO_4)_2$ dissolved in 1 cm^3 water was added to 2 mmol of the heterocyclic base dissolved in 3 cm^3 water. Stirring for 2h at *ca* 335 K in the dark completed reaction as shown by conductivity measurements. On evaporation of excess water the crystalline substance was extracted with 30 cm^3 anhydrous diethylether (to remove uncoordinated heterocycle), collected by filtration (under dry N_2 if necessary). The dried complex represented a yield of between 60-80%. Microanalysis data are collected in Table 2.4.

2.11 Preparation of 4(5)-bromoimidazole [60,61].

Synthesis of tribromo imidazole

A solution of 36 mmol (2.5 g) imidazole in 200 cm^3 chloroform in a round bottomed flask, equipped with a magnetic stirring device was brominated by the dropwise addition of 6 cm^3 Br_2 in 50 cm^3 chloroform. The reaction

was kept cooled in an ice bath, care being observed not to allow addition of excess Br_2. Once the solution remained permanently orange (slight excess Br_2) it was stirred at room temperature for 30 minutes. Removing the solvent yielded a bright orange powder to which 100 cm^3 water was added. This mixture was boiled for 20 minutes under reflux. The white precipitate was washed well with water and collected by filtration, yielding on drying *ca* 6.1 g (60%) pure tribromoimidazole, m.p. 219-222° C decomp. (literature corrected m.p. 221°C [60]) $C_3HN_2Br_3$ requires 11.8 % C, 9.2 % N, 0.3 % H, microanalysis gave 12.2 % C, 9.2 % N, 0.4 % H.

Synthesis of 4(5)-bromoimidazole

4g Tribromoimidazole dissolved in 500 cm^3 water containing 82 g Na_2SO_3 was heated under reflux for 7.5 h. The reaction was followed by thin layer chromatography (see below). The filtered, cooled straw-yellow solution was extracted with three portions of 100 cm^3 diethylether. The combined ether extract was dried with anhydrous Na_2SO_4, yielding on removal of solvent a mixture of crude mono-, di- and tribromoimidazole. This was confirmed by ^1H n.m.r. and thin layer chromatography. TLC plates (silica-gel G F_{254} 0.25 mm, Merck) developed with 50 % ethylacetate/ n-hexane, visualized by U.V. and I_2 vapour, showed the presence of tribromo-imidazole Rf 0.87, dibromoimidazole Rf 0.55, monobromoimidazole Rf 0.18 and some imidazole Rf 0. Authentic tribromoimidazole (Aldrich Chemicals) had Rf = 0.88.

Final separation of these compounds was achieved by means of a silica-gel G 60 (Merck) column using eluant of increasing polarity in the form of 5-75% ethylacetate/n-hexane. Various fractions were examined by TLC allowing a total of 0.85 g (22%) 4(5)-bromoimidazole to be collected. Crystallization from hot benzene yielded white crystals melting at 126°-128°C

(literature corrected m.p. 130 - 131°C [60]). $C_3H_3N_2Br$ requires 24.51 % C, 2.04 % H, 19.06 % N, microanalysis shows 24.4 % C, 2.1 % H, 18.8 % N.

Table 2.4: Microanalysis results of isolated platinum complexes of type *cis*-$[Pt(NH_3)(X)_2]Y_2$

			FOUND			CALCULATED		
Y	X	n	%H	%C	%N	%H	%C	%N
-	chloride	-	2.0	-	9.3	2.0	-	9.3
Cl	1H-imidazole	-	3.1	16.6	18.7	3.2	16.5	19.3
Cl	1Me-imidazole	2	4.3	18.8	17.0	4.4	19.2	16.8
Cl	2Me-imidazole	2	4.3	18.8	17.2	4.4	19.2	16.8
Cl	benzimidazole	1	3.7	30.3	14.6	3.6	30.3	15.2
Cl	adenosine	3	4.5	28.7	18.8	4.4	27.6	19.3
Cl	inosine	2	3.8	27.7	16.5	3.7	27.6	16.1
ClO_4	pyrimidine	-	2.5	16.0	14.2	2.4	16.4	14.3
ClO_4	4-methylpyrimidine	1	2.9	18.2	13.1	3.2	19.0	13.3
ClO_4	5-methylpyrimidine	1	2.9	19.0	13.4	3.2	19.0	13.3
ClO_4	pyridine	-	2.8	20.0	9.6	2.7	20.5	9.6
ClO_4	3-methylpyridine	-	3.4	24.1	9.4	3.3	23.5	9.1
ClO_4	3-acetylpyridine	1	3.1	24.4	8.1	3.2	24.5	8.2
ClO_4	3-cyanopyridine	1	2.7	22.4	12.2	2.5	22.1	12.8
ClO_4	3-methylcarboxylato-pyridine	-	2.9	23.9	7.9	2.9	24.0	8.0
ClO_4	3-iodopyridine	-	1.7	14.2	6.7	1.7	14.3	6.7
ClO_4	3-bromopyridine	-	2.1	15.8	7.4	1.9	16.1	7.5
ClO_4	3-chloropyridine	-	2.5	19.0	8.2	2.1	18.3	8.6
ClO_4	3-hydroxypyridine	-	2.6	18.9	9.1	2.6	19.5	9.1
ClO_4	3-carbinolpyridine	-	3.2	22.4	8.8	3.1	22.3	8.7
ClO_4	guanosine	1.5	3.5	23.5	15.6	3.2	24.1	16.9
ClO_4	inosine	1.5	3.4	25.0	14.0	3.1	24.9	14.5

PART II

CHAPTER III : RESULTS AND DISCUSSION

RESULTS

3.1 ^{1}H and ^{13}C n.m.r. Studies of cis-$[Pt(NH_3)_2X_2]Y_2$. X = imidazoles, Y = Cl

The title complexes were prepared according to the general reaction scheme in Figure 3.1, in which also the numbering system for the imidazole moiety is given (numbering according to IUPAC nomenclature [76].

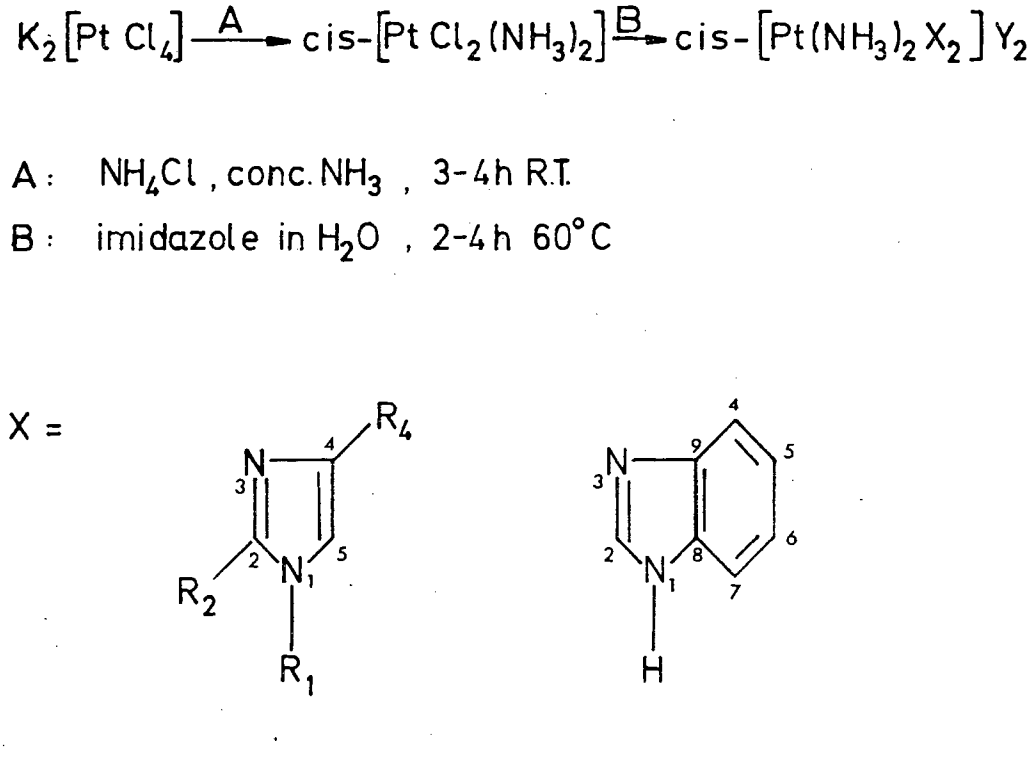

Figure 3.1: Synthesis and numbering of bis(imidazolato) platinum(II).

It is seen that the imidazoles quantitatively displace the chloride ions yielding a stable *cis*-diamino-bis(imidazolato)-platinum(II) chloride. Microanalysis data are given in Table 2.4. These compounds excepting the 4(5)-bromoimidazole and benzimidazole complexes were all found to be very soluble in water rendering them very suitable for ^{13}C n.m.r. studies.

^{1}H n.m.r. spectroscopy

The ^{1}H n.m.r. spectra of imidazole and its substituted analogues were fairly simple. In the case of ^{1}H-imidazole dissolved in $^{2}H_2O$, only two resonances of intensity 1:2 were observed. This is as a result of rapid tautomerism that 1H-imidazole is known to undergo [77], resulting in H(4) and H(5) being magnetically equivalent. In all cases H(2) resonated at lowest field, attributable to the increased deshielding effect of two adjacent N-atoms to which H(2) is subject. Figure 3.2 shows a typical spectrum of *cis*-$[Pt(NH_3)_2(imidazole)_2]Cl_2$ in $^{2}H_2O$.

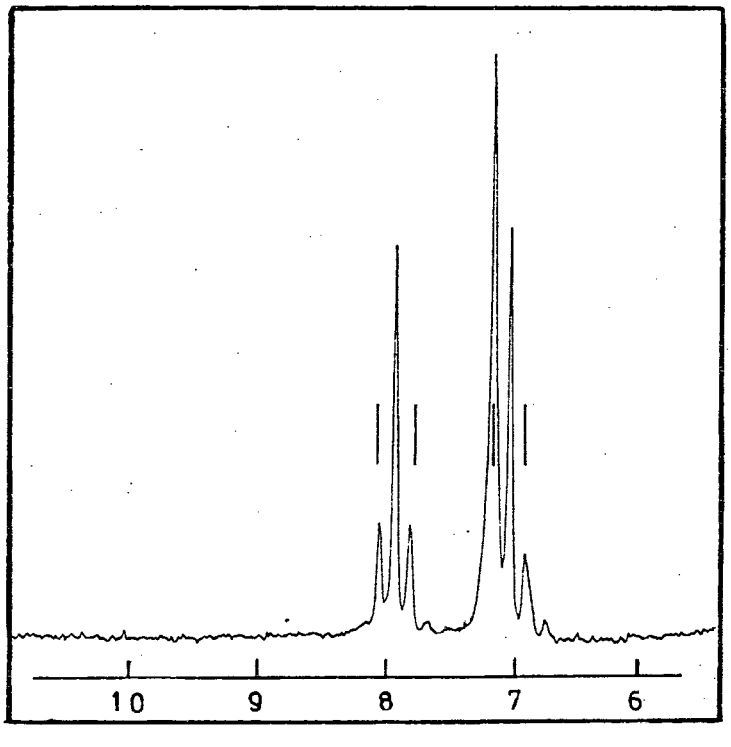

Figure 3.2: The spectrum of *cis*-$[Pt(NH_3)_2(imidazole)_2]Cl_2$ in $^{2}H_2O$.

Platinum coordinates *via* N(3) according to the numbering scheme adopted (see Figure 3.1). Evidently these Pt-N bonds are non-labile (on the n.m.r. time scale at least) so that chemical exchange/tautomerism processes do not occur leaving H(4) and H(5) in the 1H-imidazole complex non-equivalent, δ(H4) = 7.06 and δ(H5) = 7.20 ppm. Assignment of these resonances follows from two $^{3}J_{Pt-H}$ coupling constants. *The sign of these constants was not determined, and $^{3}J_{Pt-H}$ should not be taken to mean that these or other coupling constants designated by this symbolism are necessarily positive.* Table 3.1 summarizes the ^{1}H n.m.r. assignments of the various imidazoles and their corresponding platinum complexes.

It is evident that $^{3}J_{Pt-H}$ for H(2) is close to 20 ± 1 Hz for most complexes, while for H(4) $^{3}J_{Pt-H}$ covers a range of *ca* 20 - 24 Hz. No longer range coupling constants were resolved in most cases except for 4(5)-bromoimidazole. In the latter case the mode of coordination is unexpected. It appears from the ^{1}H n.m.r. spectrum Pt(II) binds to N(3) instead of N(1). The latter coordination site was considered more likely on steric grounds alone. This postulate is based on the long range $^{4}J_{Pt-H} \simeq 7.5$ Hz coupling observable in the spectrum of the 4(5)-bromoimidazole complex. This type of coupling has been very recently reported in $[Pt(NMIz)_4]X_2 2H_2O$ type complexes (in which NMIz is 1-methyl-imidazole). The following coupling constants were reported, $^{3}J_{Pt-H}$ = 19.0, 24 Hz for H(2) and H(4) respectively, while $^{4}J_{Pt-H}$ = 7 Hz for H(5) was observed [41]. Figure 3.3 shows an expanded spectrum of *cis*-$[Pt(NH_3)_2(4\text{-BrImid})_2]^{2+}$, showing clearly the $^{3}J_{Pt-H}$ and $^{4}J_{Pt-H}$ satellites in addition to long range $^{4}J_{H-H}$ = 1.6 Hz involving H(2) and H(5). The latter protons occupy a planar W conformation, hence significant coupling is not unexpected [62]. The reason for this unexpected mode of bonding is not clear, but overlap between filled metal $d\pi$ orbitals and empty $d\pi/\pi^*$

Table 3.1: ^{1}H n.m.r. data for *cis*-$[Pt(NH_3)_2X_2]Y_2$ in $^{2}H_2O$

Compound		Chemical shift / ppm from DSS[a]				$^{n}J_{195Pt-H}$ Coupling constant/(Hz)		
X	Y	H(2)	H(4)	H(5)	Other	^{3}J(H2)	^{3}J(H4)	Other
1H-imidazole	Cl	7.95 (+0.19)	7.05 (-0.08)	7.20 (+0.06)		20.2	≈24	c
1-methylimidazole	Cl	7.84 (+0.23)	7.01 (+0.01)	7.14 (+0.06)	3.70(CH_3) (+0.01)	19.8	≈22.3	c
2-methylimidazole	Cl	-	7.20 (+0.22)	7.10 (+0.12)	2.65(CH_3) (+0.29)	-	≈20.7	c
4-bromoimidazole	ClO_4	8.20[b] (+0.57)	-	7.36[b] (+0.17)	-	20.5	-	^{4}J≈7.5(H5)[b]
benzimidazole	Cl	8.7 (+0.43)	-	-	8.22(H4,7) (+0.48) 7.54(H5,6) (+0.14)	20.6	-	-
5-(2-hydroxyethyl)-4-methylthiazole	ClO_4	9.17	-	-	2.76(CH_3) (+0.46) 3.00(H1') (+0.08) 3.46(H2') (+0.05)	28.6	-	c

Complexation shifts induced by platinum relative to unbound ligand are given in parentheses. (+) deshielded, (-) shielded
a: reference, 3-(trimethylsilyl)-propanesulphonic acid (as sodium salt).
b: assignment based on long range $^{4}J_{Pt-H(9)}$ coupling constant Additional $^{4}J_{H(2)-H(5)}$ = 1.6 Hz observed.
c: not resolved.

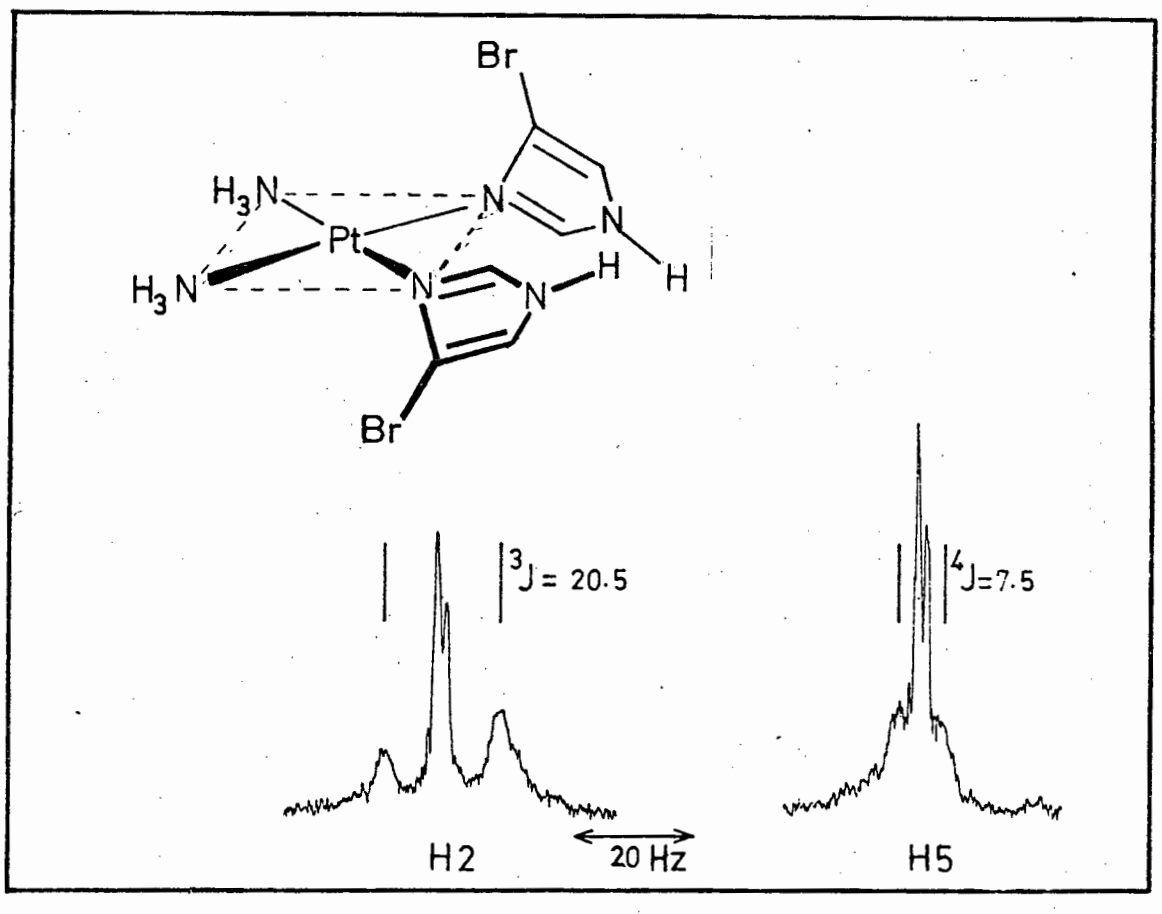

Figure 3.3: The ^{1}H n.m.r. spectrum of *cis*-$[Pt(NH_3)_2(4\text{-bromoimidazole})_2](ClO_4)_2$.

orbitals on the bromide group cannot be ruled out so producing a pseudo-octahedral Pt(II) complex [63].

Unfortunately the linewidths of the other imidazole platinum complexes were generally quite large (see Figure 3.2), so that $^{4}J_{Pt-H}$ and $^{4}J_{H-H}$ coupling constants were generally not resolved.

Finally it is worth mentioning that the analogous thiazole platinum complex *cis*-$[Pt(NH_3)_2X_2](ClO_4)_2$ where X = 5-(2-hydroxyethyl)-4-methyl-thiazole (hereafter named thiazole only) shows the expected N(3) coordination to platinum(II), since $^{3}J_{Pt-H}$ is 28.6 Hz for H(2). Only such bonding of thiazoles has been previously observed [64].

^{13}C n.m.r. spectroscopy

The ^{13}C n.m.r. spectra of imidazole and its analogues are well documented [27,43,65-67], consequently the spectra of these ligands were not re-examined unless no reliable data was available. It should be noted that various solvents were used in previous studies, thus in comparing ^{13}C shifts this must be taken into account. In general however, solvent effects were not large (<1.5 ppm) as shown by the solvent dependence study on the ^{13}C spectrum of imidazole [27]. Hence ^{13}C data collection for the ligand and complex species under identical conditions was not always warranted.

The simple imidazole platinum complexes were found to be soluble in water up to *ca* 1 M with respect to the platinum concentration. Hence spectra with suitable S/N ratios, such that the J_{Pt-C} satellites were clearly visible, were forthcoming in about 4000 transients. It must be remembered that the intensity of these satellites can only be a maximum of 17% (natural abundance of ^{195}Pt = 34%) of the main ^{13}C resonance. A prerequesite for reliable coupling constant measurement was a good S/N ratio. In less soluble *cis*-$[Pt(NH_3)_2(benzimidazole)_2](ClO_4)_2$ for instance *ca* 7.4 x 10^4 transients were required. Figure 3.4 shows some typical spectra obtained from the 2-methylimidazole, 4-bromoimidazole and benzimidazole platinum complexes.

Table 3.2 lists the ^{13}C n.m.r. parameters for the various complexes. The assignments are based on shifts induced on complex formation and the resulting coupling constants. The platinum complexes of thiazole and 4(5) bromoimidazole were prepared especially for assignment checks. Broad band and 'off resonance' decoupling techniques were used to confirm

Figure 3.4: Some ^{13}C spectra for *cis*-$[Pt(NH_3)_2(imidazole)_2]^{2+}$ complexes in ^2H_2O.

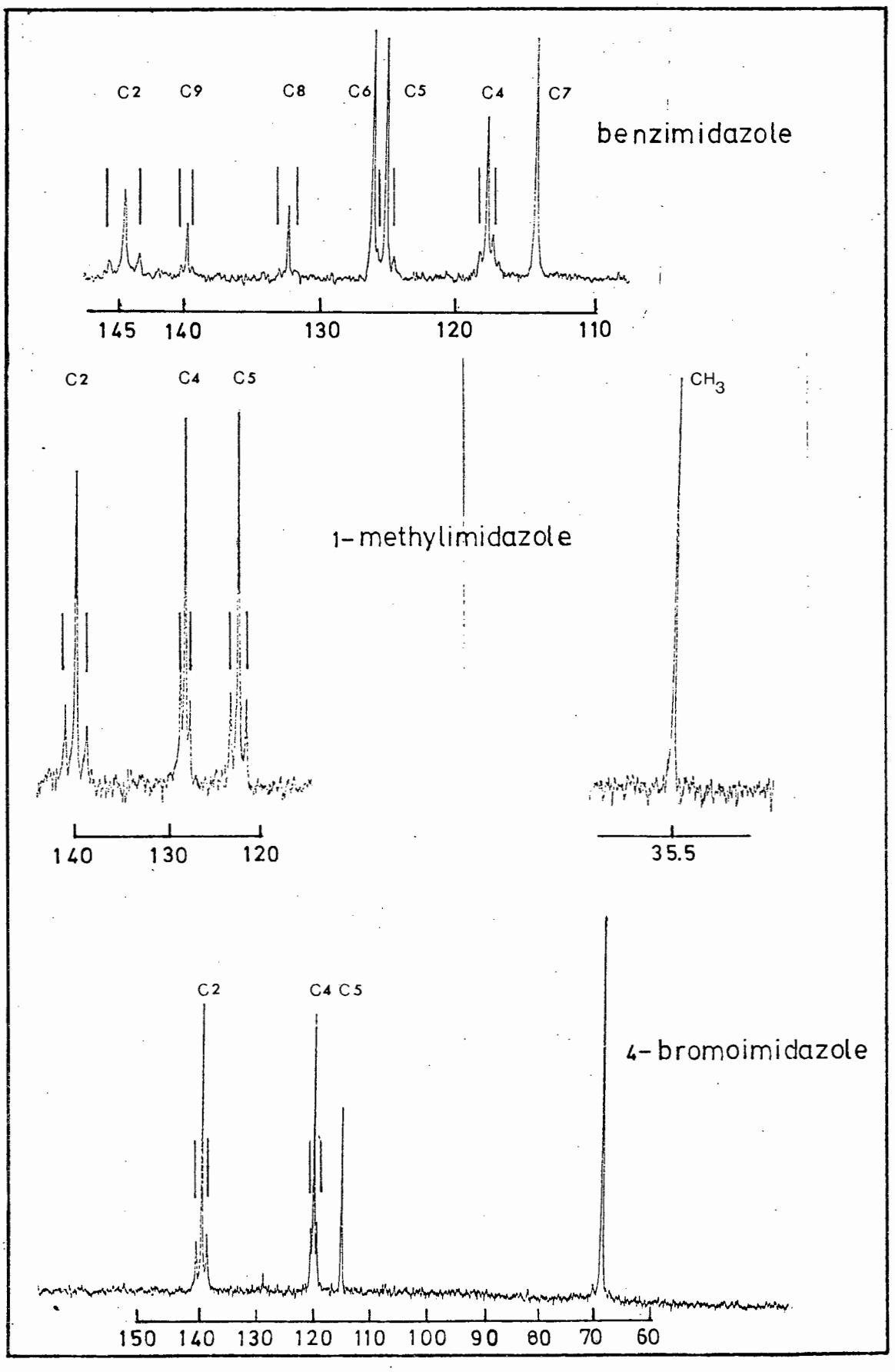

Table 3.2: 22.63 M Hz ^{13}C n.m.r. data for *cis*-$[Pt(NH_3)_2X_2]Y$ in ^2H_2O.

Compound		Chemical Shifts / ppm from TMS[a]				$^nJ_{^{195}Pt-^{13}C}$ Coupling Constants/(Hz)			
X	Y	C(2)	C(4)	C(5)	CH_3	^2J	^2J	^3J	^3J
imidazole	Cl	137.9 (+1.5)[b]	128.3 (+5.8)	119.1 (-3.4)	- -	50.5(C2)	23.5(C4)	39.5(C5)	-
1-methylimidazole	Cl	139.8 (+6.9)	128.7 (+5.5)	123.4 (+6.3)	35.5 (-1.8)	50.5(C2)	21.8(C4)	37.5(C5)	-
2-methylimidazole	Cl	147.4 (+0.8)	128.3 (+5.9)	118.5 (-3.9)	14.4 (+0.3)	45.2(C2)	22.5(C4)	44.1(C5)	23.0(CH_3)
4-bromoimidazole	ClO_4	140.0 (+2.0)	114.9 (+1.3)	120.1 (+2.3)	-	41.9(C2)	≈6 (C4)[c]	23.4(C5)	
5-(2-hydroxyethyl)-4-methylthiazole	ClO_4	157.0 (+4.9)	149.6 (-0.2)	133.1 (+1.5)	16.4 (+1.1) 30.4(C2') (-0.2) 62.1(C1') (-0.8)	35.5(C2)	25.5(C4)	35.7(C5)	20.5(CH_3)
		C(2)	C(9)	C(8)	C(4)				
benzimidazole[d]	Cl	144.3 (+2.8)[d]	139.7 (+1.8)	132.3 (+5.6)	117.8 (+2.4)	50.5(C2)	19.0(C9)	28.6(C8)	20.9(C4)
		C(5) 125.1[e] (+2.2)	C(6) 126.1[e] (+3.2)	C(7) 114.2 (-1.2)		^4J 28.0(C5)?			

Parentheses denote shift on complexation relative to free ligand parameters in water determined under similar conditions (+)downfield, (-) upfield shift.

a: relative to internal dioxane at 67.7 ppm from TMS. b: using data for free imidazole in ^2H_2O from ref. [27].

c: not clearly resolved, but estimable. d: relative to unbound benzimidazole in ethanol [66].

e: not unambiguous, based on apparent coupling constant ^4J ≈28.0 Hz.

assignments in cases of uncertainty. In general assignments so found were not at variance with data previously published [27,65-67]. The shift and coupling trends of the platinum(II) complexes will be discussed separately.

^{13}C shift trends

Figure 3.5 shows a correlation diagram of the various complexes studied. It is evident that in the majority of cases, C(2) and C(4) are both deshielded on complex formation, while the shift induced for C(5) does not appear to follow a consistent pattern.

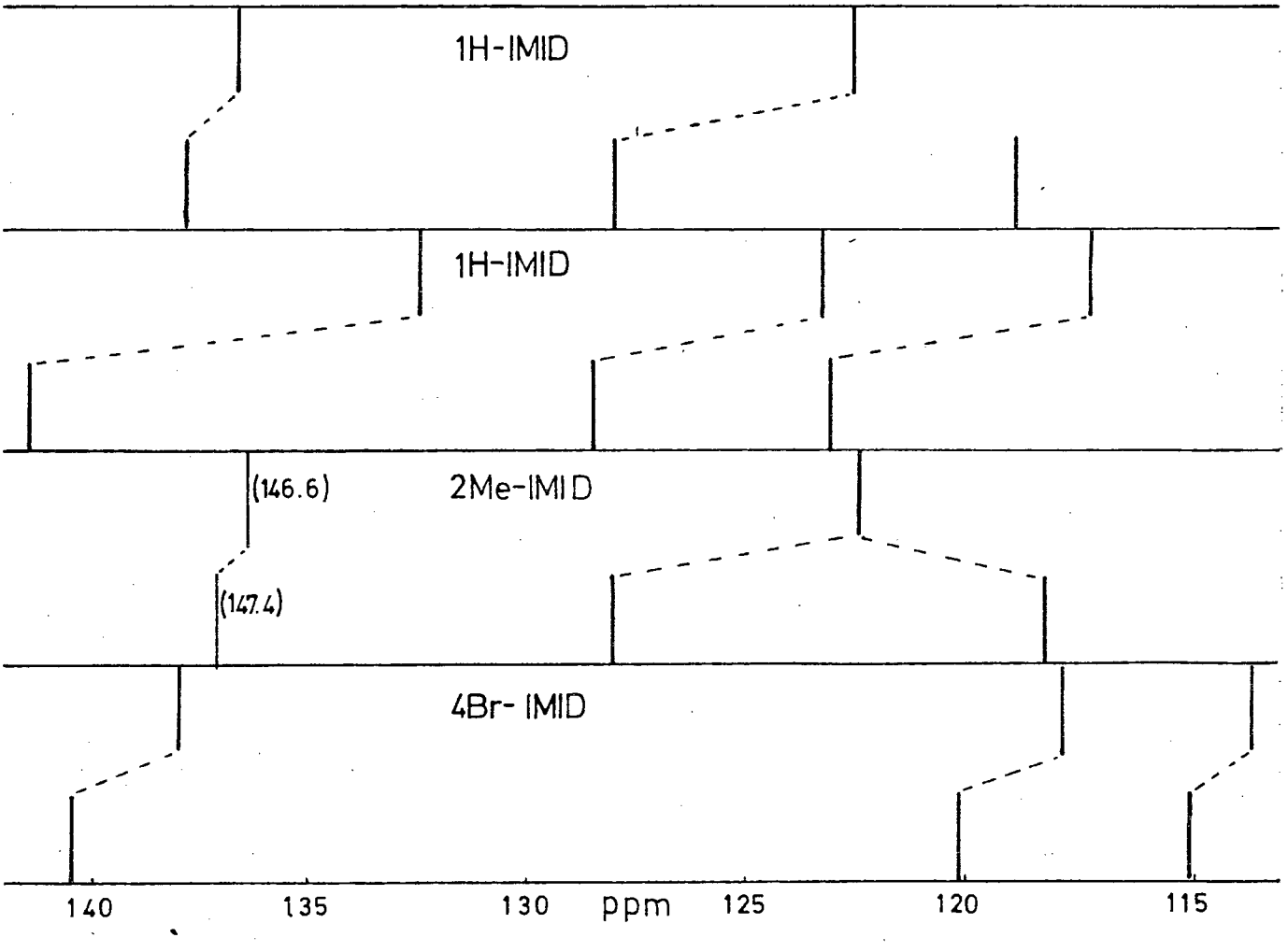

Figure 3.5: A ^{13}C shift correlation diagram for *cis*-$[Pt(NH_3)_2(\text{imidazole})_2]^{2+}$ complex cations.

In the case of 1H-imidazole and 2-methylimidazole C(4) and C(5) were not unambiguously assignable based on shifts alone. The spectrum of 1-methylimidazole had been previously assigned on the basis of europium and praseodymium induced shifts, such that C(4) and C(5) resonate at 130.2 and 121.0 ppm (relative TMS in $CDCl_3$) respectively [67]. An attempt was made to confirm this assignment by J_{C-H} coupling constants, but the undecoupled spectra of 1-methylimidazole were not sufficiently resolved to achieve this. Preparation of the 4(5)-bromoimidazole and thiazole complexes in which C(4) and C(5) were clearly distinguishable, showed complexation shift trends similar to the simple imidazole complexes. The consistency of shift trends lent support to the assignments made. It must be emphasised that consideration of coupling constant data was needed to confirm these assignments. Comparisons of complexation and protonation shifts as well as other criteria that nuclei 'close' to platinum would be expected to shift most, were *not* applicable unambiguously. For instance, in the case of imidazole Grant [65,66] has shown that protonation produces upfield shifts in C(2) and C(4), C(5) relative to neutral imidazole. The platinum complex shows a downfield shift for C(2) and C(4), while C(5) is shielded. Similarly, the C(2) shift is about half of the "further away" C(5) atom, although shifts are of opposite relative sign. Interpretation of these shift trends will be attempted in the general discussion below.

Platinum-195 to carbon-13 coupling constants

The various $^2J_{Pt-C}$ and $^3J_{Pt-C}$ coupling constants listed in Table 3.2 are illuminating. To begin with, Figure 3.6 shows the structure of the thiazole platinum complex as well as the ^{13}C parameters for this substance. It is clear that $^2J_{Pt-C(4)} < {}^3J_{Pt-C(5)} \simeq {}^2J_{Pt-C(2)}$. In addition a $^3J_{Pt-C}$ =

20.5 Hz to the exocyclic 4-methyl group is evident. It will be recalled that the ^{1}H n.m.r. spectrum of this compound clearly established N(3) binding. Nevertheless it was uncertain just how the substitution of a N atom by a S atom (going from a 1,3-diazole system to the 1,3-thiazole system) might affect the overall electron distribution in these systems (and thus the J_{Pt-C} coupling constants). Hence caution was exercised in extending the thiazole complex coupling trends to the imidazole systems.

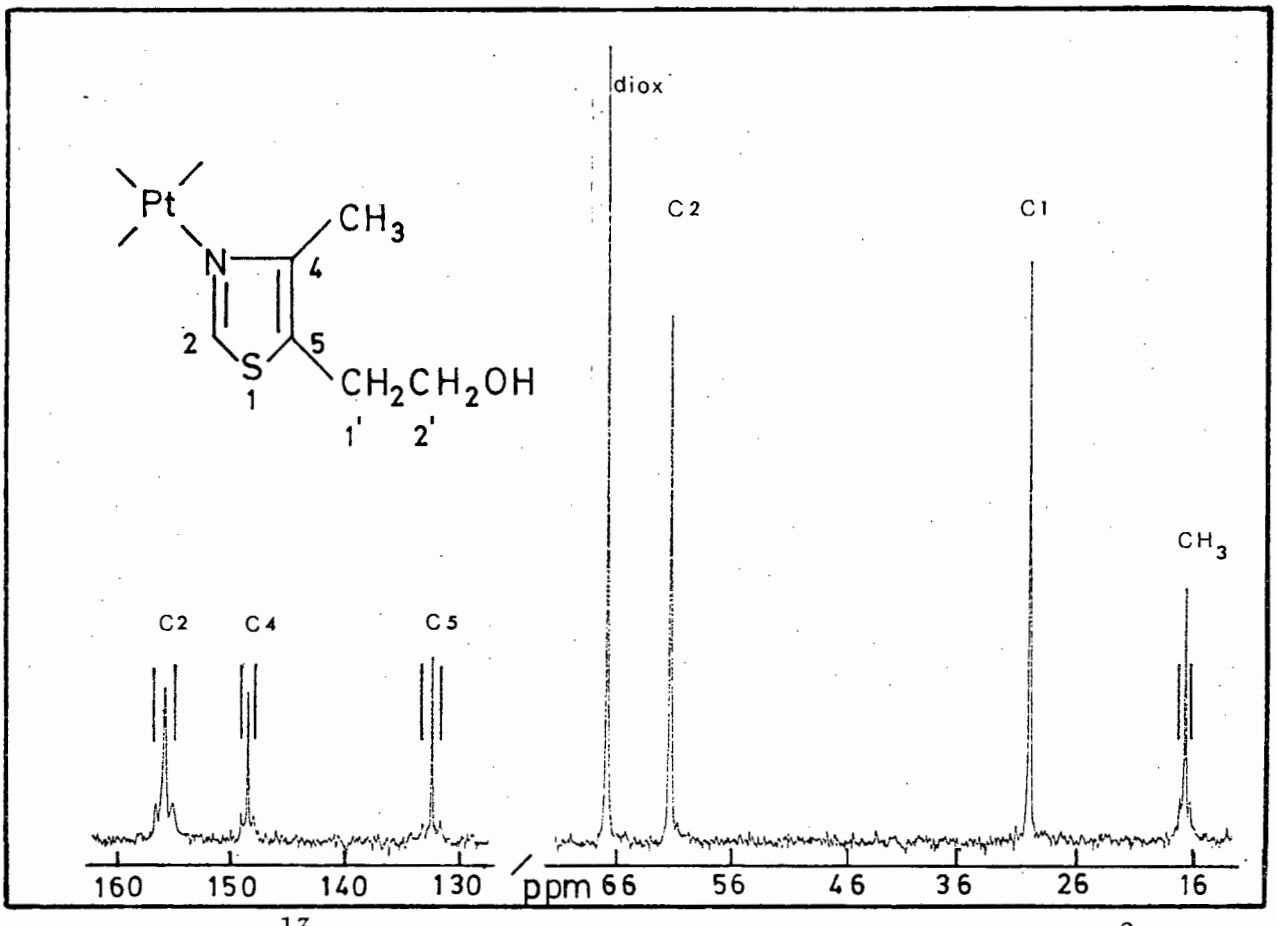

Figure 3.6: The ^{13}C spectrum of *cis*-$[Pt(NH_3)_2(thiazole)_2](ClO_4)_2$ in $^{2}H_2O$.

The 4(5)-bromoimidazole complex of platinum has been shown (^{1}H n.m.r.) bonded *via* N(3) such that possible metal to Br $d\pi$ back-bonding interactions cannot be ruled out. This compound also showed a very definite $^{2}J_{Pt-C(4)} < {}^{3}J_{Pt-C(5)}$ trend. All other imidazole complexes show very similar trends as may be verified in Table 3.2. This set of assignments is compatible

with assignments based on complexation shift trends and is the only possible self-consistent set.

Evidently then the imidazole complexes show similar heavy metal to carbon coupling constant trends ($^2J < {}^3J$) as have been observed in heavy metal phenyl compounds arylmercury [68], arylthallium [69] and arylplatinum complexes [38], all these involving σ metal to carbon bonds. The position of C(2) in the *cis*-$[Pt(NH_3)X_2]^{2+}$ complex anions (where X = 5 membered 1,3-diazoles or thiazoles) is less clear. In all compounds made in this study, $^2J_{Pt\text{-}C(2)}$ was found largest, ranging from *ca* 35-50 Hz. Attempts to qualitatively interpret these trends will be made at a later stage.

Finally it should be observed that some $^3J_{Pt\text{-}C}$ couplings to exocyclic methyl carbon atoms are resolved in complexes of 2-methylimidazole, and the thiazole complex. Similarly in benzimidazole C(4) shows a similar coupling constant of *ca* 20 Hz. From the spectrum of the bis(benzoimidazole) platinum complex an apparent $^4J_{Pt\text{-}C(5)} \sim 28$ Hz coupling is seen. Nevertheless, it has not been possible to verify this beyond all reasonable doubt, as a large resonance unfortunately obscures one satellite. Long range coupling of this magnitude is not unreasonable however, in a highly conjugated system such as benzimidazole. In general coupling constants are reported only if these were *clearly* evident, by the presence of two symmetrically placed satellites on either side of a major resonance. The possibility of spinning side-bands was always taken into account.

3.2 Some Difficulties Associated with Solvents

The complexes *cis*-$[Pt(NH_3)_2X_2]Cl_2$ where X = imidazoles were relatively simple to synthesise, and as is evident from the previous section, lent themselves successfully to ^{13}C n.m.r. studies. Attempts to make the corresponding pyridine and pyrimidine complexes were much less successful. It was not possible to make a *pure* sample of either *cis*-$[Pt(NH_3)_2(pyridine)_2]Cl_2$ nor the pyrimidine analogue, without the use of a vast excess of ligand. Such a procedure resulted in considerable practical difficulties of purification. The isolated products appeared to be mixtures of *cis*-$[Pt(NH_3)_2(pyridine)Cl]Cl$ and the desired bis(pyridine) complex. Additionally it appeared that hydrolysis reactions occurred if solutions of these complexes were kept for extended periods. Such behaviour is understandable in view of known reactions of the type:

$$[Pt(NH_3)_4]Cl_2 \xrightarrow[-NH_3]{\text{heat}} [Pt(NH_3)_3Cl]Cl \xrightarrow[-NH_3]{\text{heat}} \textit{trans}\text{-}[Pt(NH_3)_2Cl_2]$$

are considered [70,72]. Evidently chloride anions (which are known to π bond to Pt significantly [72]) are in direct competition with pyridines or pyrimidines with respect to coordination to platinum. It appears that multiple equilibria are set up in aqueous solution, such that no one species is predominantly favoured:

$$\begin{aligned} \textit{cis}\text{-}[Pt(NH_3)_2Cl_2] + X &\rightleftharpoons \textit{cis}\text{-}[Pt(NH_3)_2X\,Cl]^+ + Cl^- \\ \textit{cis}\text{-}[Pt(NH_3)_2X.Cl]^+ + X &\rightleftharpoons \textit{cis}\text{-}[Pt(NH_3)_2X_2] + Cl^- \end{aligned} \qquad (3a)$$

Such equilibria are of course a simplification since there is good evidence that in all such substitution reactions the solvent plays a significant role [70,72]. Hence *cis*-$[Pt(NH_3)_2Cl_2]$ is known to undergo substantial hydrolysis in aqueous solution (at 298 K the first and second aquation equilibrium constants are $K_1 = 3.6 \times 10^{-3}$ M, $K_2 = 1.1 \times 10^{-4}$ M) [71].

Such hydrolysis reactions as well as the comparable binding affinities of the chloride, pyridine and pyrimidine moieties are believed to be the underlying reason for above synthetic difficulties. One question that immediately springs to mind is why do no complications arise in the case of imidazoles?

The total answer to this question is not clear, although it is fairly certain that such behaviour is very much a property of the nucleophile, X, which displaces the chloride ions in reactions such as given in (3a). The greater basicity of imidazole pK_a = 7.03 (298 K, μ = 0.16) as compared with pyridine pK_a = 5.24 (208, μ = 0.1) [73], suggests that the latter ligand coordinates to platinum more feebly than imidazoles do. This suggestion is certainly consistent with the observation that *cis*-$[Pt(NH_3)_2X_2]Cl_2$ complexes are readily prepared if X = imidazole, but much less so if X = pyridine or pyrimidine molecules. It must, however also be emphasised that the role of the Cl^- anion cannot be ignored.

It turned out that the difficulties experienced in making the pyridine and pyrimidine analogues of type *cis*-$[Pt(NH_3)_2X_2]Cl_2$ were overcome by substituting the chloride ion with the perchlorate anion. The perchlorate complexes were readily prepared, isolated and were very stable for the purposes of this work.

Problems associated with solvolysis of various types of platinum complexes were even more severe in DMSO, a solvent often used by previous workers to obtain ^1H n.m.r. spectral data [27,28,34,59]. The use of DMSO proved to be an unfortunate choice of solvent for many such systems, particularly if complexes of pyridine, pyrimidine or nucleosides were studied.

Figure 3.7: The influence of solvent on the ^{13}C spectrum of *cis*-$[Pt(NH_3)_2$-(3-methylnicotinate)$_2](ClO_4)_2$.

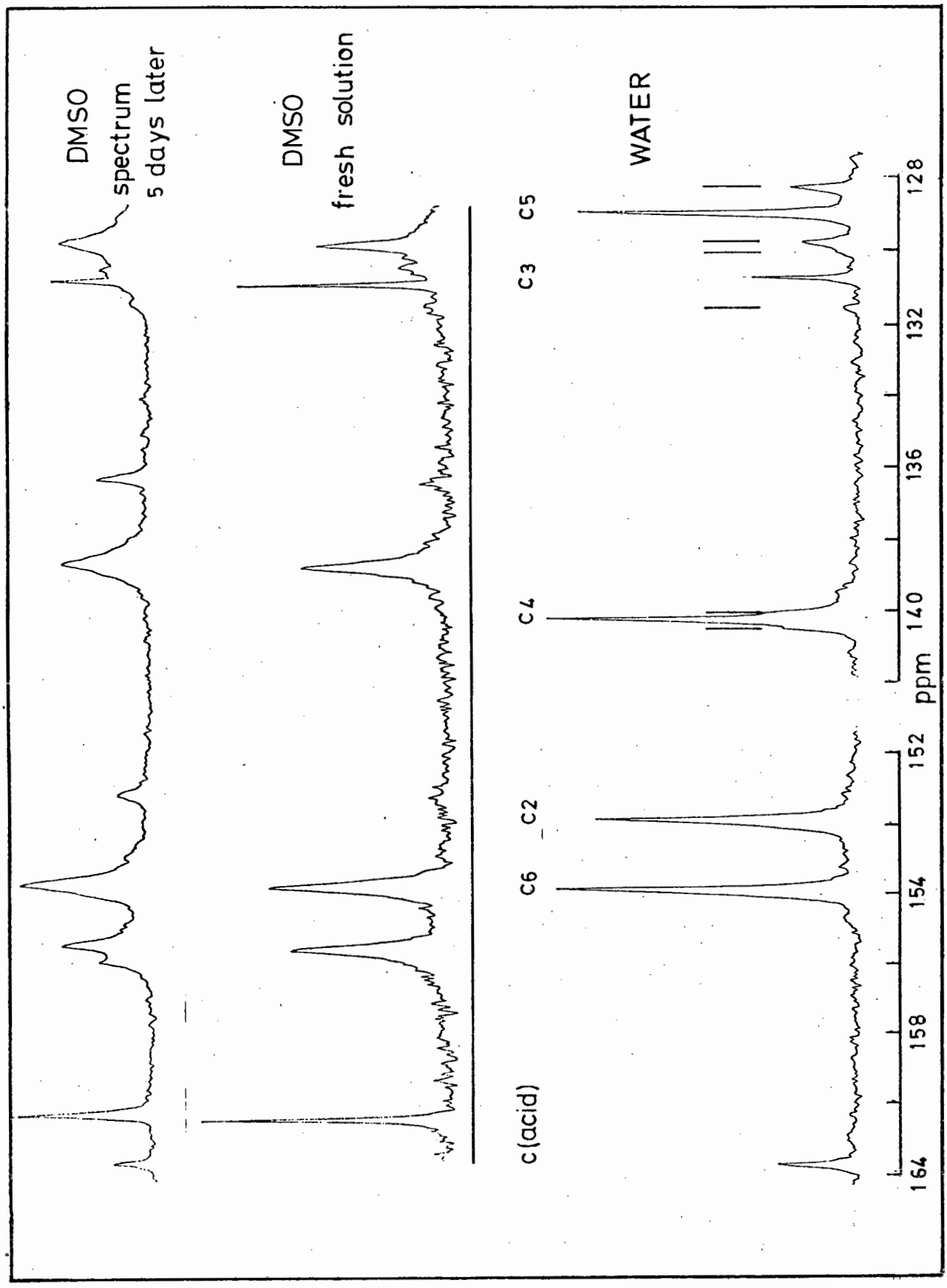

To illustrate the solvent effect Figure 3.7 shows the ^{13}C n.m.r. spectra of *cis*-$[Pt(NH_3)X_2](ClO_4)_2$ where X = 3-methylnicotinate , in water and DMSO under approximately the same conditions. The DMSO spectrum recorded five days later is also shown. It is quite clear that solvolysis reactions occur, unacceptably broadening the resonances. Evidently DMSO decomposes the complex even in the perchlorate salt. Such solvolysis however did not consistently occur as exemplified by the 3-iodopyridine complex. This was found to be quite stable for at least a few days. It appears that the kinetics of these solvolysis processes span a wide range and are highly dependent on the nature of the complex. Further remarks in this regard will be made in discussing platinum nucleoside complexes below.

3.3 The ^1H and ^{13}C n.m.r. of cis-$[Pt(NH_3)X_2](ClO_4)_2$ Complexes in ^2H_2O (X = 3 substituted pyridines)

The title complexes were readily prepared according to the scheme shown in Figure 3.8. The solubility of these complexes in water ranged from a maximum of *ca* 0.2 to 0.6 M. These complexes were characterized by C, H and N microanalysis, results of which are tabulated in Table 2.4.

^1H n.m.r. spectra

Clean 100 M Hz ^1H n.m.r. spectra were readily obtained in ^2H_2O solution. These results are summarized in Table 3.3. Assignments of the free 3-substituted pyridines are well known and have been previously measured either neat or in DMSO solution [74]. Although strictly speaking solvent and concentration effects cannot be assumed negligible in comparing the *cis*-$[Pt(NH_3)_2X_2](ClO_4)_2$ chemical shifts (in dilute ^2H_2O solution), the re-examination of all free ligand ^1H n.m.r. parameters in ^2H_2O was not

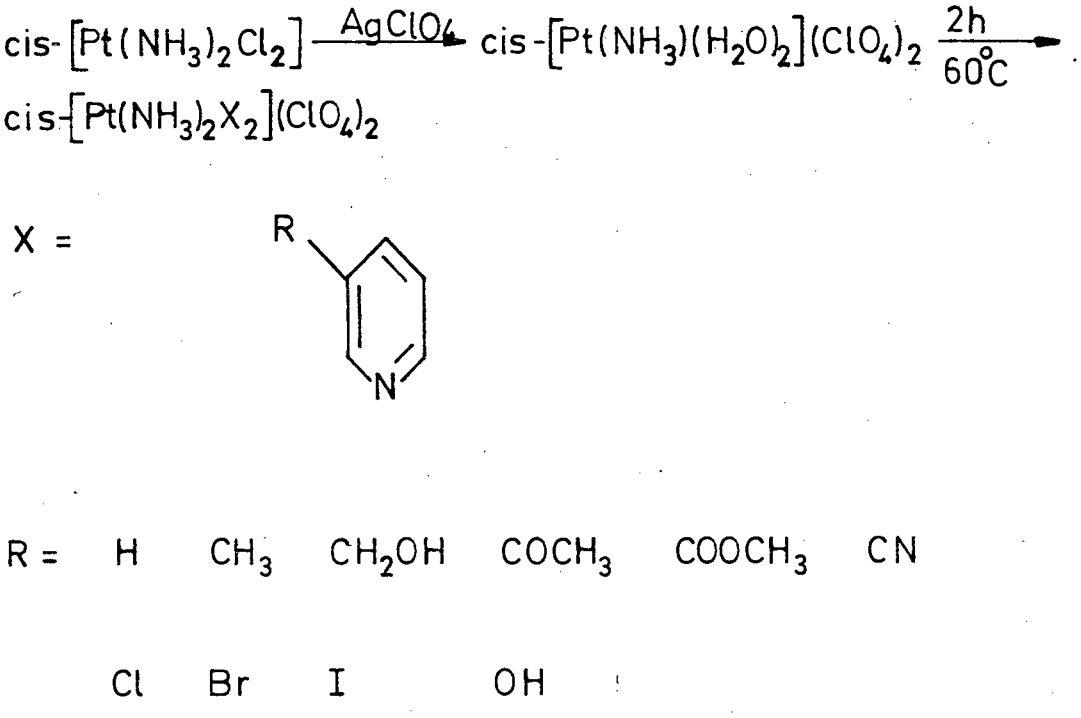

Figure 3.8: The synthesis and structure of the bis(pyridine) platinum (II) complexes studied.

considered justified for the purposes of this work. The complexation shifts shown in Table 3.3 must be considered in this light.

In general the 2,4,6-protons are all deshielded on complexation, except H(5), which is consistantly shielded with respect to the free ligand resonance. This behaviour is not entirely unexpected however if it is remembered that substituent effects are observed to be more pronounced in the *ortho* and *para* position than for the *meta* position in 6-membered conjugrated rings systems [43,75].

Table 3.3: ^1H n.m.r. data for *cis*-$[Pt(NH_3)_2(X)_2](ClO_4)_2$ in ^2H_2O.

Compounds		Chemical shift / ppm from DSS					$^nJ_{^{195}Pt-^1H}$ Coupling Constants	
X	R	H(2)	H(6)	H(4)	H(5)	Other	^3J(H2)	^3J(H6)
pyridine	$-CH_2OH$	8.89[e]	8.81[a]	8.93[b]	7.61[c]	g (CH_2)	39.0	≈40
	$-CH_3$	8.68[e] (+0.11)	8.61[d] (+0.09)	7.86[b] (+0.17)	7.44[c] (+0.15)	2.37[e] (CH_3)	40.0	39.1
	-H	8.80[a] (+0.21)	8.80[a] (+0.21)	8.02[b] (+0.27)	7.56[c] (-0.19)	-	39.0	39.0
	$-COOCH_3$	9.44[e]	9.06[d]	8.55[b]	7.43[c]	4.10[e] (CH_3)	40.0	37.5
	$-COCH_3$	9.42[e] (+0.11)	9.06[d] (+0.10)	8.55[b] (+0.12)	7.45[c] (-0.23)	2.70[e] (CH_3)	40.0	37.5
	-CN	9.34[e]	9.12[d]	8.43[b]	7.79[c]	-	≈40	≈37
	-OH	8.39[a] (-0.17)	8.31[c] (-0.04)	≈7.5[f] (+0.12)	≈7.5[f] (-0.03)	-	≈42	≈38
	-I	9.19[a] (+0.40)	8.80[c] (+0.24)	8.38[b] (+0.25)	7.37[c] (-0.13)	-	39.5	37.5
	-Br	9.08[e] (+0.29)	8.82[d] (+0.05)	8.24[b] (+0.06)	7.52[c] (-0.20)	-	40.0	37.8
	-Cl	8.95[a] (+0.16)	8.78[d] (+0.10)	8.10[b] (+0.11)	7.57[c] (0.00)	-	40.0	38.7

Parentheses denote complexation shift, (+) deshielded, (-) shielded; free pyridine data (solvent DMSO) from ref. [74].
a: Doublet, resolved $J_{H_2H_4}$ ≈1.2 - 1.7 (Hz); b: Poorly resolved doublet $J_{H_4H_5}$ ≈7.0 - 8.5 (Hz);
c: Doublet of doublets $J_{H_5H_6}$ ≈4.8 - 6.3 (Hz), $J_{H_2H_5}$ not resolved; d: Doublet $J_{H_2H_6}$ not resolved;
e: Singlet; f: Multiplet, H_4H_5 resonances superimposed; g: Obscured by ^2HOH resonance.

Only $^{3}J_{Pt-H}$ coupling was resolved, the respective values being relatively invariant, ranging from *ca* 37.8 to 41.0 Hz. These constants did not seem to reveal any sensitivity to the substituent present, although coupling to H(2) was always very slightly larger than to H(6), the difference increasing for the more electronegative substituents. Figure 3.9 shows some typical ^{1}H n.m.r. spectra of 3-acetyl pyridine and its platinum complex.

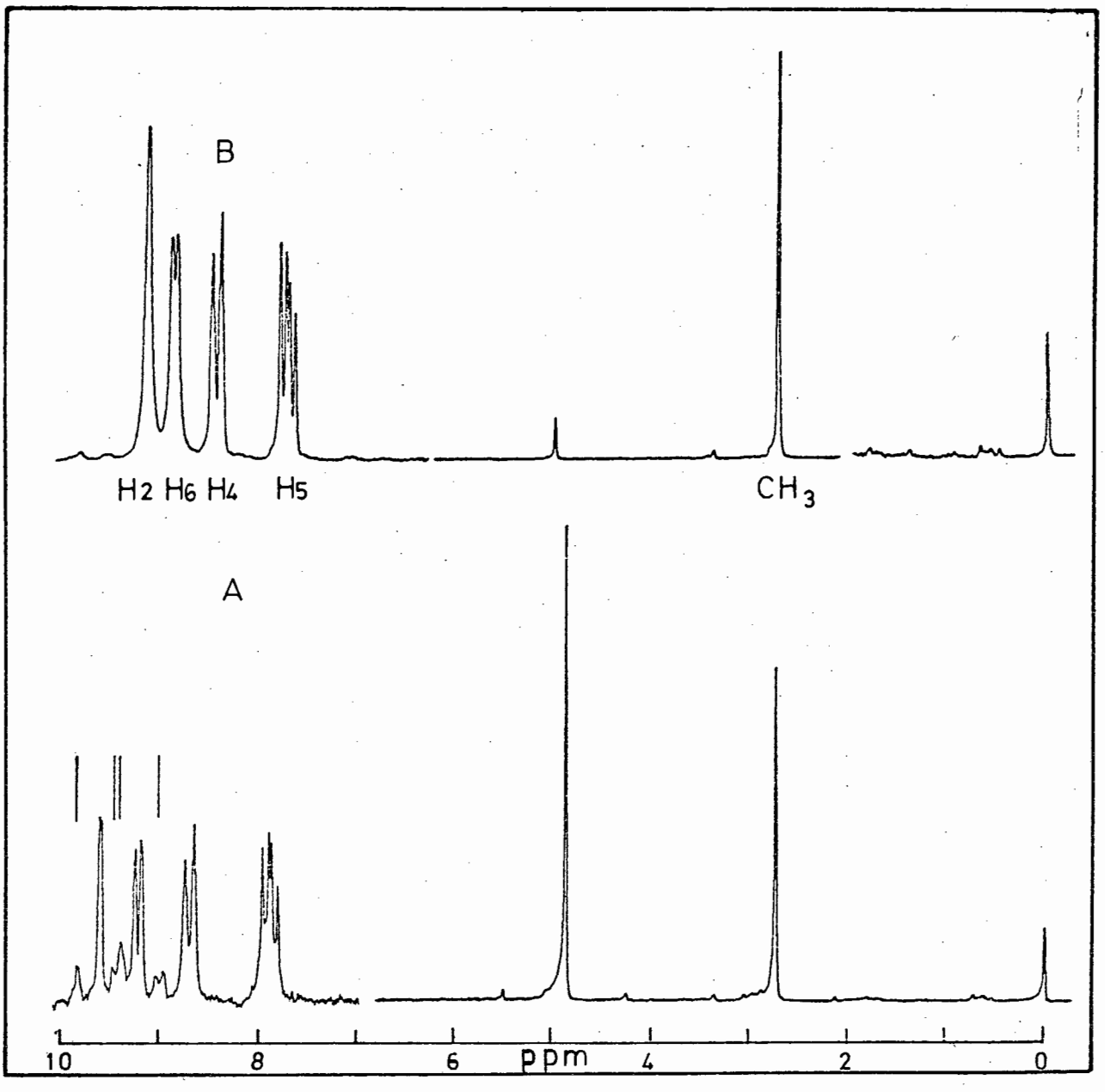

Figure 3.9: The ^{1}H n.m.r. spectrum of 3-acetylpyridine and the corresponding *cis*-$[Pt(NH_3)_2(pyr)_2](ClO_4)_2$ complex in $^{2}H_2O$.

^{13}C n.m.r. parameters

Retcofsky studied substituent effects in the ^{13}C n.m.r. spectra of 3-substituted pyridines [78]. These results were obtained from either neat or concentrated DMSO solution. These results have been discussed subsequently in terms of substituent effects by Stothers [43] and Katritzky [75]. The chemical shifts of some ligands were thus not re-examined but previous remarks on solvent and concentration effects must be kept in mind. Table 3.4 lists the ^{13}C parameters observed for *cis*-$[Pt(NH_3)_2(pyridine)_2](ClO_4)_2$ complexes dissolved in water, concentrations ranging from *ca* 0.2 M to 0.6 M. The relatively low solubility necessitated the accumulation of *ca* 2 x 10^4 transient in most cases such that J_{Pt-C} coupling satelites could be seen. In addition all these spectra were recorded in the presence of *ca* 0.05 M Gd(TTHA) (see section 2.4) as shiftless relaxation agent. Gd(TTHA) served two purposes, it allowed rapid accumulation of data (no delays between 45^o pulses were required) and relaxed the quarternary carbon atoms sufficiently such that a reasonable S/N ratio for these carbons was obtained. Figure 3.10 shows a typical spectrum obtained for the bis(3-acetylpyridine) platinum(II), plotted such that the region of pyridyl resonances is shown in expanded (5 Hz/cm) form. It is clear that resonances were sharp, $\Delta\nu_{\frac{1}{2}}$ ranged from *ca* 1.3 to 2.5 Hz which approaches the maximum resolution possible in the Fourier Transform spectrum at these conditions (at 8K memory size, and sweep width 6000 Hz maximum resolution is 1.46 Hz).

^{13}C Shift trends

Reference to Table 3.4 shown that consistent shift patterns emerged and these did not appear to depend greatly on the conditions under which the free ligand spectrum was obtained. In fact these trends were

Figure 3.10: The ^{13}C spectrum of *cis*-$[Pt(NH_3)_2(3\text{-acetylpyridine})_2](ClO_4)_2$ in ^2H_2O (expanded).

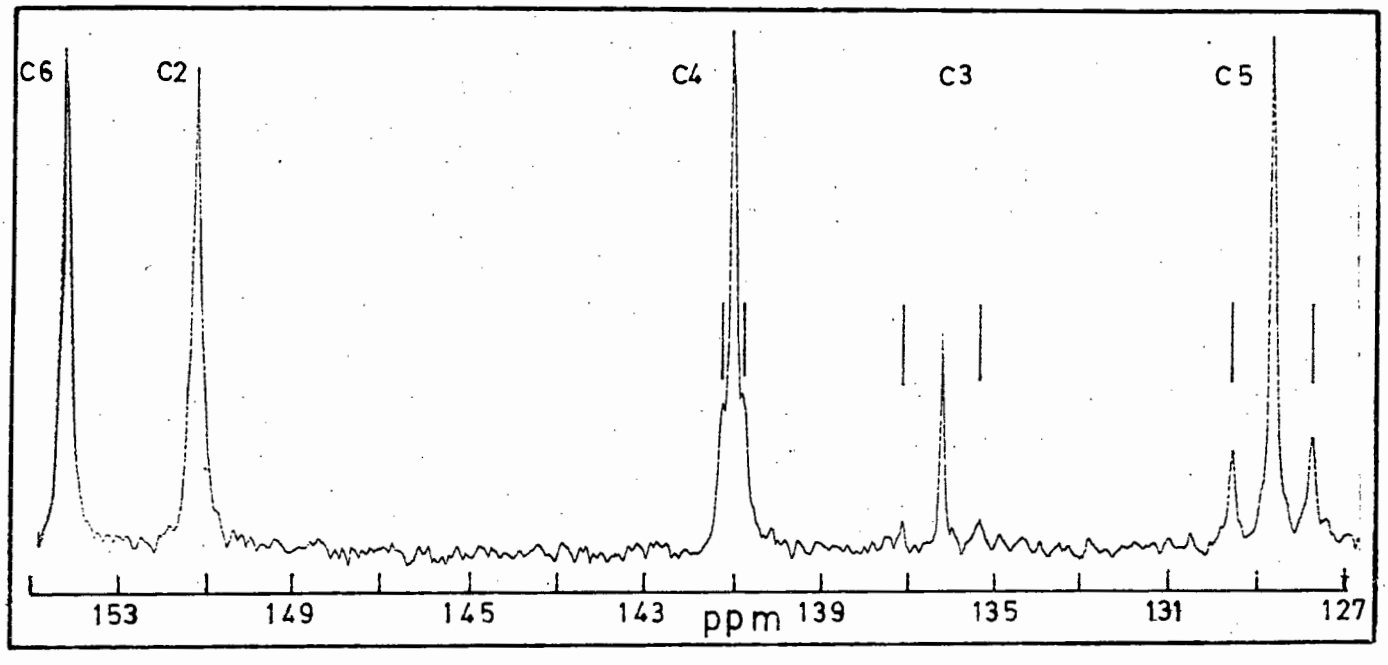

similar where the ligand and complex spectra were recorded in different solvents to the cases where identical solvents were used, although the absolute magnitude of complexation shifts varied slightly. A plot of δ(C3) of the free pyridine against δ(C3) of the complex is linear indicating that no unusual solvent effects are present, and that platinum(II) induces comparable perturbations in all pyridine systems. In all cases a general deshielding of the ring carbon atoms is observed. In fact, only C(3) in the 3-hydroxopyridine and 3-iodopyridine complexes is slightly shielded in the complex. This is attributed to an unusual substituent effect. Figure 3.11 shows a correlation diagram for the observed shifts. Evidently C(2) and C(6) undergo similar shielding in the range +1.8 to +3.4 ppm, with one obvious exception, the 3-hydroxypyridine. This anomaly is understandable if it is remembered that 2 and 4-hydroxypyridines

Table 3.4: 22.63 M Hz ^{13}C n.m.r. data for *cis*-$[Pt(NH_3)_2(X)_2](ClO_4)_2$ in ^2H_2O containing Gd(TTHA) (≈0.05M)

Compound		Chemical shifts / ppm from TMS[a]						$^nJ_{^{195}Pt-^{13}C}$ Coupling Constans/(Hz)			
X	R	C(2)	C(3)	C(4)	C(5)	C(6)	Other	^2J(C2,6)	^3J(C3)	^3J(C5)	^4J(C4)
3R-pyridine	$-CH_2OH$	152.1[d] (+2.8)	141.5 (+3.9)	140.1 (+2.8)	128.1 (+2.9)	151.6[d] (+3.1)	61.5(CH_2OH) (-1.0)	e	41.5	43.5	10.5
	$-CH_3$	152.2 (+2.0)[b]	138.9 (+5.1)	141.6 (+4.3)	127.0 (+2.9)	149.6 (+1.8)	18.3(CH_3) (-0.7)	e	41.9	43.2	11.1
	-H	153.1 (+2.5)[b]	128.5 (+4.0)	141.7 (+5.3)	128.5 (+4.0)	153.1 (+2.5)		e	42.5	42.5	≈11[f]
	$-COOCH_3$	154.1 (+3.8)	130.8 (+4.2)	142.2 (+3.8)	128.6 (+3.7)	156.3 (+2.7)	54.7(CH_3) (+1.0) 165.8 (-1.2)	e	44.0	41.5	≈11[f]
	$-COCH_3$	153.5 (+3.4)	136.4 (+3.9)	141.0 (+5.5)	128.7 (+4.4)	156.5 (+2.6)	27.8(CH_3) (+1.0) 199.5 (+2.0)	e	44.0	41.0	10.5
	-CN	156.5 (+2.8)	114.2 (+3.0)	145.4 (+4.3)	129.0 (+3.4)	157.1 (-1.8)	115.7(CN)	3	49.0	41.0	11.8
	-OH	145.0 (+7.3)	156.1 (-1.8)	128.5 (+0.2)	128.9 (+2.2)	141.3 (+4.6)		e	52.5	47.3	g
	-I[c]	158.3 (+1.8)[b]	95.3 (-2.6)	148.8 (+4.0)	128.5 (+2.3)	152.1 (+3.0)		e	53.8	42.5	g
	-Br	153.7 (+2.3)[b]	123.3 (+1.7)	144.9 (+5.7)	129.3 (+3.8)	152.0 (+3.1)		e	57.5	44.0	≈10
	-Cl	152.1[d] (+3.2)	135.9 (+3.2)	142.1 (+4.5)	129.3 (+3.9)	151.8[d] (+2.9)		e	58.0	44.5	10.5

Parentheses denote shifts relative to free ligand measured under similar conditions unless otherwise stated. (+) deshielded (-) shielded. a: Relative to internal dioxane at 67.7 ppm from TMS. b: Shifts of free ligand from ref. [43,75,79]. c: Solvent dimethylsulphoxide. d: Shifts not unambiguous. e: Not observed. f Poorly resolved. g: Unresolved.

are actually considered to be pyridones, in which the nitrogen atom carries the 'hydroxy' proton and the substituted carbon atom is in fact a ketonic carbon [75]. In the case of 3-hydroxypyridine an equilibrium between the pyridine and pyridone is also expected, which lies toward the pyridone. Hence the 'free ligand' shift is not that of '3-hydroxypyridine'. This is underlined by an abnormally large 7.3 ppm shift at C(2) on complex formation, in which the 3-hydroxypyridine is forced to exist. The atoms C(3) and C(5) tend to show the next largest complexation shifts, in the range +1.7 to +4.4 ppm (except C(3) in 3-iodopyridine). The carbon *para* to platinum(II) shows the largest shifts in general; C(4) complexation shifts range from +2.9 to +5.7. These shift trends are more readily apparent if the 'average complexation shift' is calculated (omitting the 3-hydroxypyridine anomally). The mean shifts for the various ring carbon atoms are: C(2), 2.73 < C(6), 2.79 < C(3), 3.03 < C(5), 3.58 < C(4), 4.5.

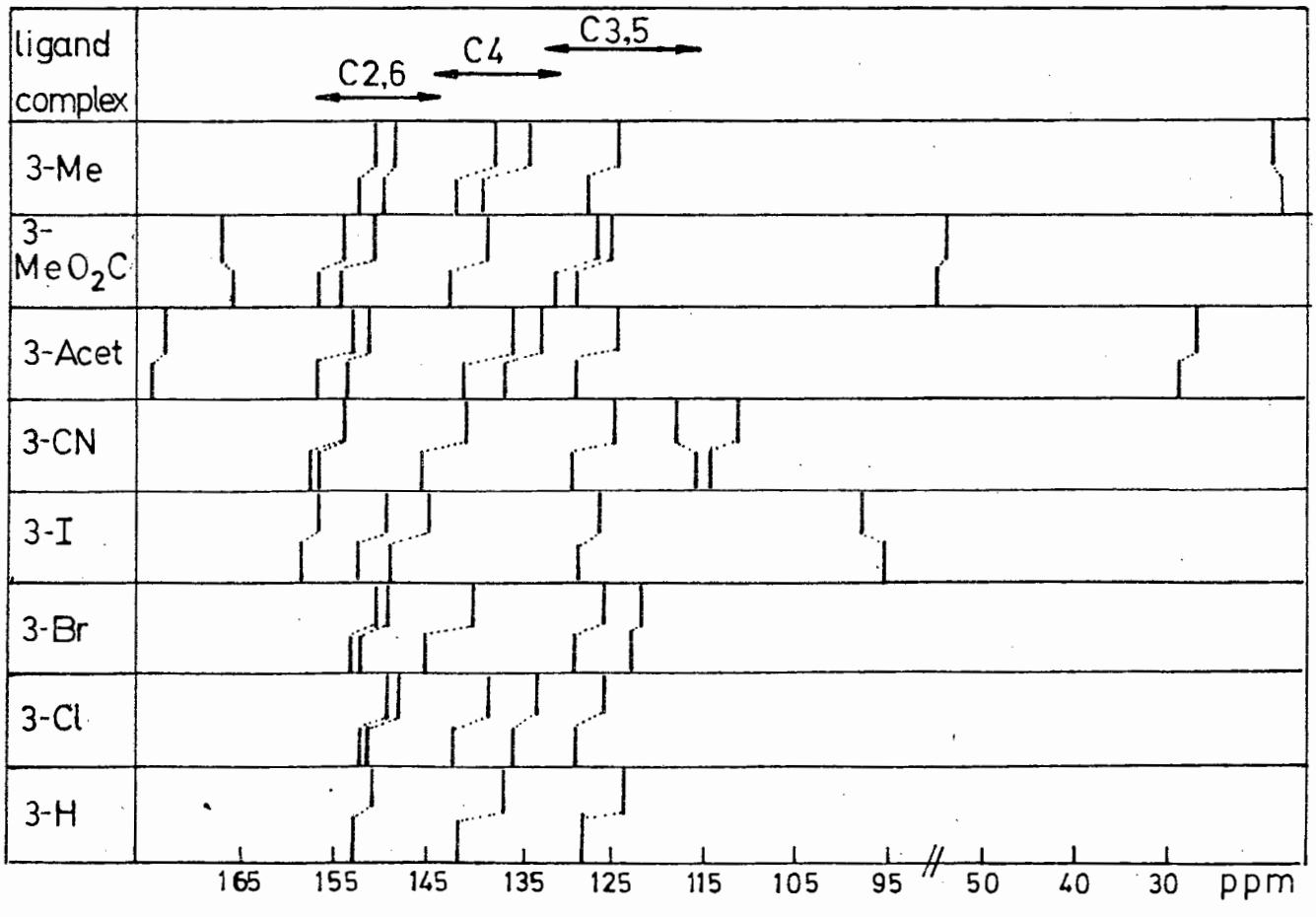

Figure 3.11: A ^{13}C shift correlation diagram for 3-substituted platinum(II) complexes.

It must of course be remembered that some solvent effects might contribute to this trend, but these are considered small because in cases where ligand and complex were examined under similar conditions the same trend is borne out. Further discussion of such trends will be given at a stage in this work.

Platinum-195 to carbon-13 coupling constants

Reference to Table 3.4 shows that for all 3-substituted pyridine platinum(II) complexes studied here, only $^{3}J_{Pt-C}$ and $^{4}J_{Pt-C}$ coupling constants were observable. The unexpected absence of any two bond coupling constants is puzzling. Indeed 3-substituted complexes were selected for two reasons (i) the substituent effect on $^{3}J_{Pt-C}$ was unknown and (ii) since substituent effects in 6-membered rings are known to perturb the carbon atoms *para* substantially a possible $^{2}J_{Pt-C6}$ was expected. Lauterbur [79] noted a correlation between the *para* carbon shieldings and the electronic effects of the substituents in mono-substituted benzenes. Retcofsky has shown that 3-substituted pyridines show similar trends to the monosubstituted benzenes, while 2 and 4-substituted pyridine shielding trends are faithful to their benzene analogues [78,43]. Vrieze [40] had previously reported $^{2}J_{Pt-C2,6}$ of *ca* 12.6 Hz (see later).

It was therefore somewhat disappointing that no $^{2}J_{Pt-C}$ coupling constants were measurable. It is evident from the spectrum in Figure 3.10 that such couplings must be smaller than *ca* 5 Hz since the base line width of C(2) and C(6) were generally of this magnitude.

Turning to the $^{4}J_{Pt-C4}$ coupling constant first, it is clear that in all cases this long range interaction is observed although in two cases it was not resolved because of excessive line broadening. The magnitude

Table 3.5: Qualitative trends of $^3J_{Pt-C3}$ in terms of Lupton-Swain substituent constants [36,38].

Substituent Constants	$\sigma_I < 0$	$\sigma_I \sim 0$	$\sigma_I > 0$
$R^n < 0$ $^3J_{Pt-C3}$	CH_3 CH_2OH 41.9 41.5		OH I 52.5 53.8 Br Cl 57.5 58.0
$R^n \sim 0$ $^3J_{Pt-C3}$		H 42.5	
$R^n > 0$ $^3J_{Pt-C3}$	No substituents known		CO_2CH_3 $COCH_3$ CN 44.0 44.0 49.0

It appears from Table 3.5 that those substituents which have $\sigma_I > 0$, (i.e. that are electron withdrawing *via* inductive effect) but capable of resonance electron donation ($R^n < 0$), result in the largest ^3J values. Intermediate ^3J values are observed for substituents which have $R^n > 0$ as well as $\sigma_I > 0$ such as the cyano, acetyl and methylcarboxylate groups. These substituents would be expected to be strongly electron withdrawing *via* a resonance effect as well as an inductive effect. Finally the 3-methylpyridine complex shows a low ^3J value, qualitatively correlated with an inductive electron release, $\sigma_I < 0$ and slight resonance donation.

These coupling trends also show no correlation with δ C(3). For example a large $^3J_{Pt-C3}$ for 3-chloropyridine is observed (58 Hz) while C(3) in this complex resonates at 135.9 ppm. In contrast the 3-methylpyridine analogue shows a C(3) chemical shift of 138.9 ppm while $^3J_{Pt-C3}$ = 41.5 Hz, whereas the 3-iodopyridine complex $^3J_{Pt-C3}$ = 53.8 Hz while C(3) resonates at 95.3 ppm. Such effects are difficult to account for, but a possible explanation for the seemingly erratic coupling trend will be discussed at a later stage.

3.4 The ^1H and ^{13}C n.m.r. Parameters of cis-$[Pt(NH_3)_2X_2](ClO_4)_2$ where X = some Pyrimidines

These substances were synthesised exactly as the pyridine complexes in the previous section, while their properties resembled the pyridine analogues closely. Figure 3.1 shows the structural formulae of the complexes studied. Microanalysis data are collected in Table 2.4.

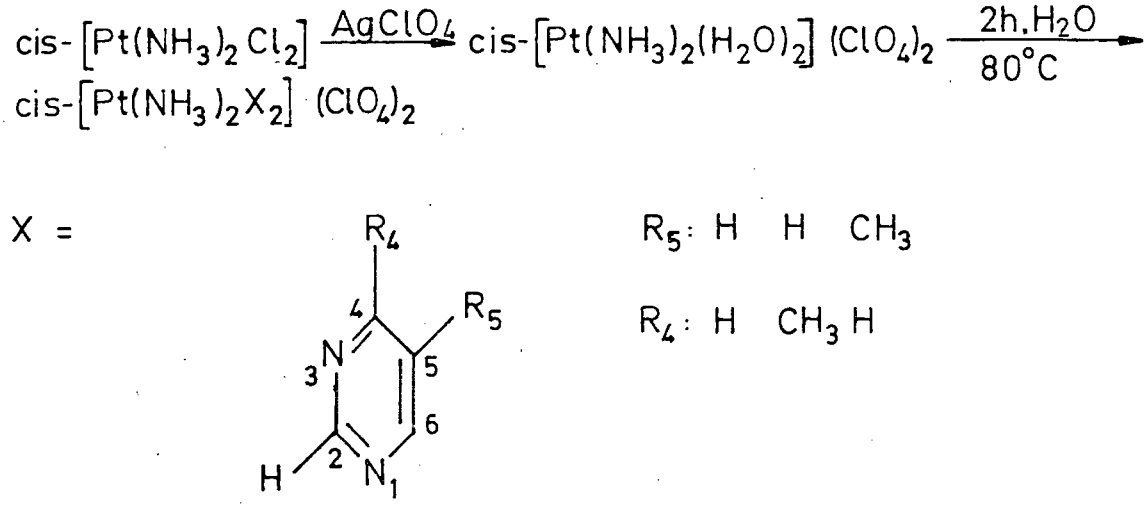

Figure 3.12: The synthesis and numbering scheme for the pyrimidine complexes studied.

^{1}H n.m.r. parameters

The *cis*-$[Pt(NH_3)_2(pyrimidine)_2](ClO_4)_2$ type complexes were only moderately soluble in water. Table 3.6 lists the various ^{1}H n.m.r. parameters for the pyrimidine complexes. The spectra of these complexes were fairly simple assignments being readily apparent. The proton flanked by the two nitrogen atoms always resonated lowest field, while the pattern of J_{HH} coupling constants fascilitated assignment of H(4), H(5) and H(6). As was found for pyridine and imidazole platinum complexes, the pyrimidine complex protons were generally all deshielded relative to the unbound ligand. H(2) shifted downfield by *ca* 0.4 ppm while H(6) showed variable shifts.

Table 3.6: ^{1}H n.m.r. parameters for *cis*-$[Pt(NH_3)_2X_2](ClO_4)_2$ in ^2H_2O

Compound	Chemical shift/ppm from DSS					$^nJ_{195Pt-'H}$ Coupling Constants (Hz)	
	H(2)	H(6)	H(4)	H(5)	Other	^3J(H2)	^3J(H6)
Pyrimidine	9.57[c] (+0.45)	9.17[a] (0.36)	8.92[b] (+0.11)	7.74[a] (+0.15)	-	24.3	39.2
4-methyl-pyrimidine	9.34[c] (+0.42)	8.88[a] (+0.29)	-	7.58[a] (+0.15)	2.59 (+0.08)	24.1	37.6
5-methyl-pyrimidine	9.34[c] (+0.44)	9.01[c] (+0.40)	8.76[c] (+0.15)	-	2.34	22.0	36.9

Parentheses denote complexation shift (+) deshielded, (-) shielded.

a: $J_{H5-H4} = J_{H6-H4} \simeq 5.4$ Hz.

b: $J_{H4-H2} \simeq 1.6$ Hz

c: no proton-proton coupling resolved.

The $^{3}J_{Pt-H}$ coupling constants are quite different for H(2) and H(6). Coupling to H(6) is very similar to the value obtained for the corresponding pyridine protons covering the range 36.9 - 39.2 Hz. On the other hand $^{3}J_{Pt-H2}$ is much smaller ranging from 22.0 to 24.3 Hz. This coupling constant is reminicent of the corresponding value in the imidazole platinum complex (19.8 - 20.5 Hz). Considering the similarity between these two sets of coupling constants it is tempting to draw the inference that the electronic environment of H(2) in these two systems is similar.

^{13}C n.m.r. parameters

The diamino-bis(pyrimidine)platinum(II) perchlorate salts were not very soluble in water. For instance the spectrum of the 5-methylpyrimidine complex had to be measured from a saturated water solution at 350 K while only limited coupling information was forthcoming under these conditions. The pyrimidine and 4-methylpyrimidine complexes were however somewhat more soluble in water. Since these salts did not contain chloride anions, it was considered profitable to try DMSO as solvent, in which these complexes were readily soluble. These DMSO solutions yielded reasonable spectra with no detectable decomposition over the period of spectral accumulation. Evidently the perchlorate salt does not readily undergo solvolysis as the corresponding chloride salt was found to do (see section 3.2).

Figure 3.13 shows the ^{13}C spectrum of the 4-methylpyrimidine platinum complex in water, and the 5-methylpyrimidine complex in DMSO. As is evident from the two spectra in the Figure, unfortunate overlap of resonances occurs, particularly so in the symmetrical 5-methylpyrimidine case. Consequently assignments were difficult to make unambiguously. Table 3.7 collects the data for both water and DMSO solutions.

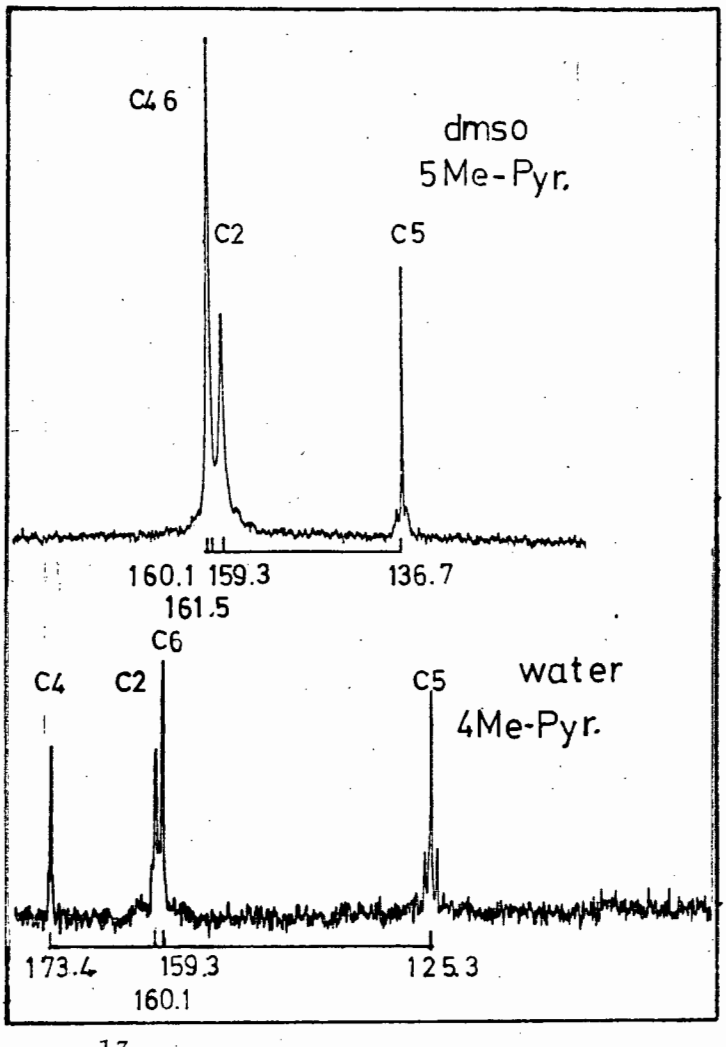

Figure 3.13: The ^{13}C spectra of bis(pyrimidine) platinum(II) complexes in $^{2}H_2O$ and DMSO-d^6.

The assignments were made by considering J_{Pt-C} coupling constants, but are not unambiguous for C(2) and C(6) (see below).

^{13}C shift trends

A correlation diagram of the complex shieldings shows that as in the case of the corresponding pyridine complexes, most carbons are deshielded relative to the free ligand. Trends are also similar to the pyridine analogues, with C(4) (*para* to platinum) most deshielded. The shieldings observed in DMSO and water show minimal solvent dependance, so that the average complexation shifts for the various carbon atoms are:

C(4), 3.6 ppm > C(5),C(2), 2.9 ppm > C(6), 1.8 ppm

A similar trend has been observed for the pyridine complexes. It should

Table 3.7: ^{13}C n.m.r. parameters for *cis*-$[Pt(NH_3)_2(pyrimidine)_2](ClO_4)_2$ in ^2H_2O (with 0.05 M Gd(TTHA)) or in DMSO (containing ≈ 0.01 M $Cr(acac)_3$).

Compound		Chemical shift / ppm from TMS[a]					$^nJ_{195_{J-}13_C}$ Coupling constants/ (Hz)		
	Solvent	C(2)	C(4)	C(5)	C(6)	Other	^2J(C2)	^3J(C5)	^4J(C4)
Pyrimidine	H_2O	160.9[b] (+1.2)	160.9 (+3.2)	125.4 (+3.1)	161.2[b] (+3.5)	-	∿22	34.8	c
	DMSO	160.7	160.7	125.2	161.5	-	c	33.0	c
4-methyl-pyrimidine	H_2O	159.3[b] (+1.6)	173.4 (+4.1)	125.3 (+2.2)	160.2[b] (+2.1)	24.7(CH_3) (+0.5)	20.0	35.5	9.5
	DMSO	159.4 (+1.7)	171.7 (+2.4)	123.8 (+0.7)	161.6 (+3.5)	24.8(CH_3) (+0.6)	c	∿23	c
5-methyl-pyrimidine	H_2O	160.1[b] (+3.6)	161.5 (+3.5)	136.7 (+3.4)	159.1[b] (+2.1)	16.1(CH_3) (-0.1)	d	∿33	d
	DMSO	160.8 (+3.5)	160.8 (+2.8)	134.6 (+1.3)	159.0 (+2.8)	16.1(CH_3) (-0.1)	c	∿32	c

Parentheses denote complexation shifts relative to ligand spectra in ^2H_2O (+) deshielded, (-) shielded.

a: measured relative to dioxane at 67.7 ppm or DMSO-d_6 at 40.4 ppm from TMS

b: assignment not unambiguous - based on $^2J_{Pt-C2}$ value.

c: unresolved coupling due to relatively large base line widths.

d: sensitivity problems due to poor solubility.

be remembered that the above assignments for C(2) and C(6) are based on apparent $^{2}J_{Pt-C}$ coupling constant.

An interesting feature of the spectra obtained in DMSO is that on average the line widths of all carbon resonances are about 50% greater than the corresponding spectra obtained in water. In point of case, the average line widths of the complex *cis*-$[Pt(NH_3)_2(r\text{-methylpyrimidine})_2]ClO_4$ are between 4-7 Hz in water but between 8-16 Hz in DMSO, and yet no visible solvolysis occured in DMSO while some J_{Pt-C} coupling was observable. A possible reason might be the greater viscosity of DMSO, which would presumably result in a longer correlation time, τ_c, for the complex cation as compared with the water solution. If this were the case, some line-broadening would be expected as a result of a shorter spin-spin relaxation time, (T_2).

Platinum-195 to carbon-13 coupling constants

Reference to Table 3.7 shows that only limited coupling data was observable. The possible obstruction of J_{Pt-C} satellites must be remembered in this regard. In water solution $^{3}J_{Pt-C5}$ coupling spans the range 33 - 35 Hz, somewhat less than the corresponding constants for the pyridine complexes. In the favourable case of 4-methylpyrimidine a $^{4}J_{Pt-C4}$ = 9.5 Hz was observed, but this long range coupling was generally not resolved in the other cases. In contrast to the pyridine analogues a two bond coupling constant does become visible in the pyrimidine complexes. $^{2}J_{Pt-C}$ of *ca* 20 - 22 Hz is observed but because C(2) and C(6) show such similar shieldings in all the pyrimidine complexes, it is not clear to which carbon coupling is actually visible. Comparing C(2) to the corresponding imidazole carbon atom, it is not unreasonable to consider the electronic environment in these to systems to be roughly similar. Extended Hückel Theory (EHT) calculations

of the σ and π electron densities of nitrogen heterocyclic molecules (and the protonation effects) yield the following results for imidazole and pyrimidine systems (Table 3.8) [80,81].

Table 3.8: Calculated ETH electron densities from referces [80,81].

Molecule	Position	Electron Densities σ	π	σ + π
Imidazole	2	2.60	0.833(0.894)[a]	3.43
	4	2.81	1.06 (1.049)	3.87
Imidazole	2	2.62	0.833	3.45
cation	4	2.82	1.06	3.88
Pyrimidine	2	2.58	0.651(0.802)	3.23
	4	2.79	0.734(0.847)	3.52
	5	3.05	1.02	4.07
Pyrimidine	2	2.60	0.651	3.25
Cation	4	2.80	0.734	3.53
	5	3.04	1.02	4.06

a: π-electron densities calculated by means of a Hückel molecular orbital (HMO) method from reference [81] are in parentheses.

Inspection of the electron densities in Table 3.8 shows that the total electron density of the C(2) atom in pyrimidine and imidazole is fairly similar. In the imidazole platinum complex, a large $^2J_{Pt-C2}$ coupling constant is observed (*ca* 45 - 50 Hz) and a relatively small $^2J_{Pt-C4}$ (*ca* 21 - 23 Hz) value. By analogy then the observed $^2J_{Pt-C}$ constant in the pyrimidine systems (*ca* 20 - 22 Hz) is assigned to C(2). Whatever effects that lead to a large $^2J_{Pt-C2}$ coupling in imidazoles are then also postulated to lead to a relatively large $^2J_{Pt-C2}$ constant in the pyrimidine case. Nevertheless, this assignment of C(2) and C(6) in the pyrimidine complexes is only tentative and must await further experimental verification. It was on this basis however, that the assignments in Table 3.7 were made.

In the spectra obtained from DMSO solutions of the *cis*-$[Pt(NH_3)_2(pyrimidine)_2]^{-}(ClO_4)_2$ complexes, only $^3J_{Pt-C5}$ was visible. This value was slightly smaller than the corresponding coupling constant measured in an aqueous solution (see Table 3.7). Puzzling is the low $^3J_{Pt-C5}$ for the 4-methylpyrimidine complex (≈23 Hz) as compared to that in water (35.5 Hz). The fact that in general the line widths of all resonances in DMSO are substantially larger than for the corresponding resonances measured in water is probably responsible that other coupling constants were not resolved in DMSO solution.

3.5 The ^1H and ^{13}C n.m.r. Spectra of some Platinum(II) Nucleoside Complexes

Reference has already been made to some difficulties experienced in the use of DMSO as solvent for platinum(II) complexes in section 3.2. In the case of nucleoside complexes problems experienced with solvents were particularly severe. In retrospect it has become clear that the 'solvent problem' had a common denominator *viz* the use of DMSO (which in many regards is a superior solvent for a large variety of substances) and the presence of a halide ion, in this case Cl^-. It turned out that the majority of solvent related problems were circumvented by substituting the Cl^- ion by the ClO_4^- ion and using water as a solvent instead of DMSO. Fortunately the perchlorate salts were quite soluble in water, as is evident from the results presented in previous sections. It might be well however, to briefly

outline the various approaches tried to obtain satisfactory ^{13}C n.m.r. spectra for some platinum(II) nucleoside complexes.

Theophanides *et al* [19-21,29] had previously prepared compounds of the type *cis*-$[Pt(NH_3)_2(nucleoside)_2]Cl_2$ and uncharged *cis*-$[Pt(nucleoside)_2Cl_2]$. The former compounds were reasonably soluble in water to yield good ^1H n.m.r. spectra such that $^3J_{Pt-H(8)}$ of *ca* 26 Hz was readily observable for the complexes of inosine, guanosine and xanthosine. Our attempts to observe ^{13}C spectra of analogous compounds were frustrated by two factors

(i) the relatively low solubility (max *ca* 0.15 M at 230 K), and

(ii) the apparent solvolysis reactions.

To obtain a suitable S/N ratio such that platinum-195 to carbon-13 coupling satellites would be clearly visible *ca* 50-60 x 10^4 transients were necessary (meaning total data accumulation times of between *ca* 10 to 12 h). Over this period it appeared that extensive solvolysis reactions occured, which were not apparent from ^1H n.m.r. spectra (generally recorded within one hour of sample preparation). Attempts to improve solubility (to *ca* 1 M, thus reducing accumulation times) using DMSO resulting in even more rapid decomposition of the complex, yielding ^{13}C spectra with broad resonances, and the appearance of several species in solution.

Similar solvolysis reactions were encountered if *cis*-$[Pt(nucleoside)_2Cl_2]$ compounds were dissolved in DMSO, although these reactions were slower.

Theophanides *et al* had examined the ^{1}H n.m.r. spectra of these substances in DMSO solution [15,59] without reporting any difficulties. Our attempts to obtain a suitable ^{13}C spectrum for *cis*-[Pt(inosine)$_2$Cl$_2$] in DMSO resulted in a very complex spectrum, showing the presence of at least three separate species in solution, as shown in Figure 3.14.

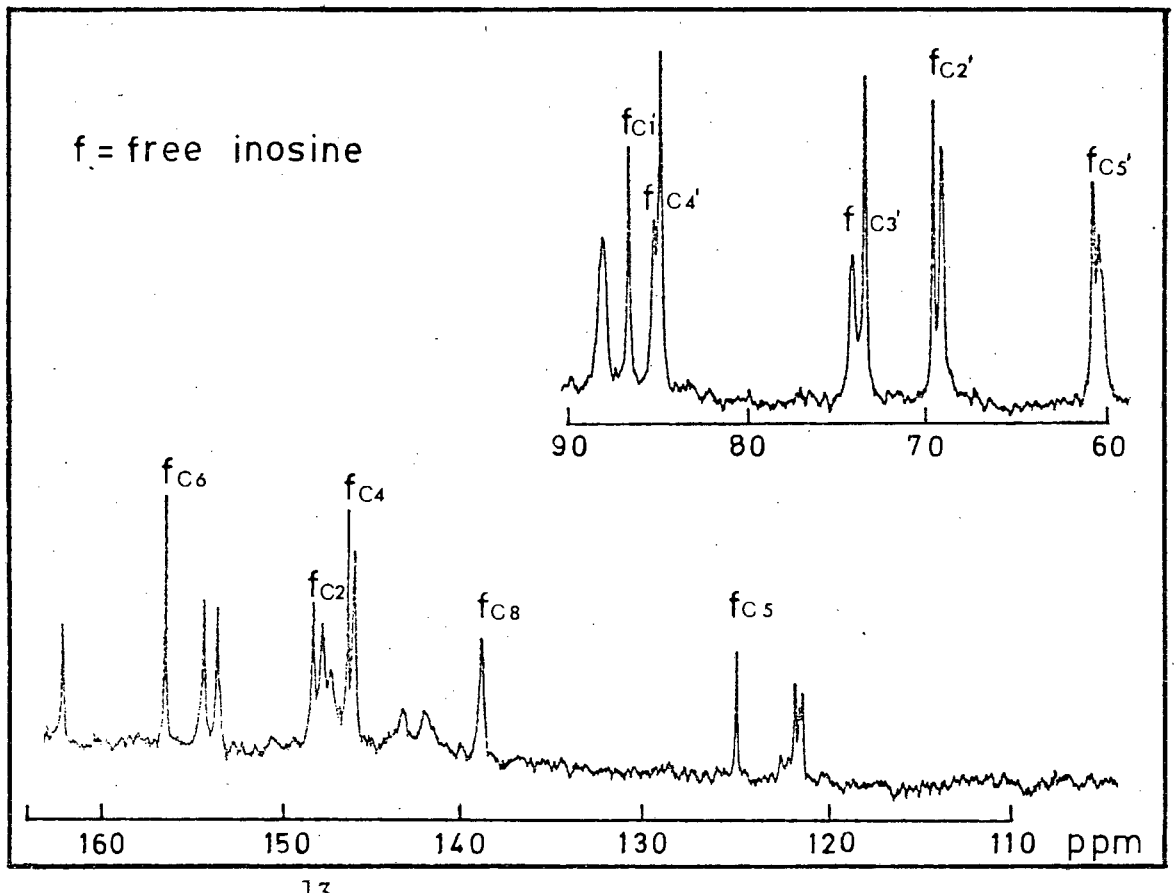

Figure 3.14: The ^{13}C spectrum for *cis*-[Pt(inosine)$_2$Cl$_2$] in DMSO - d_6.

These results all point to a slow, chloride catalysed, solvolysis of the complexes in both water and DMSO, the rate of solvolysis being much larger in the latter case. Although detailed mechanistic studies were not undertaken, it may be postulated that reactions of the following type might be responsible for the problems experienced:

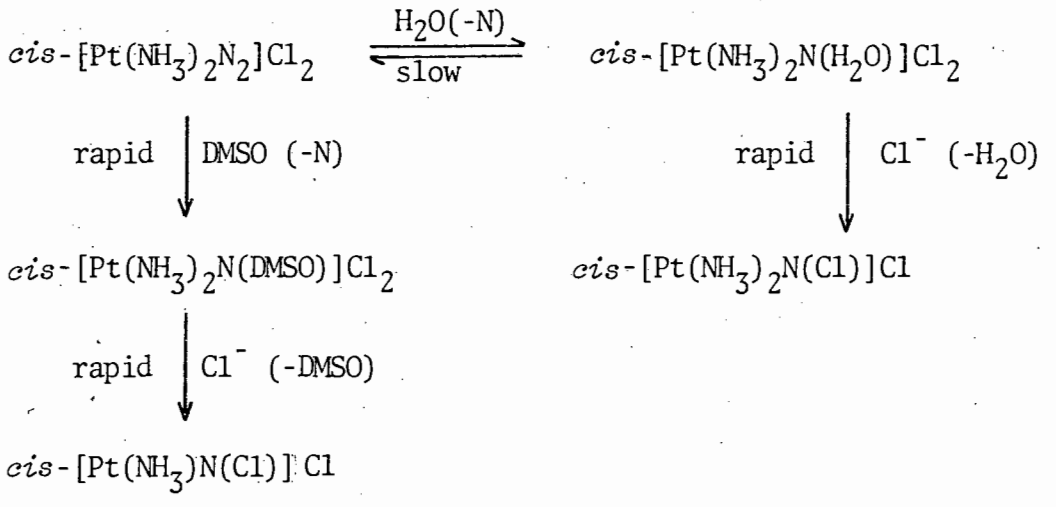

A survey of some relevant literature shows that in substitution reactions involving square planar platinum, unusual solvent dependance is well documented. It has for example been observed that DMSO increases the rate of chlorine-36 exchange in complexes such as *trans*-$[Pt(pyridine)_2Cl_2]$ by a factor about 100 (rate = 380 x 10^5 sec^{-1}) over that observed in water (rate = 3.5 x 10^5 sec^{-1}) [82]. Furthermore this rate was found to be independent on the chloride concentration. Tobe and Romeo [83] have investigated details of a reversible replacement of amines by chloride under the trans effect of DMSO, and have shown that reactions of the type

$$cis\text{-}[Pt(am)_2Cl_2] \underset{}{\overset{DMSO}{\rightleftharpoons}} cis\text{-}[Pt(am)_2(DMSO)Cl]Cl$$

$$cis\text{-}[Pt(am)_2(DMSO)Cl] \overset{H^+/Cl^-}{\rightleftharpoons} cis\text{-}[Pt(am)(DMSO)Cl_2] + amH^+$$

occur fairly rapidly *via* a complex solvolytically controlled pathway. The further possibility of *cis/trans* isomerism processes must also be taken into account [84]. Recently, a ^{195}Pt and ^{15}N investigation of the solvolysis of *cis*-$[Pt(NH_3)_2Cl_2]$ in DMSO has been published [86], which demonstrates conclusively that at least six independent species are observable over a period of time (see Figure 3.15).

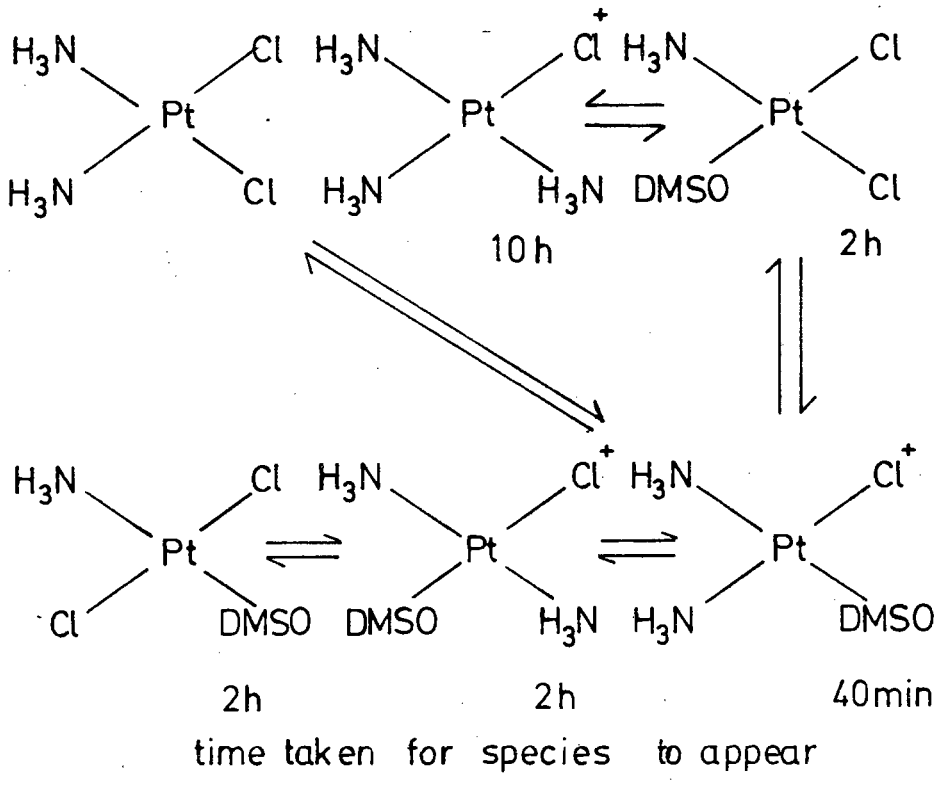

Figure 3.15: Solvolysis reactions of *cis*-$[Pt(NH_3)Cl_2]$ in DMSO (after Ref. [86].)

Kong *et al* have reported the reactions of *cis*-$[PtCl_2(DMSO)_2]$ with nucleosides, in which initially a *trans*-$[Pt(DMSO)(N)Cl_2]$ compound was formed which later isomerised completely to the corresponding *cis* complex. These authors examined the ^1H n.m.r. spectra of these complexes and reported readily assignable spectra with $^3J_{Pt-H8}$ clearly visible for inosine, guanosine and xanthosine [34]. Attempts to adapt this system for ^{13}C n.m.r. spectroscopy also failed however, presumably due to *cis/trans* equilibria resulting in a remarkable concentration and solvent dependence of the visibility of $^3J_{Pt-H8}$ in the inosine complex. Figure 3.16 shows the ^1H n.m.r. spectra of equimolar amounts of *cis*-$[Pt(DMSO)_2Cl_2]$ and inosine in DMSO, equilibrated for 24 hours at *ca* 315 K. Spectra were recorded by progressive dilution with DMSO and/or acetone.

Figure 3.16: The ^{1}H n.m.r. spectra of equimolar mixtures of *cis*-$[Pt(DMSO)_2Cl_2]$ and inosine under various conditions.

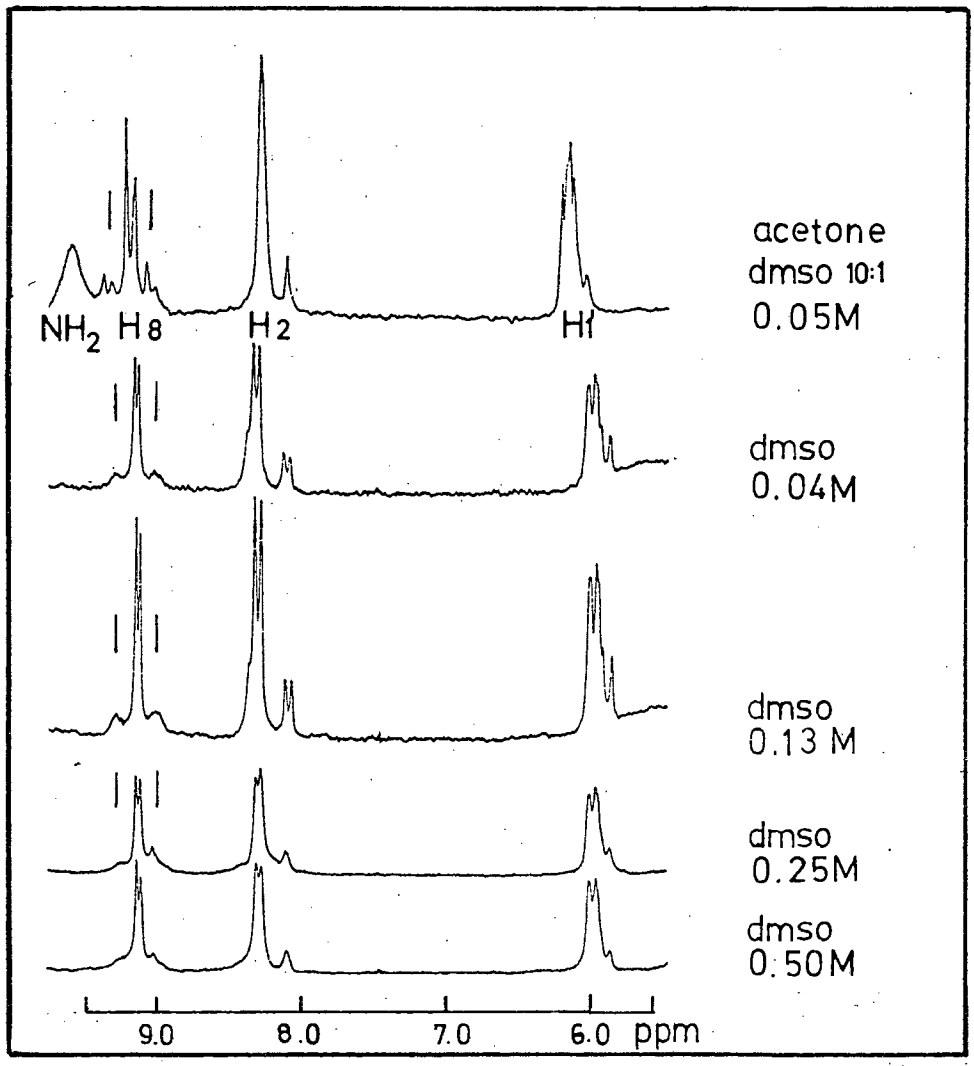

Evidently dilution and addition of acetone increases the resolution dramatically such that $^{3}J_{Pt\text{-}H8}$ coupling constants become readily apparent. The reason for this is not quite clear, but might in part be due to the high viscosity DMSO solutions which tend to be viscous at ambient temperature. Kong *et al* [34] have suggested that the *cis* isomer is exclusively present, and explained the fact that in inosine two H(8) resonances are visible at 9.16 and 9.10 ppm (c.f. Figure 3.16) by postulating different

Table 3.9: ^{1}H n.m.r. data for some *cis*-$[Pt(NH_3)_2X_2](ClO_4)_2$ in $^{2}H_2O$

Compound	Chemical shift / ppm from DSS							$^{n}J_{^{195}Pt-^{1}H}$ / Coupling Constants (Hz)	
X	H(8)	H(2)	H(1')	H(2')	H(3')	H(4')	H(5')	^{3}J	Other
Inosine	8.80 (+0.64)	8.24 (+0.18)	6.1	4.6	4.4	4.3	3.9	24.0(H8)	-
Guanosine	8.43 (+0.58)	-	5.9	4.6	4.4	4.3	3.7	24.0(H8)	-
Inosine[c]	8.98	8.45	-	-	-	-	-	26	-
Guanosine [c]	8.73	-	-	-	-	-	-	26	-

Complexation shifts in parenthesis (+) deshielded (-) shielded.

a: 3-(trimethylsilyl)-propane sulphonic acid,
b: shift of ribose protons on complexation very small,
c: from reference 21, measured as the chloride complex.

Figure 3.17: The ^{13}C n.m.r. spectrum of an equimolar mixture of *cis*-$[Pt(DMSO)_2Cl_2]$ and inosine (0.5 M) in DMSO - d_6 and acetone mixtures.

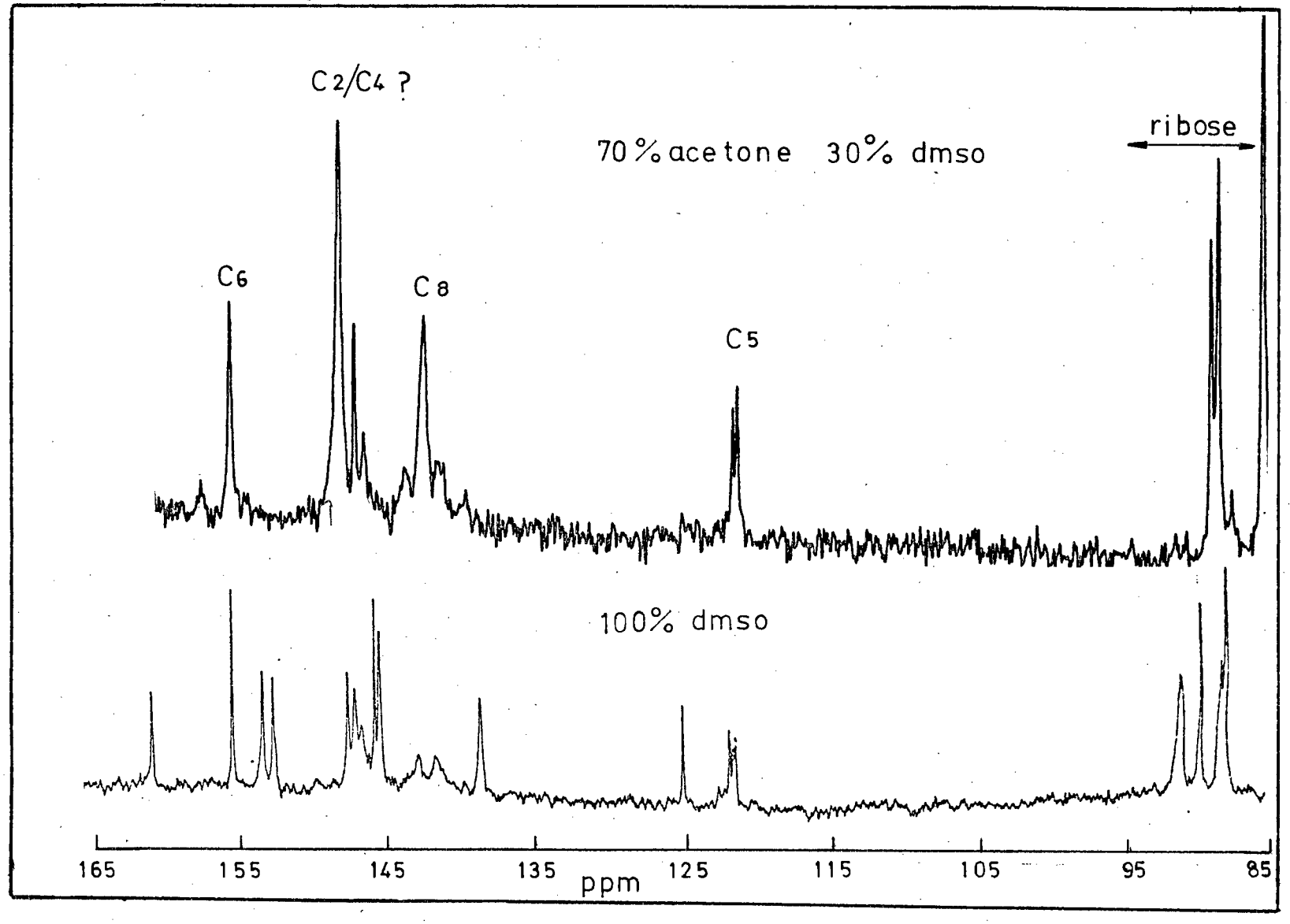

Table 3.10: ^{13}C n.m.r. data for *cis*-$[Pt(NH_3)_2(nucleoside)_2](ClO_4)_2$ in ^2H_2O containing Gd(TTHA), (≈0.05 M).

Nucleoside	Chemical shift / ppm relative to TMS[a]										$^nJ_{^{195}Pt-^{13}C}$ Coupling Constants (Hz)		
	C(8)	C(5)	C(4)	C(2)	C(6)	C(1')	C(2')	C(3')	C(4')	C(5')	^2J(C8)	^2J(C5)	^2J(C4)
Guanosine	140.9[b] (+4.0)	115.6 (-2.0)	151.5 (-0.9)	155.5 (+0.9)	157.8 (+0.0)	90.2 (+2.9)	71.0 (-0.6)	75.1 (+0.2)	86.5 (+0.1)	62.4 (+0.2)	40.2	16	27.0
Inosine	143.7[b] (+3.8)	124.5 (-0.9)	149.1[c] (-0.1)	149.4[c] (+2.4)	158.0 (+0.3)	91.7 (+2.9)	71.3 (0.0)	76.3 (+1.1)	56.9 (+0.2)	61.2 (-0.2)	38.0	12	c
	C(2)	C(6)	C(4)	C(5)									
cytidine[d]	155.8	142.4 142.9 143.5	166.6 165.3	96.7 97.1		92.6[e] 91.5	69.7[e] 70.2 70.5	75.8[e] 75.5	85.1[e] 84.7	61.7[c] 61.9	f	f	f
unbound cytidine	157.0[b]	142.8	166.7	95.7		90.1	70.6	75.1	85.4	61.9			

a: measured from dioxane at 67.7 ppm relative to TMS.
b: shifts on complexation are based on free nucleoside chemical shifts from ref. [85, page 472]. (Solvent DMSO).
c: assignment, due to resonance overlap, not unambiguous.
d: an intense blue colour developed on dissolving complex.
e: major resonance.
f: no coupling observed.

^{13}C n.m.r. parameters

Solutions of *cis*-$[Pt(NH_3)X_2](ClO_4)_2$ in water where X = inosine, guanosine and cytidine, yielded good ^{13}C spectra of which Figure 3.18 is a typical example. Generally the solution concentration ranged from *ca* 0.3 - 0. M with respect to the platinum and contained *ca* 0.05 M Gd(TTHA).

Table 3.10 lists the shieldings and coupling constants for some nucleoside complexes. Although the corresponding spectrum for the adenosine complex was also measured, it was found to be unassignable as a result of excessively broad resonances. Attempts to obtain suitable spectra with varying platinum to adenosine ratios did not yield assignable spectra either, and in all cases at least three sets of resonances appeared. This is regarded as being the result of multiple platinum coordination at N(7) and N(1) in adenosine. In high concentration it is likely that polymeric species were formed. This would account for the broad resonances observed. Efforts to obtain ^{13}C parameters from [Pt(trien)Cl]Cl and adenosine mixtures were also unsuccessful as a result of low solubility and binding of Pt(II) at N(7) and N(1) (trien = diethylentriamine).

The solution of *cis*-$[Pt(NH_3)_2(cytidine)](ClO_4)_2$ in water turned out to be unstable developing an intense blue colour shortly after dissolution. Data in Table 3.10 shows that more than one species are probably present. This phenomenon is well known in the case of platinum uracil (or other pyrimidine) complexes [26]. There is evidence that these "pyrimidine blue" complexes involve dimeric or trimeric hydroxo complexes of platinum in which the oxidation state of platinum is variable, between Pt(II) - Pt(III)-Pt(IV). These species are found to be paramagnetic, and over a period of *ca* 6 hours, result in severe n.m.r. line broadening [26]. In the case of *cis*-$[Pt(NH_3)_2(cytidine)_2](ClO_4)_2$ we are able to obtain a reasonable ^{13}C

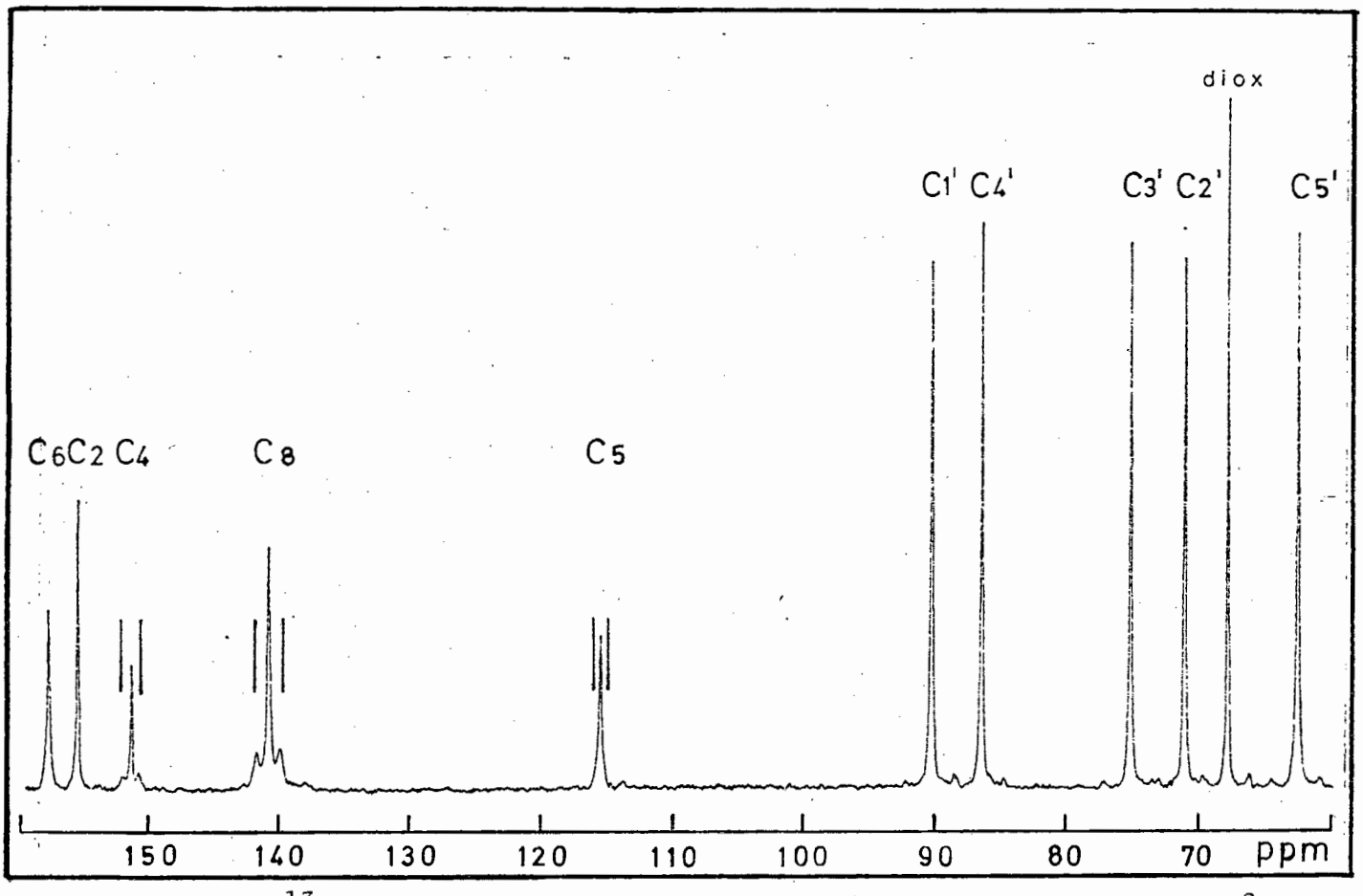

Figure 3.18: The ^{13}C spectrum of *ca* 0,4 M *cis*-$[Pt(NH_3)_2(guanosine)_2](ClO_4)_2$ in ^2H_2O.

spectrum of fresh solutions of the complex, but in all cases a blue colour appeared on dissolution, and more than a single species was evidently present in solution. In addition no J_{Pt-C} coupling, analogous to the simple pyrimidine complexes, was observable.

Reference to Table 3.10 shows that platinum exclusively coordinates *via* N(7) in both inosine and guanosine so that the ^{13}C parameters for these complexes are analogous to the imidazole compounds (c.f. Table 3.2). Very similar shielding and coupling constant trends are observed, such that $^2J_{Pt-C8}$ $^3J_{Pt-C4} > {}^2J_{Pt-C5}$ for these purine nucleosides. Incidentally, these trends confirm the assignment of the imidazole assignments, since the ^{13}C shieldings of the nucleosides have been previously assigned [85].

3.6 General Discussion and Conclusions

In this section it will be attempted to interpret the ^{13}C parameters collected for the various complexes in the previous sections. A considerable lack of detailed theoretical knowledge limits the understanding of shift and coupling trends to qualitative discussion only. Fortunately a considerable number of simple heterocycles have been subject to numerous semi-empirical quantum mechanical calculations, and to a large extent electron densities are known for imidazoles, pyridines and pyrimidines [65,66,80,81].

Some stereochemical considerations

In this work only *cis*-$[Pt(NH_3)_2X_2]Y_2$ type complexes were examined, and it is important to realize one fundamental similarity for all the complexes *viz* they all posses an effective C_{2V} symmetry axis bisecting the N $\hat{Pt}$ N angle. Furthermore, consideration of a number of crystal structures shows that in most cases the nitrogen heterocycles are not co-planar with the platinum square plane, which is by far the most preferred coordination geometry of Pt(II) [26]. For example the crystal structures of $[Pt(en)(guanosine)_2]^{2+}$, $[Pt(en)(5'\text{-IMP})_2]^{2-}$ and *cis*-$[Pt(NH_3)_2(guanosine)_2]^{2+}$ all show that the dihedral angle between the square plane of Pt(II) and the aromatic heterocycle is *ca* 70^o [37-38,87]. In the case of *cis* and *trans*-$[Pt(pyridine)_2Cl_2]$, the pyridine rings are also not copolanar with the square plane, but show dihedral planes of 55.8^o and 62^o for the *cis* isomer and 56.2^o for the *trans* case [92]. For a *trans*-$[PtCl_2(1\text{-methylimidazole})_2]$ complex the imidazole ring planes form a dihedral angle of 49.2^o with the PtN_4 plane [93]. Consideration of Drieding models of a *cis*-$[Pt(NH_3)_2X_2]Y_2$ complex where X = imidazole, pyridine and pyrimidines shows that severe steric strain would be experienced if the two heterocycles were to be forced

to be coplanar with the platinum square plane. Thus it is not unexpected to find that the two heterocycle rings form fairly acute dihedral angles with respect to the PtN_4 plane. In the solid state the dihedral angles may however also be influenced by the neighbouring molecules in the lattice; one such interaction is clearly operative in the case of the crystal lattice of *cis*-$[PtCl_2(pyridine)_2]$, in which two pyridine rings from adjacent molecules are seen to lie in parallel planes $\sim$ 0.34 nm appart [92].

It is not unreasonable to expect that in solution the bound heterocycle rings to have considerable freedom of rotation particularly if these rings lie *trans* to one another. In fact pyridine rings bound to platinum are considered to rotate rapidly in solution in some *trans* complexes [40]. On the other hand, it has been found that stereochemically demanding 2,4,6-trimethylpyridine ligand cannot rotate about a Pt-N bond, thus assuming a perpendicular orientation to the square plane [88]. For complexes in this work it is believed that in solution the two *cis*-heterocycles experience a high energy barrier to rotation about the Pt-N bond. It is thus very tempting to consider the heterocyclic rings to be on average perpendicular to the square plane, in such a way that an effective C_{2V} plane is maintained bisecting the N $\hat{Pt}$ N bond.

Considering the possible hybridization of platinum(II), it is believed that the d^8 ion forms 4 dsp^2 hybrid orbitals in the XY plane (using the *6s*, *6p* and $5d_{x^2-y^2}$ orbitals). Thus there would remain the d_{z^2}, d_{xy}, d_{yz} and d_{xz} orbitals each containing nominally two electrons [26]. It is well known that Pt(II) forms very stable bonds with π-acceptor ligands, and that platinum often, in addition to σ bonds, forms a 'back bond' involving electron transfer from filled metal *d* orbitals to $p\pi$ or π^* orbitals

of the ligand [26,72]. Although nitrogen itself is a relatively poor π-acceptor, aromatic nitrogen heterocycles show some π-acidity, in the general order pyridine > imidazole > NH_3 [90]. Recently a quantum mechanical investigation into *trans*-$[PtCl_2(pyridine)_2]$ and the corresponding Hg(II) compound showed convincingly that a considerable fraction *d* electron density is involved in the Pt-N bond [91]. Since the d_{xy}, d_{xz} and d_{yz} orbitals are essentially full, there is ample possibility of *5d* electron transfer to the pyridine π* orbitals, while the relative orientation of the pyridine ring with respect to the square plane is not critical. In fact the charge transfer absorptions observable in the u.v. spectrum are rotationally allowed, forbidden otherwise [40].

Finally it may be interesting to speculate about the structure of the *cis*-$[Pt(NH_3)_2(4\text{-bromoimidazole})_2](ClO_4)_2$ complex. ^1H and ^{13}C n.m.r. evidence strongly suggests that platinum binds through N(3) such that the bromine atom is C(4) substituted. Figure 3.19 shows the postulated structure. It is unexpected that imidazole coordinates in this fashion,

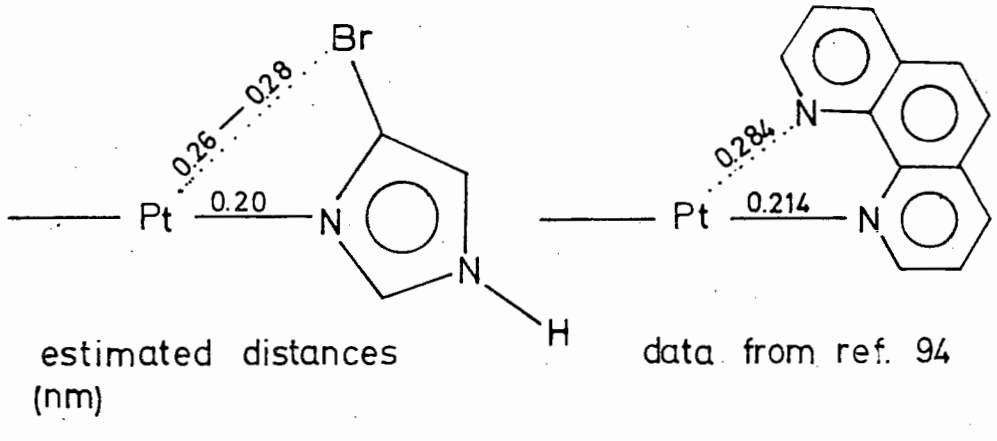

Figure 3.19: Diagram to illustrate possible Br-Pt interaction in the complex *cis*-$[Pt(NH_3)_2(4\text{-bromoimidazole})_2](ClO_4)_2$.

since N(3) is believed to be the stereochemically more crowded binding site. In view of the known capacity for halides to bind Pt(II), it is tempting to postulate some form of Br-Pt interaction, since Drieding models show the Br atom to be ideally placed for such geometry almost octahedral. Octahedral complexes of platinum(II) are known although not favoured [26]. On the other hand the complex *cis*-$[PtCl(PEt_3)_2(phen)][BF_4]$ is known to bind 1-10-phenanthroline *via* a single monodentate bond such that the phenanthroline plane is almost perpendicular to the square plane while the 'free' nitrogen appears to interact (Pt-N distance 0.28 nm) with Pt(II) [94]. In the above case, it is estimated that the Pt-Br distance is *ca* 0.26-0.27 nm. This might explain the unusual coordination mode of bromoimidazole, but in the absence of an X-ray study the structure postulated must remain tentative.

Factors influencing chemical shifts

Concerning first the unbound aromatic heterocycles, there have been numerous electron density calculations which have generally resulted in direct correlations between the ^{1}H, ^{13}C and ^{14}N n.m.r. shieldings and the electron densities calculated. Some calculated electron densities have already been given in Table 3.8. Grant *et al*[65] has examined imidazoles and purine systems in detail and has calculated the σ and π electron densities as well as bond orders for these systems [65,66]. It is interesting to consider the results of these authors in regard to protonation of the imidazole system. Figure 3.20 shows charge densities and Mulliken overlap populations as calculated with the CNDO-SCF method.

Protonation results in an upfield shift of both C(2) and C(4,5) in imidazole. It may be observed that the shielding of these atoms results not so much from changes in the actual charge densities at the various carbon atoms,

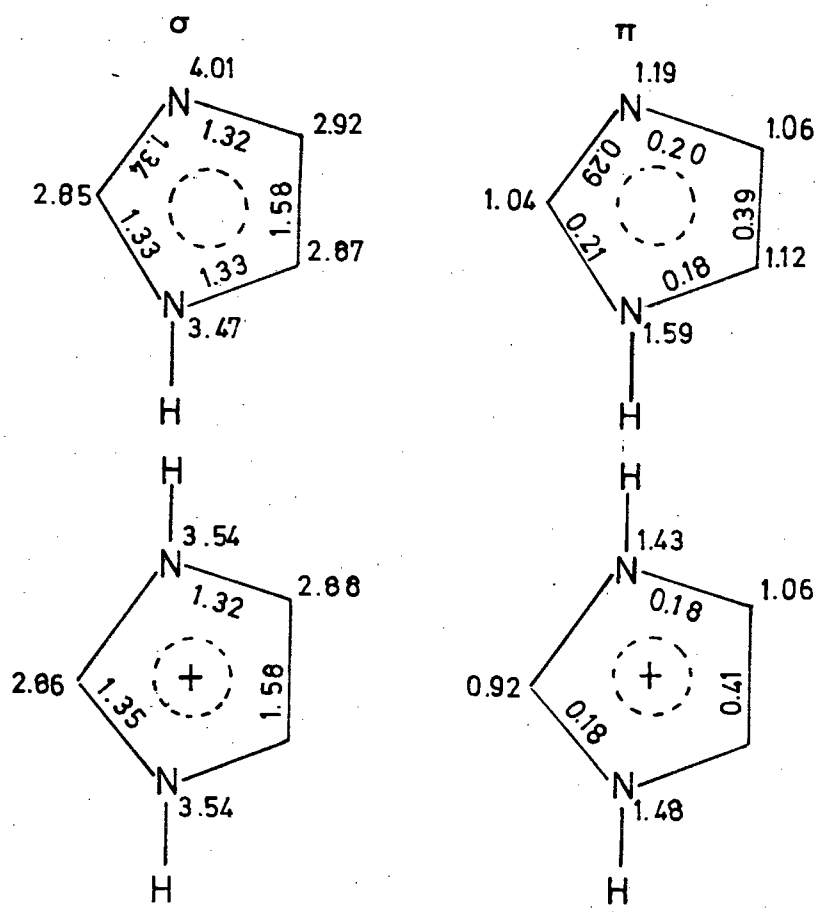

Figure 3.20: The σ/π charge densities and Mulliken overlap populations for imidazole and its cation. (From ref. [65]).

but from a significant decrease in the π overlap population of the N-C bond. It appears that changes in the σ bond population are small.

Comparing the platinum complexes of the imidazoles (Figure 3.5) shows that with the exception of 4-bromoimidazole, C(5) resonates at highest field, while C(2) is always most deshielded, i.e. coordination of platinum causes only a small downfield shift of all the resonances, as is particularly evident for the 1-methylimidazole case. It is tempting to expect the overall changes in bond-order/charge densities of the complexed imidazole moiety to be qualitatively similar to that predicted for the protonated species above. Some caution must be observed, however, because of the

possibility that platinum ligand $d\pi$-$p\pi$ back bonding that may take place. Ibusuki and Saito have found that the valence electron density of the carbon atoms in pyridine in the *trans*-$[PtCl_2(pyridine)_2]$ complex are for all practical purposes identical in the free pyridine, but no bond-order predictions were presented [91].

The origin in the general downfield shifts observed in all the complexes studied in this work cannot therefore be understood in terms of changes in σ and π electron densities and bond-order as a result of an "electron withdrawing" effect of platinum, since this would be expected to result in decreases of the π bond-order in the N-C bonds, which is associated with a shielding effect at the carbon atom [65,66]. It is believed that the overall deshielding observed for the complexes in this work is the result of one or more of the following effects:

(i) The effect of ring current anisotropy of the aromatic heterocyclic rings [19-24 part 1].

(ii) The anisotropy of the magnetic susceptibility of the square planar platinum atom. (Which has been invoked to account for the unusual high field shift of the hydride complex $[Pt\ H(X)(P\ Z_3)_2]$) [40,89].

If the heterocycle is allowed to rotate about the Pt-N bond, then an additional paramagnetic deshielding contribution is expected as a result of $5dxy \rightarrow \pi^*$ transitions (which are rotationally allowed and forbidden otherwise) [40].

Reference to equation (2.4) shows that the three major contributors to the overall shielding of a ^{13}C nucleus are σ_p, σ_d and σ', the *local* paramagnetic and diamagnetic terms, as well as the σ' term which results from electron

circulation induced in remote orbitals. Vrieze *et al* in their detailed examination of some neutral *trans*-[$PtCl_2(C_2H_2)$(pyridine)] complexes have split this σ' term into a paramagnetic (σ'_p) and diamagnetic (σ_d') contribution and estimated the relative magnitude of these terms [40]. These authors show that the paramagnetic anisotropy contribution of the metal σ'_p is small, if the pyridine ring rotation is constrained. On the other hand the diamagnetic contribution of the platinum atom was found to be a very large upfield shift (*ca* 240 ppm for C(2) in pyridine). This upfield shift was found to be offset by the large *local* paramagnetic term (σ_p). These authors also considered the possibility of ring current effects, but believed these effects small.

In the present case, while the overall chemical shifts may be considered to be grossly dominated by σ_p and σ'_d, it is an oversimplification to ignore the relative ring current contributions to the overall shieldings. If, as it is very likely, the *cis* heterocyclic rings are rotationally constrained and are on average perpendicular to the square plane of coordination, then it is impossible to ignore this contribution, which in this case would be essentially ◯shielding. Figure 3.21 illustrates the aromatic ring current anisotropy effects in a *cis*-$[Pt(NH_3)_2(pyridine)_2]^{2+}$ complex cation.

In conclusion then it is reasonable to consider that the largest contributions to the chemical shifts of the heterocyclic ring ^{13}C chemical shifts are:

(i) the local σ_p term,
(ii) the diamagnetic shielding term from the platinum metal σ'_d,
(iii) some smaller, but significant contributions from the local σ_d term as well as the ring current anisotropy contribution in this case.

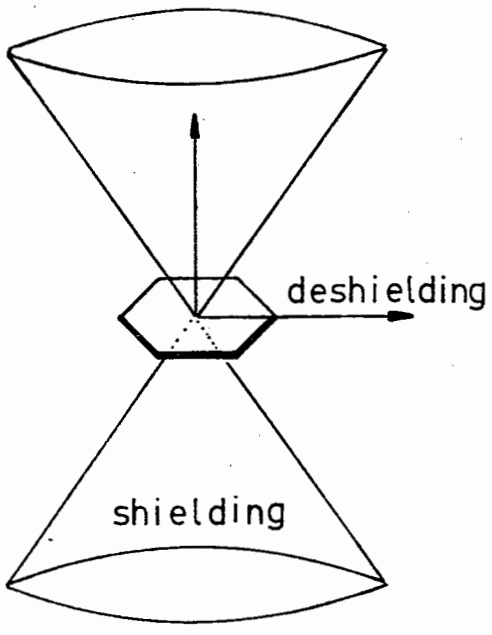

magnetic anisotropy of the benzene ring

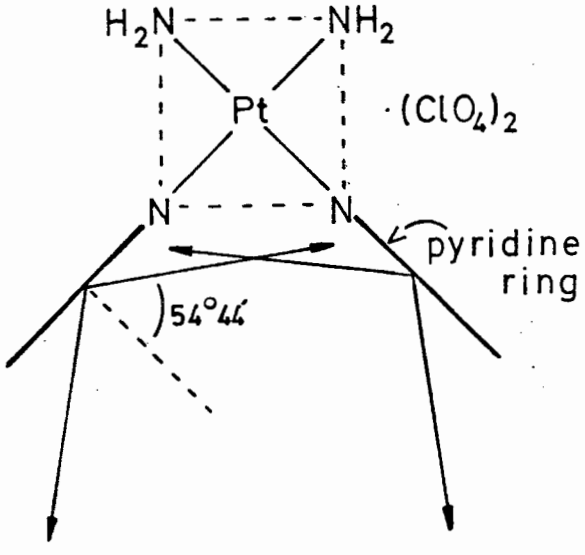

Figure 3.21: The magnetic-anisotropy of aromatic rings in the pyridine complexes.

Platinum-195 carbon-13 coupling constants

Consideration of the J_{Pt-C} coupling constants observed for the various *cis* platinum complexes studied shows that in general distinct 'types' of coupling constants are observable which all show similar trends.

(i) For a $Pt - N = C - C$ conjugated system, the trend $^{2}J_{Pt-C} < {}^{3}J_{Pt-C}$ is observed.

(ii) For a $Pt - N = C - N$ conjugated system an unusually large $^{2}J_{Pt-C}$ is observed.

(iii) $^{3}J_{Pt-C}$ in a $Pt - N = C - CH_3$ system is smaller than $^{3}J_{Pt-C}$ in (i) above and is approximately equal to the $^{2}J_{Pt-C}$ in this system for 5-membered heterocycles.

(iv) In a 6-membered ring system, generally an invariant $^{4}J_{Pt-C}$

coupling constant is observed.

(v) In pyridines no $^{2}J_{Pt-C}$ is observed.

Although it is generally accepted that one bond heavy-metal carbon coupling constants (involving a σ bond) are dominated by the Fermi contact contribution (c.f. equation 2.7), the orbital dipole and the dipole-dipole contributions to the coupling cannot be entirely ignored, and in particular will not be small if at least one π-bond order is non-zero [95]. Even in the case of a totally saturated system, considering coupling effects to be transmitted only *via* σ electrons is an oversimplification. It is well known that from hyperfine splittings in electron spin resonance spectra, that spin polarization exists between σ and π electrons. This spin polarization even if only to a small extent, may be transmitted *via* the often extensively delocalized π-electrons over a large distance so that over such distances the π electrons may have an effect which outweighs the more directly σ transmitted coupling. In general the coupling interaction should therefore be considered as a sum of two terms J^{σ} and J^{π} while it might be predicted that over a large distance J^{π} would be the predominant interaction [95]. It has also been predicted that the J^{π} contribution, in contrast to J^{σ} coupling, shows no angular dependence. This is demonstrated by the effectively equal $^{5}J_{cis-cis}$ (+ 0.6 Hz) and $^{5}J_{cis-trans}$ (+ 0.7 Hz) coupling constant in 1,3 butadiene [95]. The well known Karplus type dependence of vicinal J^{σ} type coupling, predicts a strong angular dependence, which in most cases borne out in practice. (see section 4.1, part I of this work).

It is clear from the above that the detailed factors that influence the coupling constants in the various *cis*-$[Pt(NH_3)X_2]Y_2$ complexes are complex

while their understanding is hampered by a suitable theoretical framework which J^{σ} and J^{π} are separable into quantitative terms. By means of suitable model systems however an empirical knowledge of the factors which influence the J_{Pt-C} coupling constants in 5- and 6-membered aromatic heterocyclic systems is attainable and this might stimulate greater theoretical interest in the subject.

Finally it may be interesting to compare some coupling trends that have been observed in 6-membered, aromatic heterocyclic molecules bound to Pt(II), Hg(II) and Tl(III). Considering first metal substituted phenyl systems, in arylplatinum(II) compounds $^{1}J_{Pt-C} >> {}^{3}J_{Pt-C} > {}^{2}J_{Pt-C} > {}^{4}J_{Pt-C}$ [38]. A similar trend has been observed for phenylmercury(II) [52,68] and phenylthallium(III) compounds [69]. In the arylthallium(III) case, Ernst has shown that sign of the two and three bond coupling constants are both positive while the relatively large 4-bond coupling constant is negative. Turning to the complexes of platinum(II) pyridine a very similar trend is observed in that $^{3}J > {}^{2}J$ but $^{4}J > {}^{2}J$ (not observed) in the *cis*-$[Pt(NH_3)_2(pyridine)_2]^{2+}$ complexes studied in this work, as well as for the previously reported $[Pt(pyridine)_4]^{2+}$ complex [39]. In contrast Vrieze reported a coupling pattern ^{3}J (32.5 Hz) > ^{2}J (12.6 Hz) > ^{4}J (6.4 Hz) for the *trans*-$[PtCl_2(CO)(pyridine)]$ complex [40]. The reason for this discrepancy is not clear but a tentative explanation might be that in the *cis*-$[Pt(NH_3)_2(pyridine)_2]^{2+}$ as well as for the tetrakis(pyridinato)platinum(II) cation the pyridine molecules are almost certainly restricted from rotating freely about the Pt-N bond, while in the complexes of Vrieze the single *trans* placed pyridine appears to have a larger degree of rotational freedom. This difference might affect the extent of $d\pi$-$p\pi$ back-bonding from platinum to pyridine and thus lead to the observed differences.

Conclusions

If the modest objectives of work are recalled, it is gratifying that some insight has been forthcoming into the nature of ^{13}C shifts induced and $^{n}J_{Pt-C}$ coupling constants in some simple 5- and 6-membered heterocycles. It has also been possible to observe some ^{13}C spectra of selected nucleoside platinum(II) complexes, although the properties of these compounds were such that only in idealized cases suitable ^{13}C n.m.r. spectra were obtainable.

To answer the claim that the "lack of easy discrimination between two and three bond Pt-^{13}C coupling constants may hinder their diagnostic use in identifying carbons in some types of aromatic ligands"[39], it is fair to state that by means of careful examination of suitable model systems, it is still possible to make use of the structurally very valuable J_{Pt-C} coupling constants. These coupling parameters should always be sought and used in conjunction with 'complexation shifts induced' as it may not always be possible to assign binding sites unambiguously based only on such shifts.

In conclusion then it has been shown that:

(i) The use of DMSO as solvent for the examination of chloro-amine platinum complexes is not recommended as a result of extensive solvolysis reactions that occur.

(ii) In the case of 5-membered diazole Pt(II) complexes $^{2}J_{Pt-C2} > {}^{3}J_{Pt-C5} > {}^{2}J_{Pt-C4}$ and in general all carbons are deshielded on complexation. Similar observations are made for the guanosine and inosine complexes of platinum(II). The binding site in the latter nucleosides is N(7).

(iii) In 6-membered pyridine and pyrimidine complexes, $^{3}J_{Pt-C3,5} > {}^{4}J_{Pt-C4} > {}^{2}J_{Pt-C2,6}$ for pyridines and $^{3}J_{Pt-C5} > {}^{2}J_{Pt-C2}(?) > {}^{4}J_{Pt-C4}$

for pyrimidines. The substituent in 3-substituted pyridines affects the $^{3}J_{Pt-C3}$ in a complicated way but in general may be qualitatively understood in terms of substituent constants. All ^{13}C shifts on complexation are generally downfield.

REFERENCES

1. Rosenberg, B., Van Camp, L., Trosko, R.E. and Mansour, V.H., *Nature*, 222, 385, (1969).
2. Rosenberg, B., *Naturwiss.*, 60, 399, (1973).
3. Rosenberg, B., *Cancer Chemother. Dept.*, 59, 589, (1975).
4. Howle, J.A. and Gale, G.R., *Biochem. Pharmacol.*, 19, 2757, (1970).
5. Howle, J.A., Gale, G.R. and Smith A.B., *Biochem. Pharmacol.*, 21, 1465, (1972).
6. Eichhorn, G.L. in "Inorganic Biochemistry", Vol. 2, G.L. Eichhorn (Ed.), Elsevier, New York, (1973), p. 1191.
7. Izatt, R.M., Christensen, J.J. and Rytting, J.H., *Chem. Rev.*, 71, 439, (1971).
8. Tu, A.T. and Heller, M.J., in "Metal Ions in Biological Systems, Vol. 1", H. Sigel (Ed.), Dekker, New York, 1974, p. 1.
9. Marzilli, L.G., *Prog. Inorg. Chem.*, 23, 225, (1977).
10. Mansy, S., Rosenberg, B. and Thomson A.J., *J. Amer. Chem. Soc.*, 95, 1633, (1973).
11. Harder, H.C. and Rosenberg, B., *Int. J. Cancer*, 6, 207, (1970).
12. Horacek, P. and Drobník, J., *Biochim. Biophys. Acta*, 254, 341, (1971).
13. Roberts, J.J. and Pascoe, J.M., *Nature*, 235, 282, (1972).
14. Stone, P.J., Kelman, A.D. and Sinex, F.M., *Nature*, 251, 736, (1974).
15. Macquet, J.P. and Theophanides, T., *Biopolymers*, 14, 781, (1975).
16. Harder, H.C., *Chem. Biol. Interactions*, 10, 27, (1975).
17. Guantieri, V., De Nardo, L. and Tamburro, A.M., *Inorg. Chim. Acta*, 30, 155, (1978).
18. Macquet, J.P. and Theophanides, T., *Inorg. Chim. Acta*, 18, 189, (1976).
19. Hadjiliadis, N., Kourounakis, P. and Theophanides, T., *Inorg. Chim. Acta*, 7, (2), 226, (1973).
20. Kong, P. and Theophanides, T., *Inorg. Chem.*, 13 (8), 1981, (1974).
21. Kong, P. and Theophanides, T., *Inorg. Chem.*, 13 (5), 1167, (1974).
22. Lim, M.C. and Martin, B.R., *J. Inorg. Nucl. Chem.*, 38, 1915, (1976).
23. Kong, P. and Theophanides, T., *Bioinorg. Chem.*, 5, 51, (1975).
24. Nelson, D.J., Yeagle, P.L., Miller, T.L. and Martin, R.B., *Bioinorg. Chem.*, 5, 353, (1976).
25. Sequin, J.Y. and Zador, M., *Inorg. Chim. Acta*, 20, 203, (1976).
26. Hartley, F.R., in "The Chemistry of Platinum and Palladium", Applied Science Publishers, London, 1973.
27. Coletta, F., Ettore, R. and Gambaro, A., *J. Mag. Res.*, 22, 453, (1976).
28. Ettore, R., *Inorg. Chim. Acta*, 25, L9, (1977).
29. Theophanides, T., Pneumatikakis, G. and Hadjiliadis, N., *Inorg. Chim. Acta*, 22, L1, (1977).

30. Chu, G.Y.H. and Tobias, S.R., *J. Amer. Chem. Soc.*, 98 (9), 2614, (1976).

31. Chu, G.Y.H., Ducan, R.E. and Tobias, S.R., *Inorg. Chem.*, 16 (10), 2625, (1977).

32. Chu, G.Y.H., Mansy, S., Duncan, R.E. and Tobias, S.R., *J. Amer. Chem. Soc.*, 100 (2), 593, (1978).

33. Mansy, S., Chu, G.Y.H., Duncan, R.E. and Tobias, S.R., *J. Amer. Chem. Soc.*, 100 (2), 607, (1978).

34. Kong, P.C., Iyamuremge, D. and Rochon, F.D., *Bioinorg. Chem.*, 6, 83, (1976).

35. Lippert, B., *J. Clin. Hemat. Oncol.*, 7 (1), 26, (1977).

36. Bau, R., Gellert, R.W., Lehovec, S.M. and Louie, S., *ibid*, 7 (1), 51, (1977).

37. Bau, R. and Louie, S., *J. Amer. Chem. Soc.*, 99 (11), 3874, (1977).

38. Kistenmacher, T.J., Chiang, C.C., Chalilpoyie, P. and Marzilli, L.G., *J. Amer. Chem. Soc.*, 101 (5), 1143, (1979).

39. Chow, S.T. and Martin, R.B., *Inorg. Nucl. Chem. Letters*, 10, 1131, (1974).

40. Meester, M.A.M., Stufkens, D.J. and Vrieze, K., *Inorg. Chim. Acta*, 15, 137, (1975).

41. Van Kralingen, C.G. and Reedjik, J., *Inorg. Chim. Acta*, 30, 171, (1978).

42. Yokono, T., Shimokawa, S. and Sohma, J., *J. Amer. Chem. Soc.*, 97 (13), 3827, (1975).

43. Stothers, J.B. in "Carbon-13 N.M.R. Spectroscopy", Academic Press, New York, (1972).

44. Axenrod, T. and Webb, G.A. (Editors) in "Nuclear Magnetic Resonance Spectroscopy of Nuclei other than Protons", Wiley-Interscience, New York, (1974).

45. Levy, G.C. (Editor) in "Topics in Carbon-13 N.M.R. Spectroscopy", Vol. 1, 2, Wiley-Interscience, New York, (1974).

46. Müllen, K. and Pregosin, P.S. in "Fourier Transform N.M.R. Techniques: A Practical Approach", Academic Press, New York, (1976).

47. Wehrli, F.W. in reference 45, Vol. 2, pp. 343-389.

48. Wehrli, F.W. in reference 44, pp. 157-186.

49. Noggle, J.H. and Schirmer, R.E. in "The Nuclear Overhauser Effect, Chemical Applications", Academic Press, New York, (1971).

50. Ellis, P.D. and Ditchfield, R. in reference 45, Vol. 1, pp. 2-51.

51. Ellis, P.D. and Ditchfield, R., in reference 45, Vol. 2, pp. 434-476.

52. Mann, B.E. *Advan. Organometal. Chem.*, 12, 135, (1974).

53. Swain, C.G. and Lupton, E.C., *J. Amer. Chem. Soc.*, 90 (16), 4328, (1968).

54. Coulson, D.R., *J. Amer. Chem. Soc.*, 98 (11), 3111, (1976).

55. Maciel, G.E. in reference 45, vol. 1, pp. 54-77.

56. Sherry, D.A. and Lettrin, J., *J. Mag. Res.*, 28, 459, (1977).

57. "Inorganic Syntheses", Vol. 7, McGraw-Hill, New York, pp. 239-242, (1963).

58. Kurnakov, J., *J. Prac. Chem.*, 2, 50, 480, (1894).

59. Theophanicles, T. and Hadjiliadis, N., *Inorg. Chim. Acta*, 16, 77, (1976).

60. Pyman, F.L., *J. Chem. Soc.*, 947, (1922).

61. Wahren, R., Wahlberg, K. and Stensio, K., *Acta Chem. Scand.*, 27, (6), 22, (1973).

62. Jackman, L.M. and Sternhell, S., in "Applications of Nuclear Magnetic Resonance Spectroscopy in Organic Chemistry", 2nd Ed., Pergamon Press, London, (1969).

63. Cotton, F.A. and Wilkinson, G., in "Advanced Inorganic Chemistry", 3rd Edition, Interscience Publishers, pp. 730, 1030-1031, (1972).

64. Reference [26], p. 128.

65. Grant, D.M. and Pugmire, R.J., *J. Amer. Chem. Soc.*, 90 (16), 4232, (1968).

66. Grant, D.M. and Pugmire, R.J., *J. Amer. Chem. Soc.*, 93 (8), 1880, (1971).

67. Roberts, J.D., Marzin, C. and Elguero, J., *J. Org. Chem.*, 39 (3), 357, (1974).

68. Wilson, N.K. and Zehr, R.D., *J. Mag. Res.*, 21, 437, (1976).

69. Ernst, L., *J. Organometal. Chem.*, 82, 319, (1974).

70. Reference 26, pp. 112-113, and 292-323.

71. Martin, D.S. and Lee, K.W., *Inorg. Chim. Acta*, 17, 105, (1976).

72. Basolo, F. and Pearson, R.G., in "Mechanisms of Inorganic Reactions", 2nd Edition, Wiley, New York, Chapter 5, pp. 351-454, (1967).

73. Martell, E.A. and Smith, R.M., in "Critical Stability Constants", Vol. 2, New York, 1976.

74. Brügel, W., *Z. Elektrochem.*, 66, 159, (1962).

75. Katritzky, A.R., in "Physical Methods in Heterocyclic Chemistry", Vol. 4, Academic Press, New York, Chapter 4, pp. 121-235, (1971).

76. "Handbook of Chemistry and Physics", 55th Edition, C.R.C. Press, Cleveland, (1974).

77. Hoffman, K., in "Imidazole and its Derivatives", Part 1, Interscience, New York, (1953).

78. Retcofsky, H.C. and Friedel, R.A., *J. Phys. Chem.*, 72, 290, (1968).

79. Lauterbur, P.C., *Tetrahedron Lett.*, 274, (1961).

80. Adam, W., Grimison, A. and Rodriguez, G., *Tetrahedron*, 23, 2513, (1967).

81. Mahanti, M.K., *Ind. J. Chem.*, 15B, 168, (1977).

82. Reference 72, Chapter 5, pp. 390-391.

83. Romeo, R. and Tobe, M.L., *Inorg. Chem.*, 13 (8), 1991, (1974).

84. Price, J.H., Birk, J.P. and Wayland, B.B., *Inorg. Chem.*, 17 (8), 2245, (1978).

85. Reference 43, Chapter 11, Section D, pp. 468-478.

86. Kerrison, S.J.S. and Sadler, P.J., *J.C.S. Chem. Comm.*, 861, (1977).

87. Cramer, R.E. and Dahlstrom, P.L., *J. Clin. Hemat. Oncol.*, 7 (1), 330, (1977).

88. Chottard, J.C., Mansuy, D. and Bartoli, J.F., *J. Organometal. Chem.*, 65, C19, (1974).

89. Miller, R.G., Stauffer, R.D., Fahey, D.R. and Parnell, D.R., *J. Amer. Chem. Soc.*, 92, 1511, (1970).

90. Sundberg, R.J. and Martin, R.B., *Chem. Rev.*, 74 (4), 471, (1974).

91. Saito, Y. and Ibusuki, T., *Inorg. Chim. Acta*, 19, 87, (1976).

92. Orioli, P.L. and Colamarino, P., *J.C.S. Dalton*, 1656, (1975).

93. Johnson, D.A., Fair, C.K., Cordes, A.W., Chan, N. and Carmichael, J.W., *Inorg. Chem.*, 11, (5), 1117, (1972).

94. Dixon, K.R., *Inorg. Chem.*, 16 (10), 2618, (1977).

95. Murrell, J.N., *Prog. Nuclear Mag. Res. Spect.*, 6, 1, (1971).

PUBLICATION

A ^{1}H and ^{13}C NMR study of some *cis*-$[Pt(NH_3)_2X_2]Y_2$ complexes in aqueous solution. (Y = Cl, ClO_4 and X = imidazoles, pyrimidines, 3-substituted pyridines, inosine and guanosine). G.V. Fazakerley and K.R. Koch. *Inorg. Chim. Acta.* 1979, in press.